COMPARATIVE STUDIES OF THE STEADY STATE AND R.F. PROPERTIES OF PROXIMITY EFFECT BRIDGES

Thesis by

Robert Patrick McNamara

In Partial Fulfillment of the Requirements
for the Degree of
Doctor of Philosophy

California Institute of Technology
Pasadena, California

1978

(Submitted May 3, 1978)

To my in-laws, Emilienne and Humbert Volante, who have given so much of themselves these past four years. Without them, none of this would be possible.

ACKNOWLEDGEMENTS

This work was only possible through the assistance of a great number of people who have directly or indirectly affected its completion and my own continuing education. Their contribution is gratefully acknowledged.

In particular, I would like to thank Dr. Harris Notarys, without whose aid, advice, assistance and friendship, this work could never have been accomplished.

Dr. James Mercereau who aided me in gaining deeper insight into my experimental findings and attempted to train me as a physicist.

My fellow graduate students, in particular, I would like to thank Dave Palmer, Steve Decker, Tom Ganz, Warren Lai and Dave Wilt, who, each in his own way, has directly contributed to this research.

I would also like to acknowledge Leon Strand, who has contributed much to my continuing education as a friend and coworker, and with whom I have shared many sausage and mushroom pizzas.

Mostly, I would like to thank my wife, Evelyne, who over the past four years has supported me, given me a daughter, typed my thesis and somehow never tired of a husband who had apparently dedicated his life to being a professional student.

ABSTRACT

Experimental investigations on proximity effect bridges at zero and finite voltages in the μV range are reported. Measurements have been made of the bridge/film material properties (resistivity, coherence length, penetration depth) and geometry (length, width) which have been correlated to the bridge steady state properties. The steady state properties examined include the current distribution of a thin film/proximity effect bridge, the magnetic field modulation of the critical current as a function of film geometry, and the critical current density of a proximity effect bridge. A model which correlates the bridge/film material and geometric properties has been developed to calculate the bridge critical current density for the temperature regime $T > T_n$, the bridge transition temperature.

In the nonequilibrium (finite voltage) case, one particular bridge property has been examined, the bridge rf response to external microwave irradiation. Comparison is made between the bridge rf response, and predictions based on the resistively shunted junction (RSJ) model for the behavior of a weak link. Large discrepancies were found to exist between the RSJ model and the measured bridge response. At low microwave frequencies (< 10 GHz), the supercurrent-voltage relationship for these devices was found to be

$$I_s\ (T,V) = I_0(T)\ \exp\ (-|V|/V^*)\ \sin\left(\frac{2e}{h}\int V dt\right)$$

This result appears to be consistent with a new model which is based on a concept of voltage induced pair breaking in the link.

TABLE OF CONTENTS

	Page
Acknowledgements	iii
Abstract	iv
I. Macroscopic Quantum Effects	1
1.1 Introduction	1
1.2 Macroscopic Wavefunction - Ginzburg-Landau Free Energy	2
1.3 Microscopic Theory of BCS	8
1.4 Boundary Conditions	11
1.5 Non-Equilibrium Effects	13
II. Steady State Properties of Proximity Effect Bridges	15
2.1 Introduction	15
2.2 Sample Preparation/Bridge Fabrication	18
2.3 Material Properties	20
2.4 Current Distribution of a Superconducting Thin Film and Proximity Effect Bridge	33
2.4.1 Introduction	33
2.4.2 Experimental Results	34
2.4.2a Superconducting Shield Experiment	38
2.4.2b Critical Current Density	42
2.4.2c Penetration Depth Measurement	44
2.4.3 Discussion of Experimental Results	44
2.4.4 Current Distribution of a Proximity Effect Bridge	50
2.5 Critical Current of a Proximity Effect Bridge	54
2.5.1 Introduction	54

Page

2.5.2 Critical Current vs Temperature of a Proximity Effect Bridge, $T > T_n$ 57

2.5.3 Boundary Conditions at an S-N Interface 78

2.5.4 Calculation of the Critical Current of a Proximity Effect Bridge- $T > T_n$ 90

2.5.5 Comparison of Theoretical and Experimental Results 92

2.5.6 Critical Current of a Proximity Effect Bridge, $T < T_n$ 95

2.5.7 Minimization of the Free Energy with Two Boundaries 102

2.6 Bridge Critical Current vs Applied Magnetic Field 113

2.6.1 Quantum Interface Effects in Magnetic Fields 113

2.6.2 The Effect of Film Geometry on Magnetic Field Period 116

2.6.3 Discussion of Results 125

2.6.4 Critical Current vs Applied Magnetic Field - Comparison between Bridges 139

III. R.F. Response of Proximity Effect Bridges 145

3.1 Introduction 145

3.2 RSJ Model 150

3.3 Bridge RF Response as a Function of Frequency, Temperature and RF Power 152

3.4 Discussion of Results 164

3.5 Bridge RF Response at 10 GHz 185

Appendix A 196

References 199

I. MACROSCOPIC QUANTUM EFFECTS

1.1 Introduction

A mean field description of superconductivity, that of Ginzburg-Landau (GL), has existed now for over a quarter of a century.[1] While this theory has explained many of the properties of bulk superconductors, only recently has it successfully been applied to the steady state properties of weak links and, in particular, to proximity effect bridges. The approach of this thesis has been to do a comparative study of the steady state properties of proximity effect bridges. An attempt is then made to extend these findings by treating a particular non-equilibrium case, that of irradiation of a bridge with microwave radiation, as a perturbation of the equilibrium situation.

The first chapter should serve as background to the experiment and analysis which will follow. It will introduce the Ginzburg-Landau formalism and describe concepts which are applicable to superconductors in general, not specifically proximity effect bridges.

Chapter 2 will deal with the steady state properties of proximity effect bridges. Measurements have been made of the bridge/film material properties (resistivity, coherence length, penetration depth). The steady state properties examined include the current distribution of a thin film/proximity effect bridge, the magnetic field modulation of the critical current

as a function of film geometry, and the critical current density of a proximity effect bridge. A model which correlates the bridge/film material and geometric properties has been developed to calculate the bridge critical current density for the temperature regime $T > T_B$, the bridge transition temperature.

Chapter 3 examines one particular non-equilibrium situation - that of the rf response of proximity effect bridges. Comparison is made between the steady state critical current, bridge rf response and predictions based on the resistively shunted junction (RSJ) model for the behavior of a weak link. Large discrepancies are found to exist between the RSJ model and measured bridge response. A new model is proposed which attempts to explain the experimental findings.

1.2 Macroscopic Wavefunction - Ginzburg-Landau Free Energy

The concept of a superconducting electron condensate being treated as a single wavefunction originated with London in 1935.[2] This idea was extended by Ginzburg and Landau (GL) when they proposed a phenomenological theory of superconductivity in which a psuedo-wavefunction, ψ (r), was introduced as a complex order parameter.

The order parameter, ψ (r), characterized the degree of superconductivity at various points in a material. Ginzburg-Landau's basic postulate was that a Taylor's series expansion of the free energy density, f, could be made in powers of the order parameter $\psi(r)$, with coefficients that depended on the temperature, T. Only the leading terms in the expansion were

kept. $|\psi(r)^2|$ was to represent the local density of superconducting electrons, n_s. This approach was later shown (Gor'kov 1958)[3] to be a limiting case of the more exact BCS formalism. The true value of the GL formalism lies in treating the macroscopic behavior of a superconductor in cases where the free energy is more important than the detailed spectrum of excitations.[4] Since the entire state can be considered as a single, position dependent, macroscopic wavefunction, a description of the overall behavior of a system is simplified to prescribing the behavior of ψ under the constraints of certain boundary conditions and keeping the free energy of the system minimized.

Ginzburg-Landau postulated that near the transition temperature, T_c, if ψ is small and varies slowly in space, the free energy of the system can be expanded in a series of the form

$$f_s = f_n + \alpha|\psi|^2 + \frac{\beta}{2}|\psi|^4 + \frac{1}{2m^*}\left|\left(\frac{\hbar}{i}\vec{\nabla} - \frac{e^*\vec{A}}{c}\right)\psi\right|^2 + \frac{h^2}{8\pi} \qquad (1.2.1)$$

where α and β are real coefficients. They are also material and temperature dependent. The fourth quantity contains the kinetic energy terms of the expansion while the last term is the magnetic energy density if the superconductor was not present. It is interesting to note that no odd order terms are present since f_s cannot depend on either the sign or phase of ψ. It is illuminating to consider the term containing the fields and gradients and its effect on the free energy. If one writes the wavefunction $\psi = |\psi|e^{i\phi}$, it takes the form

$$\frac{1}{2m^*}\left[\hbar^2(\vec{\nabla}|\psi|)^2 + (\hbar\vec{\nabla}\phi - \frac{e^*\vec{A}}{c})^2|\psi|^2\right] \qquad (1.2.2)$$

The first term gives the energy contribution due to gradients in the amplitude of the wavefunction, the second term gives the kinetic energy associated with supercurrents in a gauge-invariant form. With $|\psi|^2 = n_s$, the kinetic energy density term can be written as $n_s(\frac{1}{2}m^*v_s^2)$ where the supercurrent velocity is given as

$$m^*\vec{v}_s = \vec{P}_s - \frac{e^*\vec{A}}{c} = \hbar\nabla\vec{\phi} - \frac{e^*\vec{A}}{c} \qquad (1.2.3)$$

Therefore, the final expression for the GL free energy can be written as

$$f_s = f_n + \alpha|\psi|^2 + \frac{\beta}{2}|\psi|^4 + |\psi|^2\tfrac{1}{2}m^*v_s^2 + \frac{\hbar^2}{2m^*}(\vec{\nabla}|\psi|)^2 + \frac{h^2}{8\pi} \qquad (1.2.4)$$

By minimizing the volume integral of f_s with respect to variations in ψ the first GL differential equation is obtained.

$$\alpha|\psi| + \beta|\psi|^2\psi + \frac{1}{2m^*}\left(\frac{\hbar}{i}\vec{\nabla} - \frac{e^*\vec{A}}{c}\right)^2\psi = 0 \qquad (1.2.5)$$

The second GL equation is found by applying the quantum mechanical current operator to ψ.

$$\vec{J}_s = \frac{e^*\hbar}{2m^*i}\left(\psi^*\vec{\nabla}\psi - \psi\vec{\nabla}\psi^*\right) - \frac{e^{*2}}{m^*c}\psi^*\psi\vec{A} \qquad (1.2.6.a)$$

which can also be written as

$$\vec{J}_s = 2e|\psi|^2\vec{v}_s \qquad (1.2.6.b)$$

From the expression for the free energy, certain special and obvious solutions of the GL equations can be found and used to evaluate the constant terms α and β. Consider first the case of no fields or gradients. Then the expression for the free energy reduces to

$$f_s = f_n + \alpha|\psi|^2 + \frac{\beta}{2}|\psi|^4 \qquad (1.2.7)$$

By inspection of 1.2.7, one can see that β must be positive, otherwise f_s has no minimum value (a relative minimum is found at $|\psi|^2 = 0$). If α is positive, then f_s is a minimum when $|\psi|^2 = 0$, which corresponds to the normal case (keep in mind that $|\psi|^2 = n_s$). However, if $\alpha<0$, the minimum of f_s occurs when

$$|\psi|^2 = -\frac{\alpha}{\beta} = |\psi_\infty|^2 \qquad (1.2.8)$$

where $|\psi_\infty|^2$ is defined by 1.2.8. The energy difference between the super-normal state can be expressed as

$$f_s - f_n = \frac{-H_c^2}{8\pi} = \frac{-\alpha^2}{2\beta} \qquad (1.2.9)$$

where H_c is the thermodynamic critical field.

At this point, it is worthwhile to introduce the two

characteristic lengths of superconductivity - the penetration depth and the coherence length.

The penetration depth was first introduced by London and London to explain the Meissner effect.[5] It is the characteristic length for the variation of the magnetic field and current density. It can be derived by taking the curl of $\vec{j}_s$ in equation 1.2.6.a and assuming that the order parameter in a weak field is identical to the zero field case. Thus

$$\nabla x \vec{j}_s = \left(\frac{e^{*2} \psi_\infty^2}{m^* c} \right) \vec{h} \qquad (1.2.10)$$

Combining this with the Maxwell equation $\nabla x h = 4 \frac{\pi}{c} j$, one has

$$\nabla^2 h = \left(\frac{4\pi e^{*2} \psi_\infty^2}{m^* c^2} \right) h \qquad (1.2.11)$$

with λ_L defined as

$$\lambda_L^2 = \left(\frac{mc^2}{4\pi e^{*2} \psi_\infty^2} \right) \qquad (1.2.12)$$

which is exactly the London result with $n_s = |\psi_\infty|^2$.

The coherence length was first introduced by GL and is the characteristic length for variation of the order parameter. While it can be related to the intrinsic properties of the superconductor by microscopic (BCS) theory, we will examine how it appears in the GL formalism. Consider the special case of the first GL differential equation where there is no external field, that is A = 0, and the order parameter ψ is normalized with

respect to ψ_∞. Letting $f = \psi/\psi_\infty$ one can rewrite 1.2.5 as

$$\frac{\hbar^2}{2m^*|\alpha|}\nabla^2 f + f - f^3 = 0 \qquad (1.2.13)$$

Therefore, the characteristic length introduced into the problem is

$$\xi^2(T) = \frac{\hbar^2}{2m^*|\alpha|} \qquad (1.2.14)$$

which sets the scale for variations in the order parameter, ψ .

One other concept will be introduced here - that of the Ginzburg-Landau order parameter. Upon application of a magnetic field, superconductors show two separate and distinct trends, and are classified as type I or type II. The simplest possible definition for type I behavior is that a type I superconductor excludes a magnetic field until superconductivity is destroyed suddenly and completely, and then the field penetrates. A type II superconductor excludes a magnetic field completely only for relatively weak fields, then the flux penetrates the sample, the super and normal states are able to coexist. The coexistence of the super and normal states is characteristic of a type II behavior. Now, the Ginzburg-Landau parameter is defined as

$$\kappa = \frac{\lambda}{\sqrt{2}\xi} \qquad (1.2.15)$$

and is of importance for calculating the surface energy of a superconductor in the intermediate state. Since λ and ξ have the

same approximate temperature dependence, κ is approximately constant in temperature. What is of relevance is that for $\kappa < 1/\sqrt{2}$, the superconductor behavior is type I, while for $\kappa > 1/\sqrt{2}$, the behavior is type II.

1.3 Microscopic Theory of BCS

While London, Ginzburg, Landau and others were working on a phenomenological description of superconductivity, it was the work of Bardeen, Cooper and Schrieffer (BCS), first introduced in 1957, which explained the actual mechanism of the superconducting state.[6] Its basic premise is that an electron gas, under the influence of a weak, attractive interaction, can bind pairs of electrons (Cooper pairs). Ample background and details on the BCS theory are presented elsewhere and are beyond the scope of this section. This introduction is included since the microscopic theory provides a means for calculating the parameters of the phenomenological Ginzburg-Landau theory.

The parameter that will be necessary in evaluating the GL formalism is the BCS energy gap, Δ_k, which is ½ the binding energy of a Cooper pair and where the subscript k denotes a pair of electrons with momentum $(k_1 - k)$ and opposite spins (The factor of 2 comes from the fact that two quasiparticles are created when the pair is destroyed). It is important here that Δ be represented in terms of a measurable quantity, ie, with respect to temperature. It can be shown that the BCS gap may be expressed in terms of

$$\frac{1}{V} = \tfrac{1}{2}\sum \frac{\tanh\left(\frac{\left(E_k^2 + \Delta^2\right)^{\frac{1}{2}}}{k_B T}\right)}{\left(E_k^2 + \Delta^2\right)^{\frac{1}{2}}} \tag{1.3.1}$$

where V is the strength of the attractive interaction between electron pairs, E_k is the energy of an excitation measured relative to the Fermi energy and T is the temperature. The dependence of the energy gap as a function of temperature is shown in Fig. 1. It is seen that at the transition temperature T_c, $\Delta(T) \rightarrow 0$. Near the transition temperature, T_c, the energy gap can be expressed in the form

$$\Delta^2(T) = \left[\frac{8}{7\lambda(3)}\right] \left(\pi k_B T_c\right)^2 \left(\frac{T_c - T}{T_c}\right) \tag{1.3.2}$$

while at lower temperatures $T << T_c$, the energy gap is approximately constant and can be written

$$\Delta(T) = 1.76\ kT_c \tag{1.3.3}$$

In 1958, Gor'kov was able to show that under certain conditions the GL order parameter, Ψ, is equivalent to the energy gap Δ. Therein lies the method that will be used throughout this work. The boundary conditions on Ψ will be expressed in terms of the BCS energy gap, Δ, which in turn will be expressed as a function of temperature.

The relation between energy gap, Δ, and Ψ can be expressed in the dirty limit (that is, the intrinsic coherence length ξ_0

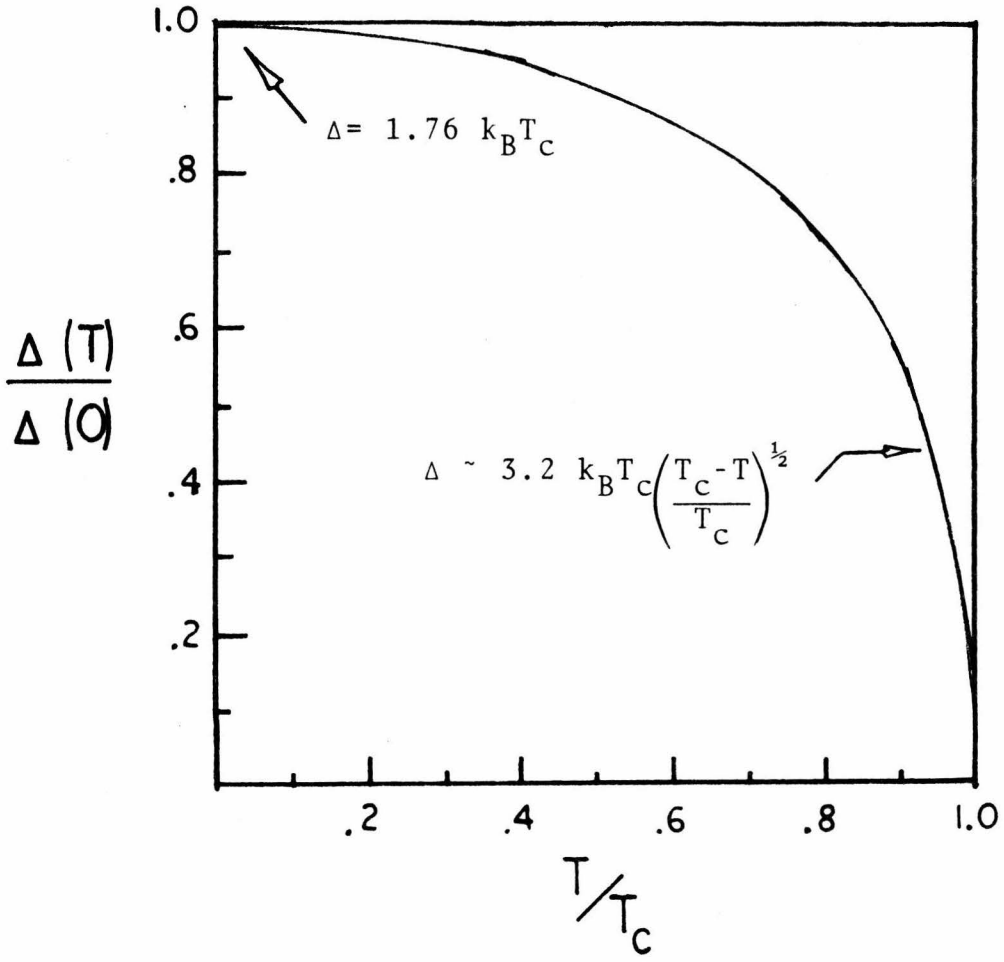


Figure 1 - BCS Energy Gap, $\Delta(T)/\Delta(0)$, as a Function of Reduced Temperature, T/T_c.

is much greater than the electronic mean free path, l) as[8]

$$\Psi = \left(\frac{\pi}{8}\frac{nl}{v_F T}\right)^{\frac{1}{2}} \Delta \qquad (1.3.4)$$

where n is the number of conduction electrons per unit volume and v_F is the Fermi velocity of the sample. This expression can be rewritten in terms of measurable parameters to within a numerical constant as

$$\psi = K\left(\frac{1}{T\lambda^2(0)T_c}\right)^{\frac{1}{2}} \Delta \qquad (1.3.5)$$

where $\lambda^2(0)$ is the penetration depth at $T=0^oK$ and T_c the transition temperature of the sample. In subsequent discussions ψ and Δ will be used interchangeably with the proper normalization.

1.4 Boundary Conditions

In the solution of the GL differential equations 1.5 and 1.6, of primary importance will be specifying the value of the order parameter at an S-N or S-S' interface. Consider the simple S-N case shown in Figure 2. The order parameter in the superconducting film, ψ_s, is depressed below its equilibrium value $\psi_{s\infty}$ near the interface for a distance of about ξ_s, the coherence length in the superconducting film. Inside the normal material, the order parameter eventually decays to zero. Note that at the boundary, ψ is shown to have a discontinuity of $\delta\psi$. The discontinuity in ψ can be most easily understood by

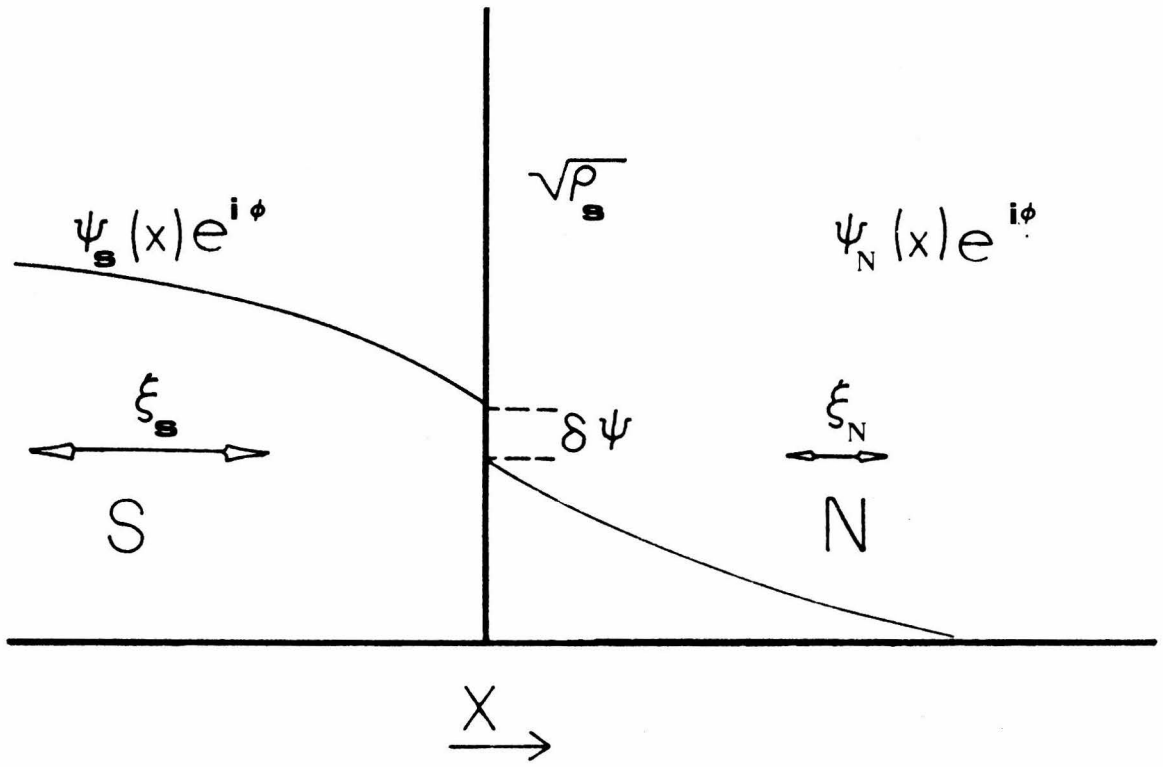


Figure 2 - Variation of ψ, the Ginzburg-Landau order parameter, at an S-N interface (not to scale). The characteristic decay lengths in the super/normal material are defined as ξ_s and ξ_n, respectively

observing 1.3.4, and noting that there is no reason that the number density of conduction electrons must be the same in both the super and normal material. The amount of depression of ψ in the superconducting film and its subsequent behavior in the normal material will be considered in more detail in chapter 2, however, suffice it for now to say that the behavior at an interface will depend on the material properties of both the super and normal materials, a point which does not seem to be generally appreciated.

1.5 Non-Equilibrium Effects

As was noted in the development of the GL theory, this approach should be feasible in situations where the overall free energy is more important than the effect of excitations of the system and should be applicable for the steady state (equilibrium) properties of the proximity effect bridges if one allows for effects due to a spatially varying order parameters. Implicit in this sort of development is that the superconducting condensate, the quasiparticle excitations, and the lattice are in equilibrium with each other. Recently, considerable attention has been focused on the problem of the behavior of a superconductor which is not in equilibrium (due to excess quasiparticles, heating, etc.) and the corresponding relaxation phenomenon.

For the case of proximity effect bridges, some effort has been expended to employ these devices as high frequency radiation detectors and as computer elements. The ability to develop

such elements has seemingly been blocked by some form of non-equilibrium process. More specifically, when a voltage is developed across a bridge, the simplest possible model of the electrodynamics is usually based on a two fluid picture of the current flow. This can be expressed as

$$I = \frac{V}{R} + I_s \sin \phi \qquad (1.5.1)$$

where R is the normal resistance of the bridge, and V, the voltage, is related to the Josephson relation by $V = (\hbar/2e)d\phi/dt$. Typically, in most modeling of weak links, I_s is taken to be equal to I_c, the critical current of the sample. However, for the case of a bridge irradiated with microwaves, experimentally I_s is found to be a function of microwave power and frequency.[9-10] I_s is found to vary from I_c at low frequencies (~1-2 GHz) and to approach zero at very high frequencies (~100-300 GHz). Since I_s is proportional to the size of the order parameter, ψ, in the bridge center (Chapter 2) any reduction in I_s can be seen to be a measure of the reduction of ψ. Stated another way, the quantum interference characteristic of the bridge seemingly is being preserved (that is, V is still proportional to $d\phi/dt$) but the amplitude is being decreased. The reduction of I_s as a function of microwave power and frequency will be considered in more detail in Chapter 3 .

II. STEADY STATE PROPERTIES OF PROXIMITY EFFECT BRIDGES

2.1 Introduction

A description of the superconducting state by the GL formalism introduces an order parameter, ψ, which is related to the degree of superconductivity in the material. While ψ is a complex quantity (Section 1.2, $\psi=\psi(r)e^{i\phi}$),it is seen that the absolute phase cannot be determined by the GL equations. It should be pointed out though, that phase differences are determined in the GL theory since they are independent of the absolute value of ϕ. Consequently, the phase of ψ is a quantity possessing long range order, that is, fixing its value at one point determines its value at another. The long range order of the phase of ψ can be understood in that it is a cooperative effect brought about by the motion of the conduction electrons from one part of the superconductor to another.

Consider a system consisting of two superconductors which are isolated from each other, that is, electrons cannot flow from one to the other. In such a situation, one would not expect any correlations between the phases in either material. If the two superconductors are coupled by some means which permits electrons to flow, then under certain circumstances this coupling results in the appearance of correlations between the phases of the order parameter in each. The coupling link is seen to exhibit properties, quantum interference effects, considerably different from a bulk superconductor.

One measure of the degree of coupling is the amount of current (denoted the critical current, I_c) which can pass through the link before phase coherence breaks down and a voltage develops across the link.[1] The quantum interference properties of the link are usually observed in the diffractionlike behavior of the critical current upon application of a magnetic field.

In general, there are two ways in which the coupling between two superconductors can be produced. First, a superconducting link between two systems can have its cross section reduced, as in the case of a Daym bridge. In the second case, the two superconductors are coupled through a link which is not superconducting. Pair diffusion through the non-superconducting region allows the transmittal of phase information provided the link is sufficiently short. The particular weak link considered in this work is the proximity effect bridge. It should be emphasized that while the fabrication of a proximity effect bridge is a specific technique for making weakly connected superconductors, the experiments run on proximity effect bridges yield results applicable to weak links in general.

Proximity-effect type bridges have been produced in various ways and with many materials. Sequential layering, anodization[2], ion etching[3] and ion implantation[4] have all been used with photographic or electron beam lithography. The main characteristic of this type of bridge is a well defined, dimensional geometry of a material whose electronic and superconducting properties are also well defined. To date there does

not exist a complete study of the steady state behavior of proximity effect bridges as a function of the bridge parameters. A partial study[5] with results being catalogued and examined in the following sections has been attempted, and while not complete, does provide enough information to correlate the dimensional and material properties of the bridge to its quantum-effect behavior. The steady state properties of this study, the critical current vs magnetic field and critical current vs temperature, are investigated as a function of both bridge and film materials, fabrication, transition temperature bridge and external film geometry, coherence length and penetration depth.

This work is organized into three main areas:

1) the current distribution through a thin film/proximity effect bridge ;
2) the effect of external film/geometry on critical current vs magnetic field and a comparison of the critical current vs magnetic field for various bridges;
3) critical current vs temperature as a function of dimensional as well as material parameters of the bridge region ;

By far the largest piece of experimental work and analysis lies in the steady state critical current vs temperature behavior of the bridges. The justification for emphasizing the steady state critical current work is twofold:

1) In any analysis of the steady state properties of proximity effect bridges, the critical current beha-

vior should be the simplest case to consider, and;

2) The critical current behavior seems to be related to the dynamic properties of the bridge (Rf response). This area will be considered in greater detail in Chapter 3 .

2.2 Sample Preparation / Bridge Fabrication

Figure 1 illustrates the generalized structure and geometry of the proximity-effect bridge. It consists of a strip of material S_o, having transition temperature T_{co}, bisected by a narrow region of a different superconducting material, S, having a transition temperature T_c, such that $T_c < T_{co}$. The dimension of the region S along the current direction will be referred to as the length, L. For the bridges described here, the S material in the narrow region is made by modifying the S_o material in the narrow region by ion implantation or anodization of a layered film. Films and bridges used in two parts of this chapter - the study on current distribution and external geometry effects on magnetic field response - were $100A^0$ of Niobium on $200A^0$ of Tantalum on a sapphire substrate. Bridges used in this part of the study were formed by standard photolithography-anodization techniques.

For the study of critical current as a function of various bridge-film parameters both anodized layered film and ion implant bridges were employed. Films for ion implant samples were Ta with $t = 460A^0$.

Implantation with Cu ions at 60 KEV formed the S region.

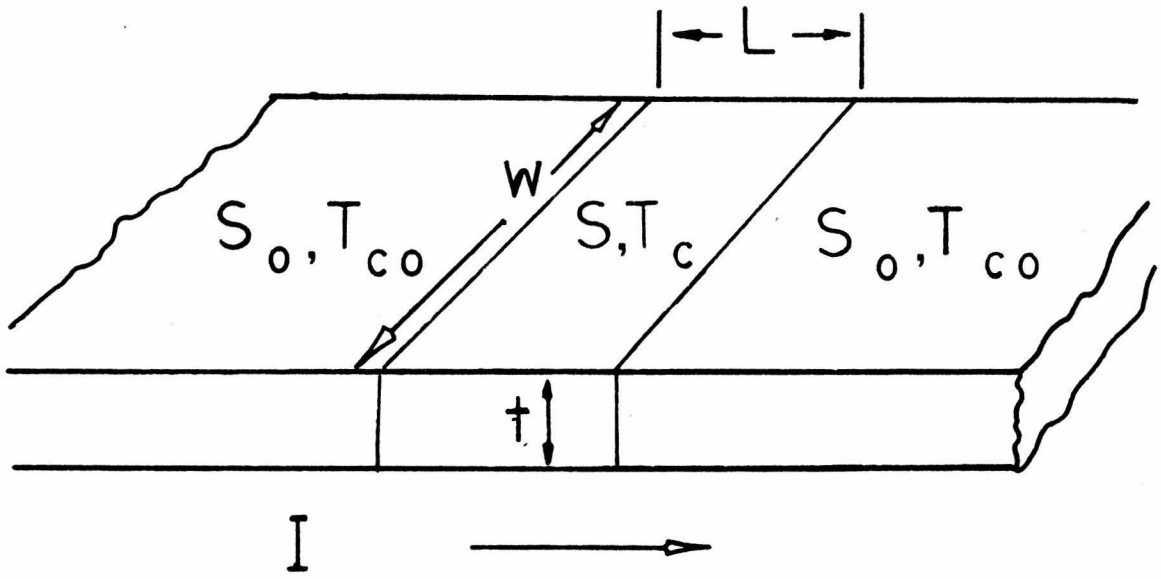


Figure 1 - Generalized structure of a Proximity Effect Bridge.

Four dosages were used; $1x10^{15}$, $3x10^{15}$, $1x10^{16}$, $3x10^{16}$ ions/cm. No attempts were made to achieve a constant implant concentration throughout the thickness of the film (only one implant energy was used) nor to anneal the implanted films. The double layered films for the anodization bridges consisted of two sets of films: $260A^0$ of Tantalum on $100A^0$ of Titanium designated Ta/Tl) and $250A^0$ of Tantalum on $100A^0$ of Hafnium (Ta/Hf). Regions of the film to be implanted or anodized to form the S region were defined by photolithography. The completed samples varied in length from .5 μm to 3.0 μm and had widths typically 20 to 30 μm.

2.3 Material Properties

Selected determinations of the electronic and superconducting properties of various S film materials were made to provide a general picture of the material properties.

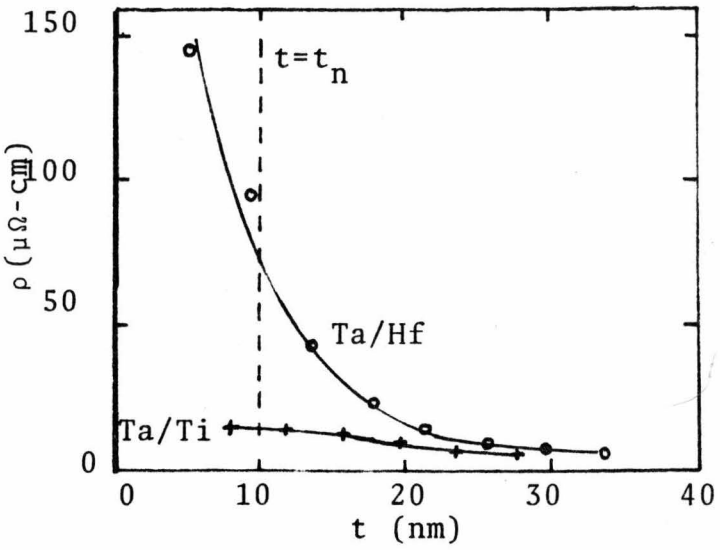
Figure 2 presents the observed dependence of superconducting transition temperature, T_c, and resistivity, ρ, on ion dosage for implanted materials and on thickness for the Ta/Ti, Ta/Hf anodized materials. For ion implanted films and bridges, the depression in transition temperature, $T_{co}-T_c$ is seen to have approximately a square-root dependence on an ion dose. The dose-dependence and magnitude are roughly the same as found by previous workers[6] and are felt to be consistent with the depression of transition temperature being primarily a result of induced damage, that is, lattice disordering. Note the large increase in resistivity with dose. For the anodized films and bridges, two bottom materials (T_i and

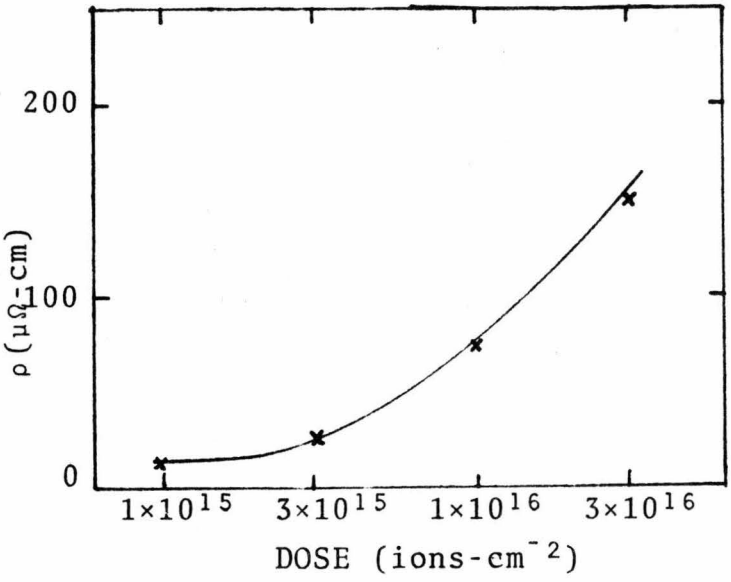
Figure 2

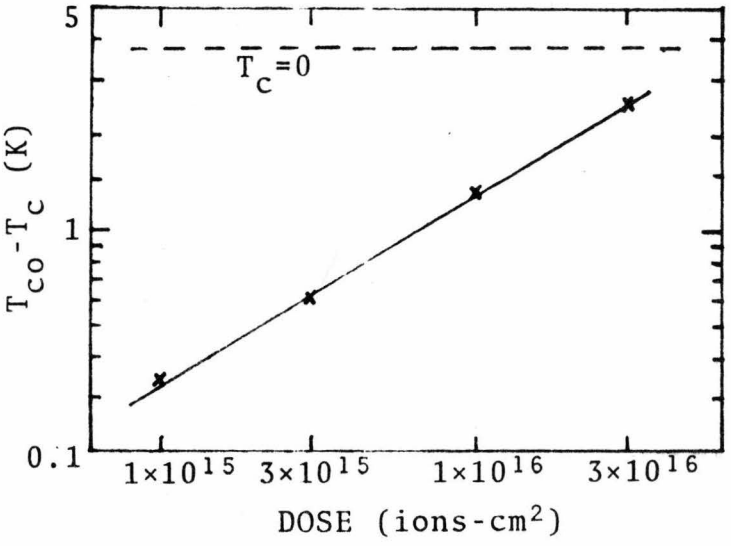
A) Resistivity of the layered Ta/Hf and Ta/Ti films as a function of film thickness, t.

B) Resistivity of the ion implant samples as a function of ion dosage.

C) Depression in the transition temperature of the ion implant samples (T_{co}-T_c) as a function of ion dosage.


150
100
50
0
ρ (μΩ-cm)
t=t_n
Ta/Hf
Ta/Ti
0
10
20
30
40
t (nm)


200
100
0
ρ (μΩ-cm)
1×10^15
3×10^15
1×10^16
3×10^16
DOSE (ions-cm^-2)


5
1
0.1
T_co-T_c (K)
T_c=0
1×10^15
3×10^15
1×10^16
3×10^16
DOSE (ions-cm^2)

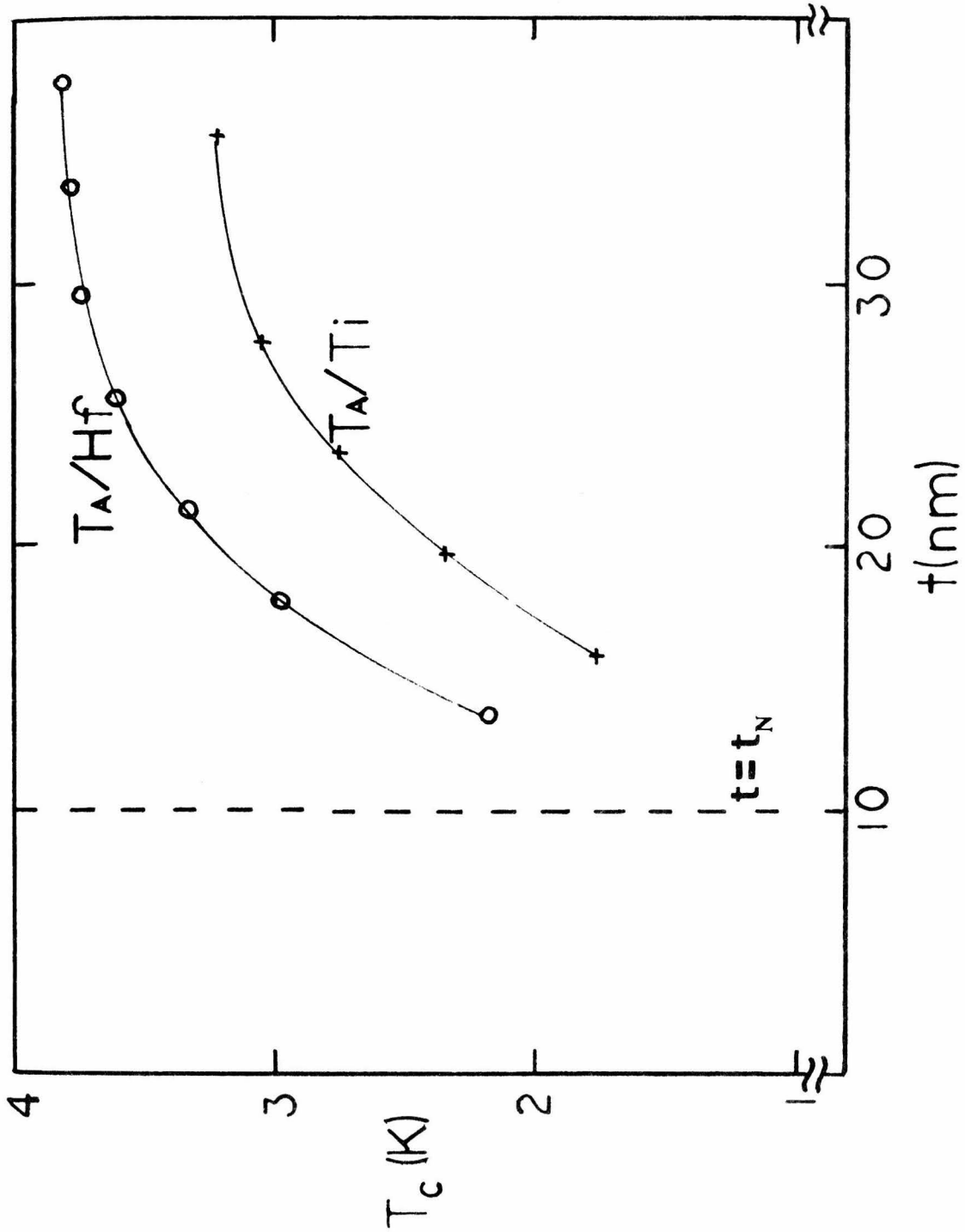
Hf) of the same thickness were used with the same top material (Ta). As is shown in figure 3, the bottom material effectiveness in depressing the transition temperature of the entire film strongly depends on its resistivity as well as the ratio of top to bottom film thickness. Bottom films of low resistivity are more effective in reducing the entire film transition temperature. Comparison of the resistivities of the ion implant and anodization films shows the resistivities of the anodization films appreciably lower. Attempts were made to determine the mean free path, 1, of the films from the resistivity data.

The usual method of determining the mean free path is to measure the sample resistivity ratio between room temperature and 4.2^0K keeping in mind that a substantial portion of the resistivity at low temperature may arise from scattering of conduction electrons at external film surfaces.[7] The critical piece of information necessary is the product $\rho 1$ (where ρ is the resistivity and 1 the mean free path), which is a constant at all temperatures and found to be

$$\frac{1}{\rho 1} = \frac{2e^2}{3} N(E_f) v_f \qquad (2.3.1)$$

$N(E_f)$ is the density of states at the Fermi level and v_f is the Fermi velocity. However, the Fermi velocities for Hafnium and Titanium are not known. This difficulty is usually overcome experimentally by measuring the resistivity ratio over several decades of film thickness and then empirically deter-

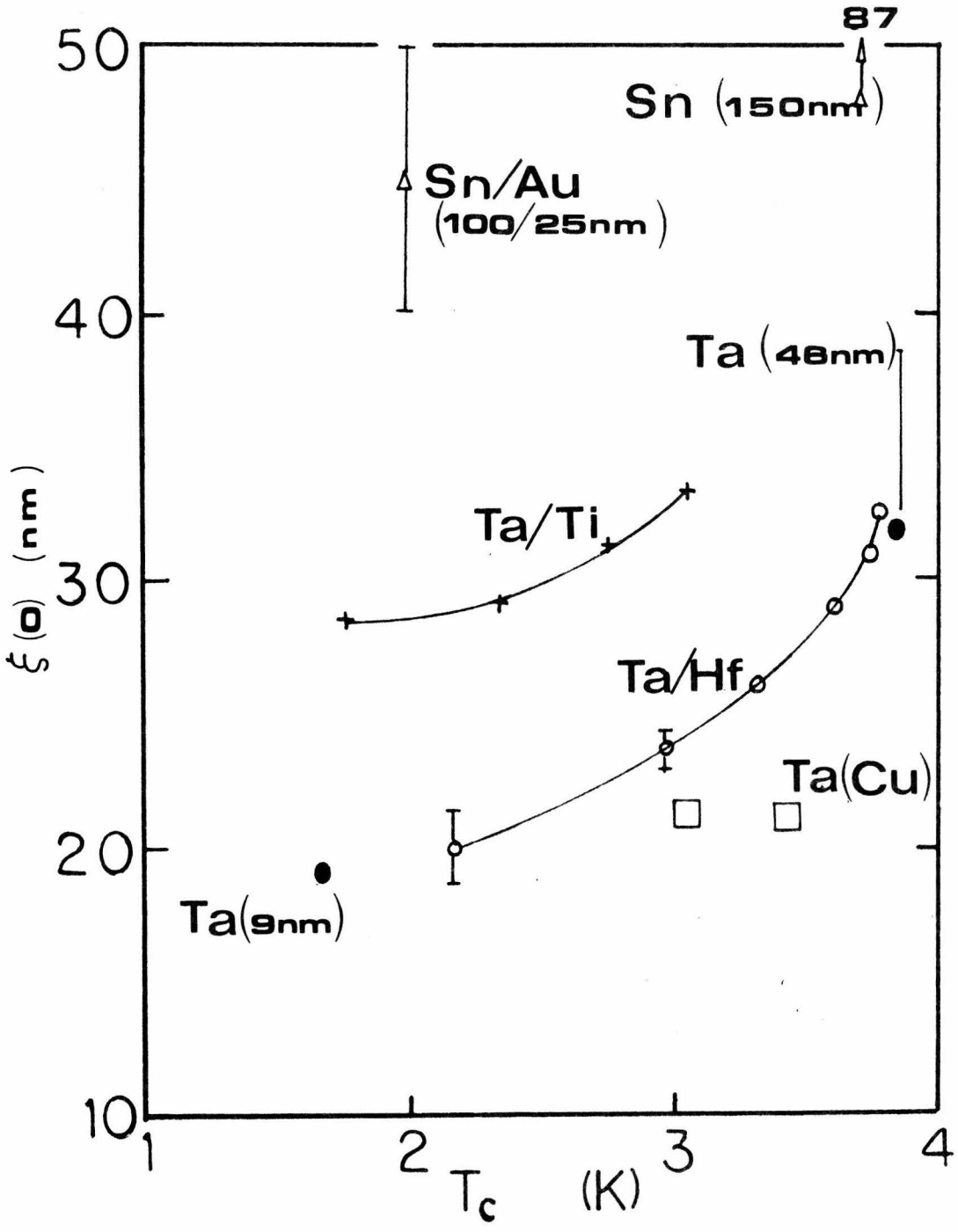
Figure 3 - Transition temperature, T_c, as a function of thickness, t, for the layered Ta/Hf and Ta/Ti film materials.


T_A/Hf
T_A/Ti
$t = t_N$
T_c (K)
t(nm)
4
3
2
1
10
20
30

mining the product ρl and the mean free path. Unfortunately, this was not attempted here. For the case of Tantalum, using tabulated values from the literature for v_f (5.1×10^7cm/sec) and $N(E_f)$ (6.9 states/R_y/atom/spin), the product ρl was calculated and a mean free path of $77A^0$ was determined for a film $380A^0$ thick. This figure is felt to be typical for Tantalum and other films (The only exception to this value is probably the ion implanted area of the Ta films, in which l is probably shorter due to lattice disordering) in this study and comparable with tests run on films of Niobium ($l \sim 50\text{-}100A^0$) of similar thickness.[8] However, it should be emphasized that no direct determination of the mean free path has been made for the Titanium, Hafnium, or layered films. Therefore, it would seem more meaningful to use the resistivity as an indication rather than a measure of the mean free path in the analysis which follows.

Figure 4 gives measurements of the zero temperature Ginzburg-Landau (GL) coherence length, $\xi(0)$ for several of the S and S_0 materials. The GL coherence length was determined by applying a magnetic field, $H_\perp$, perpendicular to a strip of the film material. $H_{c\perp}$ was defined as the field at which the resistance of the strip was one half the normal values and was measured as a function of temperature for a given strip resistance.[9] $H_{c\perp}$ is assumed to be H_{c2}, the largest magnetic field at which superconductivity can nucleate in the interior of a bulk superconductor, and is defined near T_c as

Figure 4 - Ginzburg-Landau zero temperature coherence length, $\xi(0)$ as a function of transition temperature, T_c, for various bridge and film materials.


87
Sn (150nm)
Sn/Au
(100/25nm)
Ta (46nm)
Ta/Ti
Ta/Hf
Ta(Cu)
Ta(9nm)
50
40
30
20
10
ξ(0) (nm)
1
2
3
4
Tc (K)

$$H_{c\perp} = H_{c2} = \frac{\phi}{2\pi\xi^2(0)} = \frac{\phi}{2\pi\xi(0)^2}\,\frac{(T_c - T)}{(T_c)} \qquad (2.3.2)$$

A plot of $H_{c\perp}$ vs T produced a straight line whose slope yielded the value of the GL coherence length (The value of the slope did not change when $H_{c\perp}$ was taken at 20% or 70% the normal resistance).

A comparison is now made between the results measured experimentally here and those predicted for the cases of Tantalum and Tin. Using the values of the Fermi velocity and mean free path from the last section ($v_f = 5.1 \times 10^7$ cm/sec, $l = 77A^0$) and the transition temperature for a $460A^0$ tantalum film ($T_c = 3.9^0$K), the coherence length is calculated from the relation

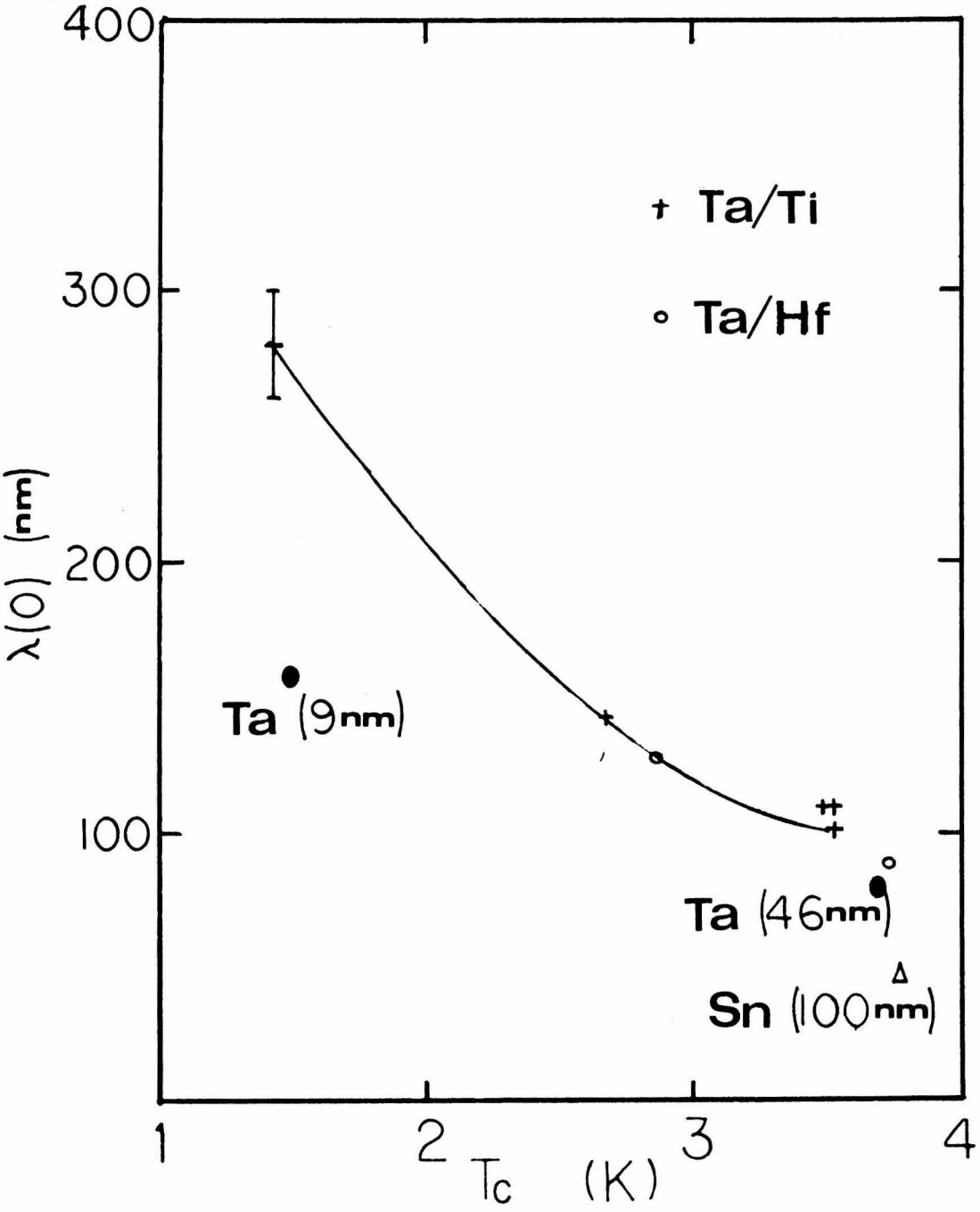
$$\xi(0) = .85 \left(\frac{.18\hbar v_f l}{k_B T_c}\right)^{\frac{1}{2}} \qquad (2.3.3)$$

The theoretical value, $\xi_{TH}(0) = 313A^0$, is found to be in good agreement with the measured value of $\xi_{exp}(0) = 320A^0$.

For the case of tin, comparison is made with a film of mean free path $500A^0$ and $\xi_0 = 2300A^0$. For this situation, the calculated value $\xi_{TH}(0) = 910A^0$ is found to be in reasonable agreement with the measured value of $\xi_{exp}(0) = 870A^0$.

Figure 5 gives measurements of the zero temperature GL penetration depth, $\lambda(0)$, for several of the S and S_o materials. To determine the penetration depth, a flat coil was fabricated by standard photolithographic techniques from a film of the

Figure 5 - Ginzburg-Landau zero temperature penetration depth $\xi\lambda(0)$ as a function of transition temperature T_c for various bridge and film materials.


400
300
200
100
λ(0) (nm)
+ Ta/Ti
∘ Ta/Hf
Ta (9nm)
Ta (46nm)
Sn (100nm)
1
2
3
4
Tc (K)

material. The induction of the coil as a function of temperature was then determined by measuring the resonant frequency of an L-C circuit formed by connecting a capacitor to the coil The inductance this measured is assumed to be the sum of a temperature-independent "classical" inductance and a kinetic inductance, L_k, defined as

$$L_k = \frac{\mu_0 L \lambda^2(T)}{wt} = \frac{\mu_0 L}{wt} \lambda^2(0) \quad \frac{T_c}{T_c - T} \tag{2.3.4}$$

where μ_o is the free space permeability and w, t and L are the width, thickness and length of the film strip.[10] The value t was taken to be the full thickness of the film. The basic assumption is that the layered films act like a homogeneous material. Plotting $1/L_k$ vs T produced a straight line whose slope yielded $\lambda(0)$.

The data for $\xi(0)$ and $\lambda(0)$ in figures 4 and 5 are given as a function of T_c, the film transition temperature, since this parameter is more relevant to the bridge experiments described here.

As before, comparison is made between experimental and calculated values of the penetration depth for tin. In the literature, typical values for the London penetration depth (Tin) are listed as $\lambda_L(0) = 350A^0$. The measured value, $\lambda(0)$, is related to the London result by the relation

$$\lambda(0) = .64\lambda_L(0) \left(\frac{\xi_0}{l}\right)^{\frac{1}{2}} \tag{2.3.5}$$

Using the same values for ξ_o and 1 from before one obtains $\lambda_{theory}(0) = 440A^0$ which compares with $\lambda_{exp}(0) = 470A^0$.

It should be pointed out that comparison of $\xi(0)$ and $\lambda(0)$ as measured here with other values in the literature is difficult at best. Not only does one have to compare coherence lengths and penetration depths, but also the mean free path information must be included in order to assess the data. Presently, very little literature is readily available with coherence length, penetration depth and mean free path for hard materials. In the case of layered films, even less information has been published, therefore, no comparison is made between layered film values obtained here and other values in the literature. Where data exist , good agreement has been found between the experimentally determined values and the theoretical values of $\xi(0)$ and $\lambda(0)$. To the author's knowledge, no other data on $\xi(0)$ and $\lambda(0)$ exist for films of construction similar to those used in this study. Therefore, the values of $\xi(0)$ and $\lambda(0)$ obtained here will be used to analyze the experimental results throughout the remainder of this thesis.

2.4 Current Distribution of a Superconducting Thin-Film and Proximity Effect Bridge.

2.4.1 Introduction

The first area to be considered is that of the current distribution in a thin, superconducting film with the work being extended to include the case of a proximity effect bridge.

The problem arises in that superconductors exhibit the property of expelling magnetic flux (Meisner Effect). The simplest possible model of the current distribution of a superconducting thin film would be to expect shielding currents to pile up where the magnetic field is largest. For the case of a thin film of dimension wide compared to the penetration depth, this would be at the film edge. (See Appendix A - Magnetic Field of a Current Carrying Thin Film). It is easily seen that a description of the current carrying capabilities of a superconducting film is complicated by this non-uniform current distribution.

For the case of a proximity effect bridge, it seems reasonable to assume that the current distribution through the bridge might be influenced by the current carrying properties of the superconducting film on both sides of the bridge structure (Figure 1). In order to determine the current distribution of a superconducting film and its influence on the current distribution of a proximity effect bridge, this study was undertaken.

2.4.2 Critical Current of a Thin Superconducting Film

The most observationally distinct property of a superconductor is zero resistance at low current. However, if the current is increased, a critical value, I_c, is reached at which the superconducting state is destroyed and a voltage appears across the sample. This behavior can easily be understood by a simple model, first proposed by London. Consider

the case where there is no current, then the energy difference between the super-normal state, Δf_{ns}, is simply $\Delta f_{ns} = H_c^2 (T)/8\pi$. As current is applied, the difference in free energy, Δf_{ns}, is reduced since the superconducting condensate has now acquired a kinetic energy of $n_s (\frac{1}{2}mv_s^2)$, where n_s is the number of superconducting pairs, m is the mass of an electron pair ($2m_e$) and v_s is current velocity. The film will remain superconducting as long as the kinetic energy of the superconducting condensate, $n_s (\frac{1}{2}mv_s^2)$ is less than the condensation energy, $H_c^2 (T)/8\pi$. When the kinetic energy of the condensate becomes equal to the condensation energy, the superconducting state is destroyed. While this description is correct if not complete (since the superconducting condensate, n_s, also adjusts itself to the current flow, this point will be considered shortly), the essential features of the critical current and destruction of the superconducting state can readily be perceived.

One means of determining the current distribution of a thin, superconducting film is to observe the critical current behavior. If the current distribution is non-uniform, with shielding currents piling up at the film edge, one would reasonably expect that the critical current density would be reached at the film edge before it is reached at the film center.[11] When the critical current density is exceeded at the film edge, the superconducting state is destroyed there and the film appears resistive. Comparison of the experimental and theoretical critical current density would be a strong indication of the current distribution in a superconducting thin film.

An adequate description of the critical current behavior of a thin film can be obtained by the simple GL formalism.[12] It is useful to go through it as a point of reference in reviewing the experimental results.

The free energy density of a thin film (thickness, $t < \xi(T)$) can be written as

$$f_s = f_n + \alpha|\psi|^2 + \frac{\beta}{2}|\psi|^4 + |\psi|^2 \frac{mv_s^2}{2} + \frac{\hbar^2}{2m}|\nabla\psi|^2 + \frac{h^2}{8\pi} \qquad (2.4.1)$$

The following simplifications will be made. First that the current density across the film thickness and width is uniform. Secondly, ψ is assumed to have a constant value everywhere, that is there is no $\nabla\psi$ terms for the case under consideration. Lastly, since the total energy due to the field term $h^2/8\pi$ is less than the kinetic energy of the current by a factor of the order of the ratio of the cross sectional area of the conductor to λ^2, it can be always neglected in a sufficiently thin conductor. Therefore, the free energy expression simplifies to

$$f_s = f_n + \alpha|\psi|^2 + \frac{\beta}{2}|\psi|^4 + |\psi|^2 \tfrac{1}{2}mv_s^2 \qquad (2.4.2)$$

Using 1.2.8, $|\psi_\infty|^2 = -\alpha/\beta$, the free energy can be written as

$$f_s = f_n + \alpha|\psi|^2 \left(1 - \frac{|\psi|^2}{2|\psi_\infty|^2}\right) + |\psi|^2 \tfrac{1}{2}mv_s \qquad (2.4.3)$$

and after minimizing f with respect to $|\psi|^2$ ($\frac{\partial f}{\partial \psi^2} = 0$), one

finds that the optimum value of $|\psi|^2$ is

$$|\psi|^2 = |\psi_\infty|^2 \left(1 - \tfrac{1}{2} \frac{mv_s^2}{|\alpha|}\right) \tag{2.4.4}$$

Substituting $|\psi|^2$ into the expression for the current, 1.2.6b, one finds that the corresponding current is

$$J_s = 2e\psi_\infty^2 \left(1 - \tfrac{1}{2} \frac{mv_s^2}{|\alpha|}\right) v_s \tag{2.4.5}$$

J_s has a maximum value when $\partial J_s / \partial v = 0$, that is when

$$v_s = v_c = \sqrt{\frac{2|\alpha|}{3m}} \tag{2.4.6}$$

Therefore, the expression for a maximum (critical) current simplifies to

$$J_s = 2e\psi_\infty^2 \frac{2}{3} \left(\frac{2}{3} \frac{|\alpha|}{m}\right)^{\frac{1}{2}} \tag{2.4.7}$$

Noting that $\psi_\infty^2 \propto 1/\lambda^2$ and $|\alpha| \propto 1/\xi$, the final expression for the critical current is written near T_c as

$$J_c = \frac{c\phi_0}{12\sqrt{3}\pi^2 \xi(0)\lambda^2(0)} \left(\frac{T_c - T}{T_c}\right)^{3/2} \tag{2.4.8}$$

where the temperature dependence of ξ and λ has explicitly been expressed. It would seem that the critical current density of a thin film should be dependent only on $\xi(0)$ and $\lambda(0)$, and vary as $\Delta T^{3/2}$.

Initially, experimental observation of this result was somewhat difficult.[11] The key assumption is that the current density in the film sample is uniform, which, as has already been mentioned, is not the situation for a film wide compared to the penetration depth. This difficulty can be overcome by controlling the magnetic field distribution of the current carrying film by shielding it with another superconducting film. In this situation, the superconducting shield forces the field lines to be parallel to the film, which in turn requires a uniform current density in the film. Experiments by Newhouse and Bremer on type I Sn strips using Pb superconducting shield planes show agreement with the GL model, that is, J_c varies as $\Delta T^{3/2}$. Without shield planes, their measurements show that J_c is at least a factor of 3 to 4 times smaller than J_{GL}. Measurements of J_c vs T made by Skocpol[13] on type I Sn strips as a function of film width indicates the temperature behavior varies from $\Delta T^{3/2}$ on the narrowest (1μm) samples to a temperature dependence of ΔT on the widest (8 μm).

2.4.2 Experimental Results

Three experiments were run to examine the current distribution behavior of a type II thin film as a function of strip width. The first experiment compared the critical current vs temperature behavior of a thin film with and without a superconducting shield plane. As already pointed out, the effect of a shield plane should force the field lines to be parallel to the film, which in turn requires the current density in the

film to be uniform. The second experiment involved monitoring the critical current vs temperature behavior of a superconducting strip as a function of the width of the strip. If the current density is non uniform, the measured critical current density, j_c, should be different for the same film at different widths. The third experiment was an indirect determination of the current distribution of a strip below the critical current and was inferred from the penetration depth measurements.

2.4.2 A Superconducting Shield Experiment

The superconducting strips employed in the first two experiments were anodized from 276A^0 of Nb on 272A^0 of Tantalum on a sapphire substrate. The top layer of Nb was completely anodized for two reasons - first, the unanodized film had a transition temperature in excess of 4.2^{0}K, which is difficult to reach without pressurizing the glass dewar, and second, the anodized Nb layer formed an insulating oxide Nb_2O_5, approximately 750^{0}A thick. This allowed the superconducting shield plane to be evaporated directly over the film strip without shorting out the two main films.

Two samples were run in this test. The first consists of a strip 16 μm wide and 30 μm long, with a transition temperature, T_c, of 3.9^{0}K. Critical current vs temperature tests were run with no shield plane, a 1000A^0 thick Pb shield plane and a 1 μm thick Pb shield plane and are shown in Figure 6. The results indicate no difference between all three cases.

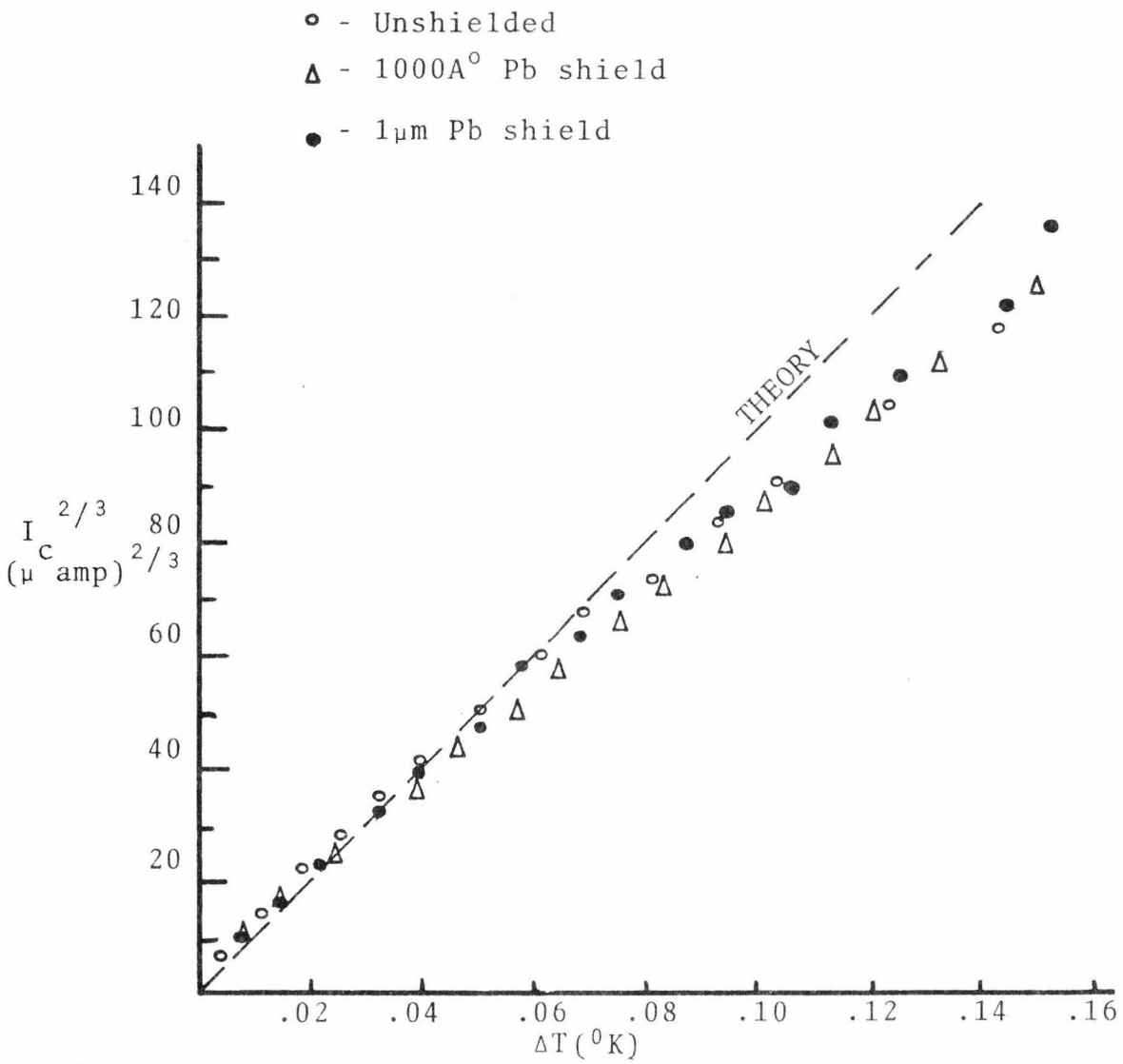


Figure 6 - $I_c^{2/3}$ vs ΔT - Strip film samples with and without Pb shield planes.

The critical current is proportional to $\Delta T^{3/2}$, with no ΔT dependence observed as contrasted to Skocpol's findings for tin strips. While no measurement of $\xi(0)$ and $\lambda(0)$ were performed on this particular film, reasonable estimates of the coherence length and penetration depths for the Tantalum film would be $\xi(0)=300A^0$ and $\lambda(0)=1000A^0$. A plot of the theoretical I_{GL} vs T using these values is also shown in Figure 6. Good agreement is seen between theory and experiment. Over the temperature range studied the penetration depth varies from ∞ at $T = T_c$ to $\lambda = 2920A^0$ at the lowest temperature observed. For any temperature below $T = 3.87^0K$, the film should be wider than 2λ. Yet, in this temperature range a uniform current distribution is indicated from the experimental results.

One possible explanation for this result is that the shield plane is not effectively shielding the film from the magnetic flux. For the superconducting plane to effectively shield the film from the magnetic flux, H_c of the shield material (H_{c1} if shield were type II) must be greater than the magnetic field generated at the edge of the sample. A calculation of the magnetic field as a function of film geometry (width and thickness) is given in Appendix A. Lead, the shield material, has a transition temperature of 7.2^0K and H_c of 803 gauss. The temperature dependence of H_c[14] in a thin film can be expressed as

$$H_c(T) = H_{co}\left(\frac{T_c - T}{T_c}\right) \qquad (2.4.9)$$

In the temperature region of interest $H_c(T)$ of the Pb shield

material is exceeded only when $I_c > 2500$ μ amp. No difference was observed above or below this current.

These results were rechecked on other samples, but no difference in the behavior described above was ever observed in any of these tests. The temperature dependence of the critical current was seen to vary as $\Delta T^{3/2}$ and the current density prefactor adequately described by 2.4.8. Therefore, one must conclude that the current is uniformly distributed across the width of the film - somewhat in contradiction to the electrodynamics which indicates that the current should tend to pile up at the film edges and the experimental work of Newhouse, Bremer, and Skocpol. This discrepancy will be considered and discussed in detail later.

2.4.2b Critical Current Density

The second experiment, to monitor the film critical current vs temperature as a function of film strip width, is just an extension of the first experiment. In this case a superconducting strip is successively narrowed, with the critical current density, J_c, vs temperature, T, being measured at each film width. Figure 7 shows J_c vs T for two widths, 16 μm and 6 μm, of the same film. These results are typical of those taken on other film strips. As in the first part of the experiment, the experimental results indicate a uniform current across the width of the film strip.

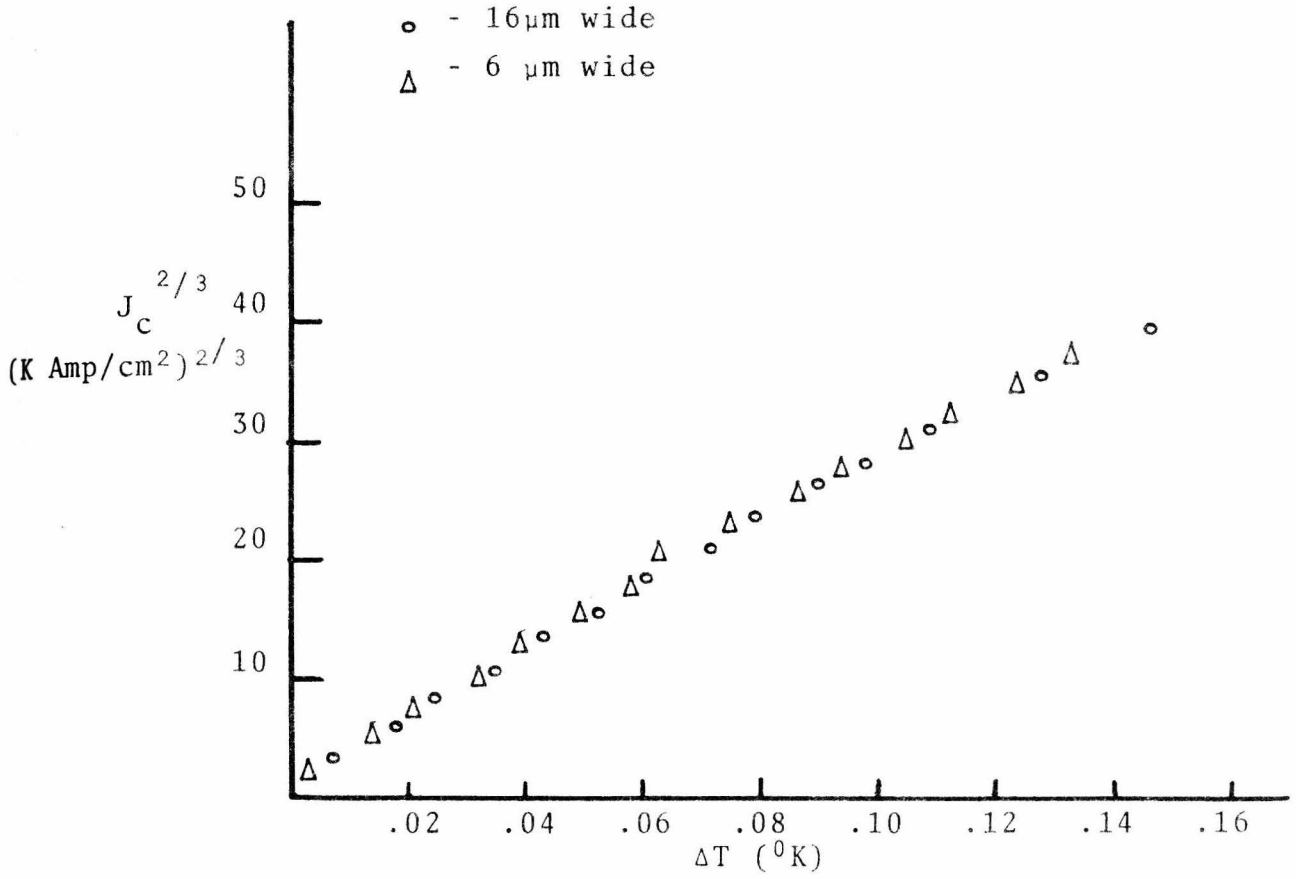


Figure 7 - $J_c^{2/3}$ vs T - A strip film for two different film widths - 16μm and 6μm.

2.4.2c Penetration Depth Measurement

Figure 8 shows a typical plot taken in the measurement of the penetration depth of the thin film samples vs temperature, using a flat coil 30 μm wide. As noted in Section 2.3, the penetration depth is related to L_k, the kinetic inductance by relation 2.3.4. This relation assumes a uniform current distribution across the film width. Consider for the moment that the current density is non-uniform and runs along a width of approximately λ on each edge of the film. The effective width of the film would then be 2λ which is now temperature dependent and the kinetic inductance would then be given as

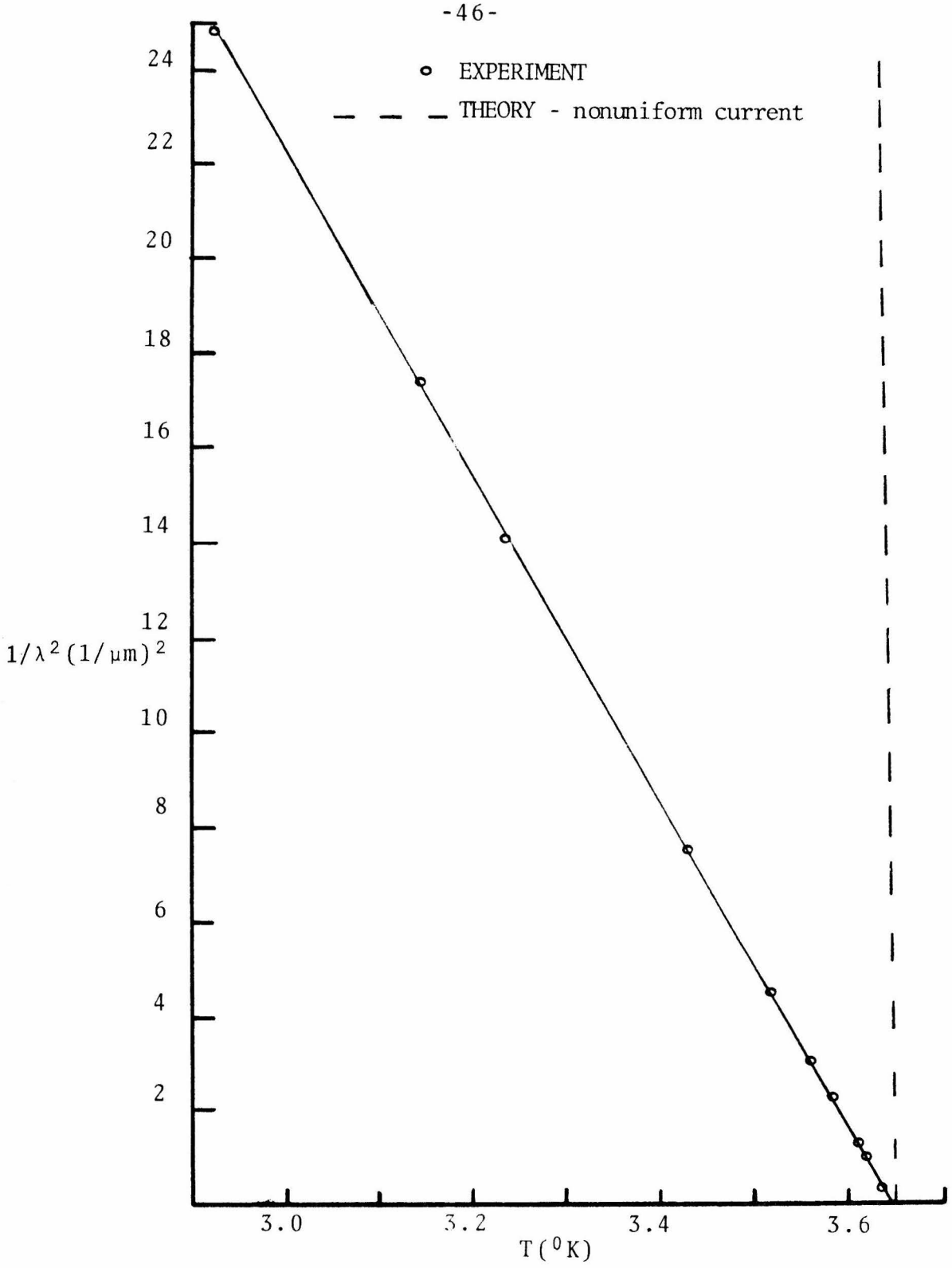
$$L_K = \frac{\mu L}{2t}\lambda(T) = \frac{\mu L}{2t}\left(\frac{T_c}{T_c - T}\right)^{\frac{1}{2}} \qquad (2.4.10)$$

Note, this new expression would lead to a much larger value of the kinetic inductance than is measured. The deviation is shown by the dotted lines in Figure 8. Certainly this is not the situation observed here. As before, the only explanation to the linear behavior of $1/\lambda^2$ vs T observed that of the current being uniform across the width of the film strip.

2.4.3 Discussion of Experimental Results

At first glance, it would seem that some discrepancy exists between these experiments and those of previous investigators. Newhouse and Bremer showed that the critical current behavior proportional to $\Delta T^{3/2}$ was only observed for the case where a superconducting shield plane was employed. No corres-

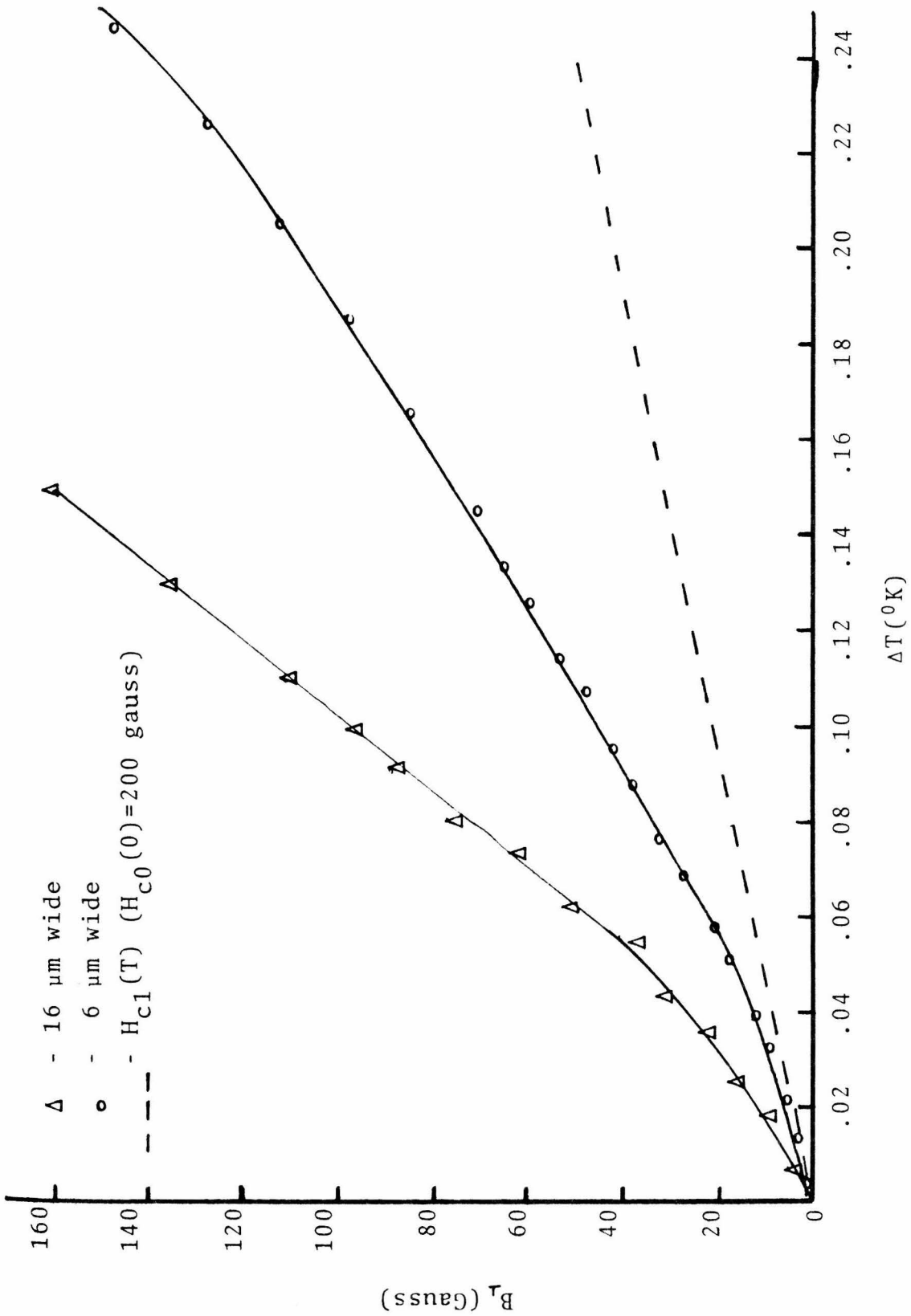
Figure 8 - $1/\lambda^2$ vs T as determined by measuring the kinetic inductance of a superconducting flat coil. Note that if the effective width of the film were to vary as a function of temperature the deviation would vary as shown by dotted line.


EXPERIMENT
THEORY - nonuniform current
24
22
20
18
16
14
12
10
8
6
4
2
$1/\lambda^2 (1/\mu m)^2$
3.0
3.2
3.4
3.6
T (^{0}K)

ponding observation is seen here. Skocpol showed that the film width strongly affected the critical current behavior. Again, no corresponding observation is seen here. One difference between experiments is that previous work has been conducted on tin, a type I material while these findings have been obtained on a type II superconductor, that is, tantalum.

One possible explanation is as follows. In the case of a type I tin film, the current distribution is non uniform. As the current increase through the film, the magnetic field at the film edge, $B_{\perp}$, increases until $B_{\perp} = H_c(T)$, the thermodynamic critical field, the superconducting state at the film edge is destroyed and a resistance is developed across the sample. Experimentally this is recorded as the critical current. For the case of a type II material, when the magnetic field at the film edge reaches $B_{\perp} = H_{c1}(T)$, a quantum of flux enters the film but the superconducting state is not destroyed, only altered slightly. It is suggested that as the current through the film is increased, the magnetic flux become distributed in such a way that the current is spread uniformly across the entire film width (it should be noted that the current distribution on a macroscopic scale appears to be uniform, on a microscopic scale it is anything but uniform). A plot of the magnetic field generated at the film edge, $B_{\perp}$, by a current equal to the critical current vs temperature and $H_{c1}(T)$ vs temperature is shown in figure 9. $H_{c1}(0)$ is calculated using a penetration depth of $\lambda(0) = 1000A^0$. In all cases, $B_{\perp}$ at the film edge is greater than $H_{c1}(T)$. This explanation has

Figure 9 - $B_{\perp}$, the magnetic field at the edge of a thin film calculated using the critical current, I_c, of the film vs temperature, T. Also shown is H_{c1} vs T with $H_{c1}(0) = 200$ gauss. As can be seen, $B_{\perp}$ is always greater than $H_{c1}(T)$ for all temperatures.


Δ - 16 μm wide
o - 6 μm wide
- - - $H_{c1}(T)$ ($H_{c0}(0)$=200 gauss)
$B_\perp$ (Gauss)
0
20
40
60
80
100
120
140
160
.02
.04
.06
.08
.10
.12
.14
.16
.18
.20
.22
.24
ΔT(°K)

two consequences - first it accounts for the uniform current distribution in these experiments and second it explains the apparent discrepancy in the magnitude and temperature dependence of the critical current between this and other shield plane experiments. The agreement of the tests with and without a shield plane (that is, with and without flux penetrating the current carrying test film strip) suggests that for the thin films employed in these studies, the critical current is adequately described by the GL theory.

2.4.4 Current Distribution of a Proximity Effect Bridge

The last and most important area to be considered is the current distribution through a proximity effect bridge. It would seem a simple step to generalize that since the current distribution to and from the bridge region is uniform (on a macroscopic scale), then the current distribution of the bridge itself is uniform. However, as will be mentioned here and discussed in more detail in the next section, a proximity effect bridge is not necessarily superconducting. Its supercurrent carrying capabilities above and below the bridge transition temperature, T_N are entirely different. (The bridge transition temperature, T_N is defined as the temperature at which the S material in the bridge center becomes superconducting if it were isolated and not joined to the adjacent superconducting sections - see Figure 1). In order to determine whether the current distribution is uniform or affected by the main superconducting films on either side of the bridge region,

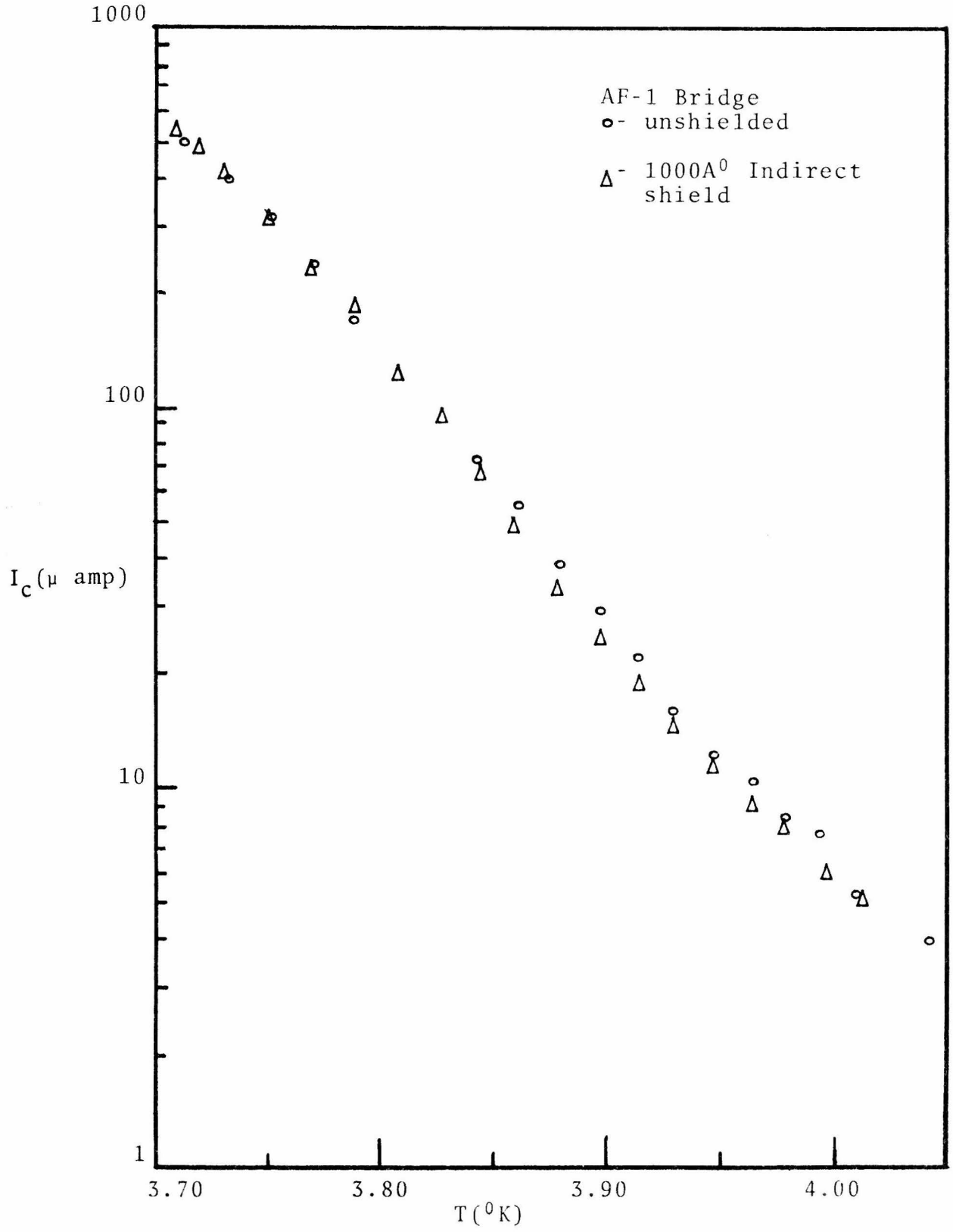
the superconducting shield experiments were repeated for the case of shielded and unshielded proximity effect bridges.

In this part of the study, a type II shield material, Indalloy II, was used. It consisted of 95% Pb and 5% Indium with an $H_{c1}(0)$ = 170 gauss and T_c = 6.5 ^{0}K. Critical current vs temperature tests were run on an unshielded, 1000A^0 thick Indalloy and 1 μm thick Indalloy shields. In order to explain any possible discrepancies, the bridge data shown here were taken on the same Nb/TA film as the previous thin film tests. These results, though, are typical of results run on other bridges and films. The test results are shown in figure 10. One must conclude that the current distribution is uniform (on a macroscopic scale) across the width of the bridge.

As an added check to the effectiveness of the superconducting plane to shield the bridge from magnetic fields, an external magnetic field of $B_\perp \cong 5$ gauss was placed on the sample with a 1 μm Indalloy shield. No effect was observed on the critical current behavior, that is, the critical current of the proximity effect bridge did not show the modulation characteristic of a quantum interference device. (Behavior of the critical current as a function of magnetic field will be discussed in detail in a later section). Modulation was observed in the unshielded test.

As a conclusion to this section, it is felt that this series of tests indicate that the current distribution of a thin superconducting film and a proximity effect bridge is uniform (at least when considered on a macroscopic scale).

Figure 10 - I_c vs T - AF-1 Bridge with and without 1000 A^0 Indalloy Shield Plane


1000
100
10
1
AF-1 Bridge
o- unshielded
Δ- 1000A⁰ Indirect shield
I_C(μ amp)
3.70
3.80
3.90
4.00
T(⁰K)

All further descriptions of the behavior of proximity effect bridges in this thesis will be 1 dimensional, that is, along the current direction, unless otherwise specified.

2.5 Critical Current of a Proximity Effect Bridge

2.5.1 Introduction

The next area to be considered will be the case of two weakly coupled superconductors. The following operational definition will be employed in the subsequent discussion: Two superconductors are weakly coupled if the coupling link exhibits quantum interference effects. Historically, this was first achieved by means of a super-insulator - super (SIS) tunneling junction.[15] In the case of an SIS tunnel junction, it was observed that if a small enough current was impressed across the sample, no voltage was measured until a critical value, I_c, was reached. This critical value, I_c, was defined as the critical current, however, it should be pointed out that I_c is not related to the destruction of the superconducting state as contrasted to the case of a superconducting strip. For a Josephson junction (or as will be shown, any weakly coupled superconductors) the magnitude critical current is a measure of the degree of coupling between the two superconducting systems. As an example of this point, consider the following simplified model of a Josephson junction consisting of two identical superconductors seperated by a thin oxide.[16] A Schroedinger equation for the coupled superconductors may be

written as

$$i\hbar \frac{\partial}{\partial t} \begin{pmatrix} \psi_1 \\ \psi_2 \end{pmatrix} = \begin{pmatrix} \mu_1 & k \\ k & \mu_2 \end{pmatrix} \begin{pmatrix} \psi_1 \\ \psi_2 \end{pmatrix} \tag{2.5.1}$$

where ψ_1 and ψ_2 are the macroscopic wavefunctions in the superconductors, k is the coupling between them (and is real) and μ_1 and μ_2 are the electrochemical potential (per electron) for pairs in the two superconductors. Noting that $\psi_1 = \psi_1 e^{i\phi_1}$, and $\psi_2 = \psi_2 {}^{i\phi_2}$, one obtains

$$\dot{\phi} = \frac{\partial}{\partial t} (\phi_2 - \phi_1) = \frac{2(\mu_2 - \mu_1)}{\hbar} \tag{2.5.2}$$

and

$$\dot{\psi} = -k\sqrt{\psi_1 \psi_2} \sin \Delta\phi \tag{2.5.3}$$

where $\dot{\psi}$ is the rate of pair density loss that would occur if an external source did not supply more electrons. The supercurrent flowing through a current biased junction is

$$J_s = 2e \; k\sqrt{\psi_1 \psi_2} \sin \Delta\phi = J_c \sin \Delta\phi \tag{2.5.4}$$

where the critical current density is defined as $J_c = 2e\, k\sqrt{\psi_1 \psi_2}$. From this simple analysis, one can see that the critical current density, J_c, depends directly on the coupling constant, k, and that a measure of J_c is also a measure of k.

The physical situation, however, is not so straightfor-

ward for the case of a proximity effect bridge. The bridges in this study can be adequately described as two identical superconductors of transition temperature, T_s, coupled by a "weakened" superconducting strip of transition temperature, T_n, such that $T_n < T_s$. The transition temperature, T_n, of the bridge region itself is defined as the intrinsic transition temperature of the coupling (bridge) region if it were isolated and not joined to the stronger superconducting sections. This temperature is not a measurable parameter in other types of weak links. The critical current behavior above and below T_n is usually quite different. For the temperature region above the bridge transition temperature, T_n, the critical current is observed to vary approximately exponentially as a function of temperature. For the temperature region below the bridge transition temperature, T_n, the critical current density is observed to vary proportionally to $(T_n - T)^{3/2}$.[17] The different temperature dependence of the bridge critical current can be readily explained if one considers that above the bridge transition temperature, T_n, the bridge should be described as two superconductors coupled by a strip of normal metal. Below the transition temperature of the coupling region, the bridge should be modeled as two superconductors coupled by a superconducting strip. Since the critical current behavior above and below T_n is observed to be different and is probably governed by different physical situations, they will be considered separately in the following discussions.

It should be pointed out here that a study of the critical current behavior of a proximity effect bridge allows one the unique opportunity to observe the coupling between two systems which varies from weak to strong, that is, the bridge properties are changing from those of a weak link to those of a type II superconductor.

The difference in the strength of coupling is evidenced in that the largest portion of quantum interference effects observed (B field modulation, rf response) were in the critical current region $T > T_n$. As T decreased below T_n, the relative magnitude of quantum interference effects was always seen to diminish. Therefore, the emphasis in this work (both here and in subsequent sections) will be in the temperature region $T > T_n$.

2.5.2 Critical Current vs Temperature of a Proximity Effect Bridge: $T > T_n$

The critical current vs temperature dependence of Nb/TA proximity effect bridges has previously been considered by Palmer.[17] This study was incomplete in that, except for bridge length, no attempt was made to correlate the critical current behavior to the bridge and film material characteristics (they were not measured). The study described here investigates the critical current behavior of proximity effect bridges as a function of bridge length, film transition temperature, material and bridge fabrication (ion implant and anodized).

The bridge and film properties, including bridge length, width, film transition temperature, bridge transition tempera-

ture, and bridge/film coherence lengths, penetration depths and resistivities are listed in Tables 1 through 4 for the samples examined. The bridge length and width were measured optically. The film coherence lengths and penetration depths were obtained from the measurements in Section 2.3 on the material properties of the films while the bridge coherence length and penetration depth were taken as those of a film with the same transition temperature as that of the bridge. The same method was employed for the resistivity measurements. The bridge transition temperature was obtained by observing the temperature region where the critical current density varied as $(T_n - T)^{3/2}$ In this temperature region, the strong superconducting films adjacent to the bridge should not seriously affect the superconducting behavior of the bridge. The bridge transition temperature, T_n, is obtained by plotting $I_c(T)$ vs temperature (Figure II), and then extrapolating the linear behavior of the critical current to zero critical current. The intercept at zero current is the bridge transition temperature, T_n. It has been shown by Palmer that the value of the transition temperature agrees experimentally with large regions of superconducting film weakened to the same thickness as the bridge region. Such a large region does not have its transition temperature changed by its strong superconducting surroundings. As an added check, comparison of bridges with different length constructed nearly identically is shown in Figure [11] .

These four bridges vary in length from .5 to 3.0 μ m, and were fabricated by implanting Ta with 10^{15} ions/cm Cu. The bridge transition temperature for all samples is $3.53^0K \pm .015^0K$

TABLE 1

Film Characteristics

Material	Thickness	ρ	$\xi(0)$	$\lambda(0)$	T_F	θ_s
Tant	$460A^0$	10 μohm-cm	$320A^0$	$800A^0$	3.86^0K	240^0K

Bridge Characteristics

Bridge	t	L_0	w	ρ	$\xi_n(0)$	$\lambda_n(0)$	T_n	θ_n
BW 5 d	$460A^0$	.5 μm	20 μm	10 μ ohm-cm	$210A^0$	$900A^0$	3.515^0K	240^0K
BW 5 f	$460A^0$	.6 μm	20 μm	10 μ ohm-cm	$210A^0$	$900A^0$	3.544^0K	240^0K
BW 5 g	$460A^0$	1.0 μm	20 μm	10 μ ohm-cm	$210A^0$	$900A^0$	3.515^0K	240^0K
BW 5 I	$460A^0$	3.0 μm	20 μm	10 μ ohm-cm	$210A^0$	$900A^0$	3.538^0K	240^0K

TABLE 2

Film Characteristics

Material	Thickness	ρ	ξ(0)	λ(0)	T_F	θ_s
Ta/Hf	$250A^0/100A^0$	6 μohm-cm	330	880	3.77^0K	243^0K

Bridge Characteristics

Bridge	t	L_0	w	ρ	$\xi_n(0)$	$\lambda_n(0)$	T_n	θ_s
BU-13	$220A^0$	.5 μ	26 μ	14 μohm-cm	$255A^0$	$1080A^0$	3.34^0K	245^0K
BU-24	$216A^0$	1.1 μ	28 μ	14 μohm-cm	$255A^0$	$1080A^0$	3.336^0K	245^0K
BU-11	$208A^0$	1.9 μ	32 μ	14 μohm-cm	$255A^0$	$1080A^0$	3.265^0K	245^0K

TABLE 3

Film Characteristics

Material	Thickness	ρ	$\xi(0)$	$\lambda(0)$	T_F	θ_s
Ta/Ti	$260A^0/100A^0$	6 μohm-cm	$340A^0$	1050	323^0K	290^0K

Bridge Characteristics

Bridge	t	L_o	w	ρ	$\xi_n(0)$	$\lambda_n(0)$	T_n	θ_n
BS-14	$235A^0$	.5μm	25μm	7.5 μohm-cm	$315A^0$	$1360A^0$	2.765^0K	318^0K
BS-23	$226A^0$	1.0μm	19μm	8.0 μohm-cm	$310A^0$	$1400A^0$	2.655^0K	320^0K
BS-7	$226A^0$	2.0μm	29μm	8.0 μohm-cm	$310A^0$	$1400A^0$	2.659^0K	320^0K

TABLE 4

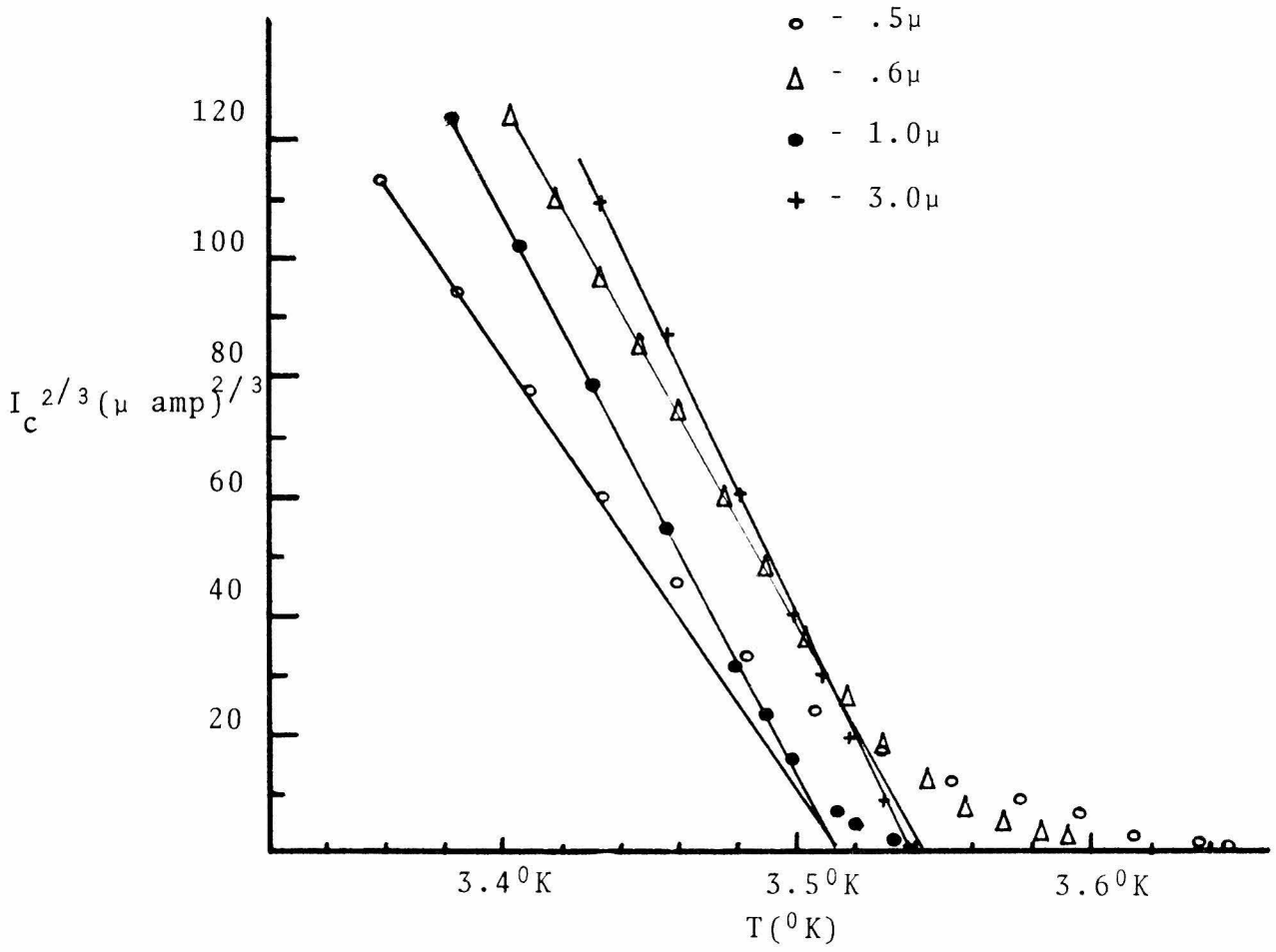
Film Characteristics

Material	Thickness	ρ	$\xi(0)$	$\lambda(0)$	T_F	θ_s
Ta/Ti	$260A^0/100A^0$	6 μohm-cm	$340A^0$	$1050A^0$	3.23^0K	290^0K

Bridge Characteristics

Bridge	t	L_0	w	ρ	$\xi_n(0)$	$\lambda_n(0)$	T_n	θ_n
BS-24	$180A^0$	.5μm	26 μm	10 μ ohm-cm	$290A^0$	$1960A^0$	2.100^0K	331^0K
BS-29	$150A^0$	1.0μm	25 μm	13 μ ohm-cm	$280A^0$	$2600A^0$	1.576^0K	360^0K
BS-11	$142A^0$	1.9μm	21 μm	14 μ ohm-cm	$280A^0$	$2700A^0$	1.483^0K	363^0K

Figure 11 - $I_c^{2/3}$ vs temperature for a set of ion implant bridges of different lengths. The bridge transition temperature are all seen to be $3.53^0K \pm .015^0K$.


o - .5μ
Δ - .6μ
● - 1.0μ
+ - 3.0μ
120
100
80
60
40
20
$I_c^{2/3}$ (μ amp)$^{2/3}$
3.4°K
3.5°K
3.6°K
T(°K)

which is felt to be within experimental error. The deviation is not felt to be a function of bridge length, L.

The general features of the bridge critical current density versus temperature are shown in Figures 12 through 15. The bridges examined in each figure consist of a set. Each set consists of bridges of differing length and approximately the same transition temperature, T_n. Four sets were considered in this study. Set 1 consists of four bridges implanted with 10^{15} ions/cm^2 of Cu into a Tantalum film. Set 2 consists of three anodized bridges on a Tantalum/Hafnium film with the bridge transition temperature approximately .5^{0}K below the main film transition temperature, T_s. Sets 3 and 4 consist of three anodized bridges each on a Tantalum/Titanium film. The bridge transition temperatures for sets 3 and 4 are approximately .5^{0}K and 1.2^{0}K, respectively, below the film transition temperature.

The following general conclusions can be drawn by examination of the experimental results in Figures 12 through 15.

1) Except for the longest bridges examined (in this case between 2.0 and 3.0 μm), the critical current density, j_c, is non zero above T_n.

2) Shorter bridges are seen to have larger critical current densities than longer bridges in the temperature regime $T>T_n$ within the same set. The critical current density above the bridge transition temperature, T_n, is observed to vary roughly as $j_c \propto \exp(-k(T-T_n)/T_n)$ for bridges of intermediate length (.6 to 1.1 μm) and even more rapidly for the shortest (.5μm) bridges.

Figure 12 - Critical Current Density vs Temperature for a set of four bridges. This set consists of four bridges implanted with 10^{15} ions/cm^2 of Cu into a Tantalum film.

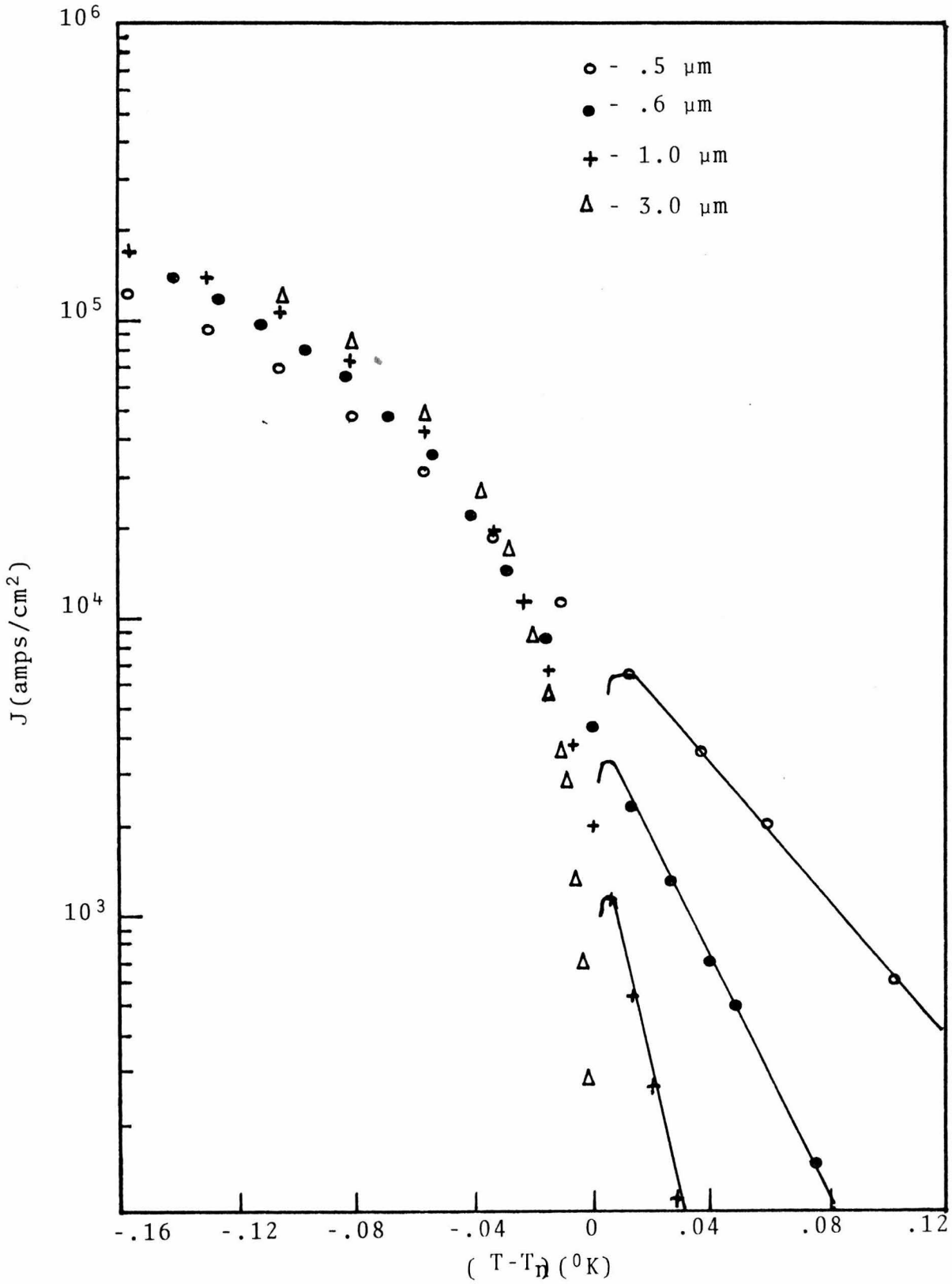

10^6
10^5
10^4
10^3
J (amps/cm^2)
o - .5 μm
● - .6 μm
+ - 1.0 μm
Δ - 3.0 μm
-.16
-.12
-.08
-.04
0
.04
.08
.12
(T-T_n) (°K)

Figure 13 - Critical Current Density vs Temperature for a set of three anodized bridges on a Tantalum/Hafnium film. The bridge transition temperature is ~.5^{0}K below the film transition temperature.

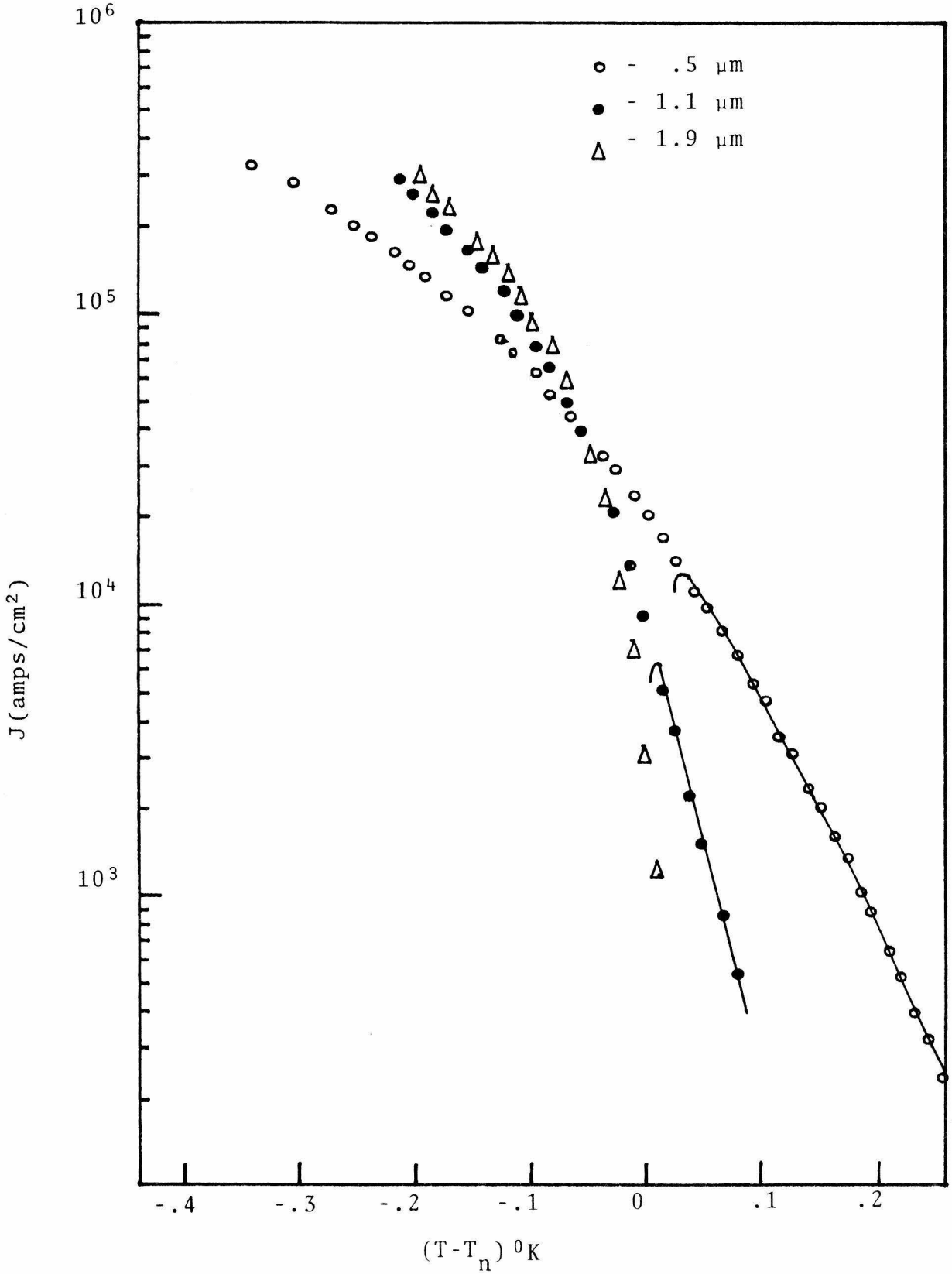

10^6
10^5
10^4
10^3
J(amps/cm^2)
o - .5 μm
● - 1.1 μm
Δ - 1.9 μm
-.4
-.3
-.2
-.1
0
.1
.2
(T-T_n) ^0K

Figure 14 - Critical Current Density vs Temperature for a set of three anodized bridges on a Tantalum/Titanium film. The bridge transition temperature is approximately $.5^{0}K$ below the film transition temperature.

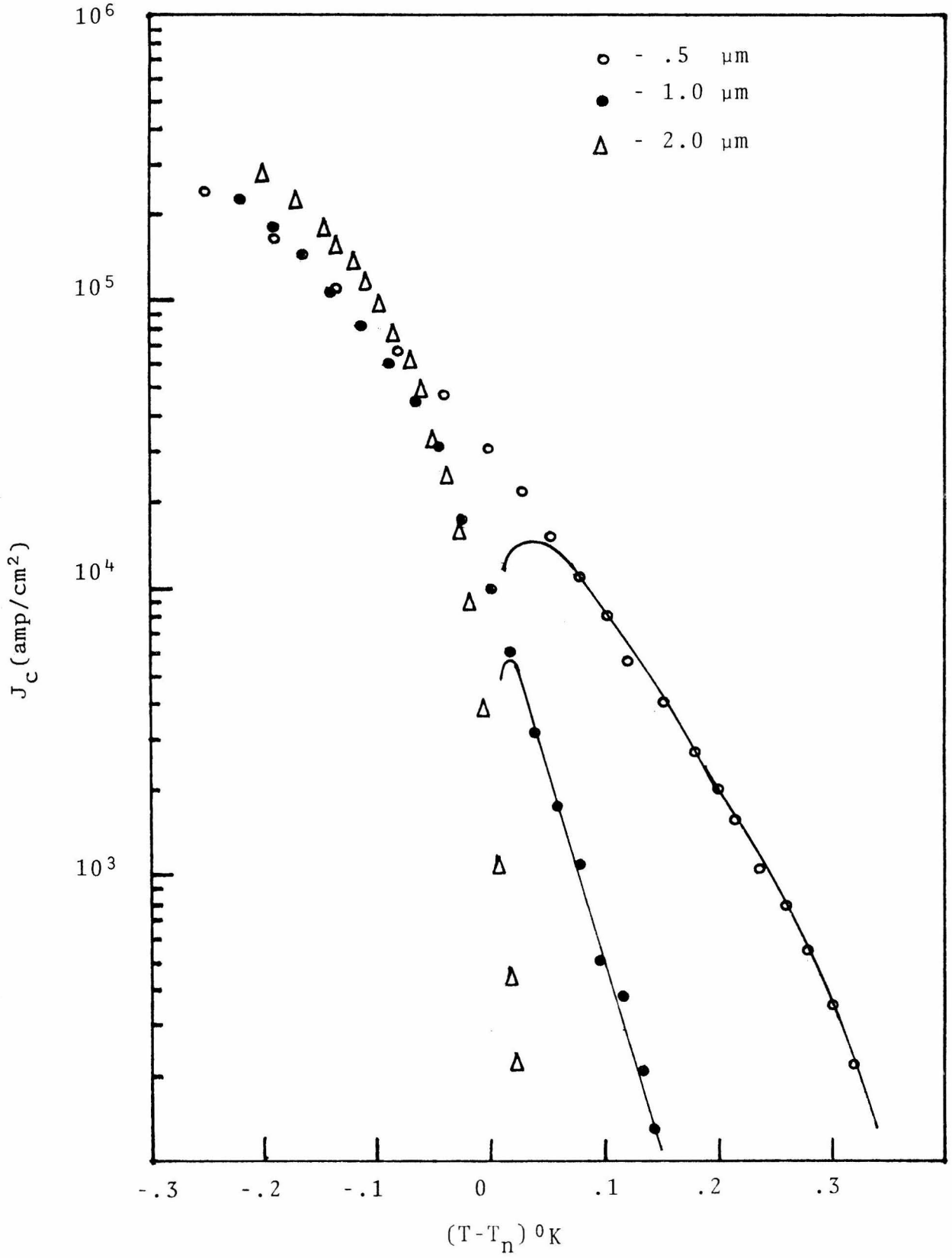
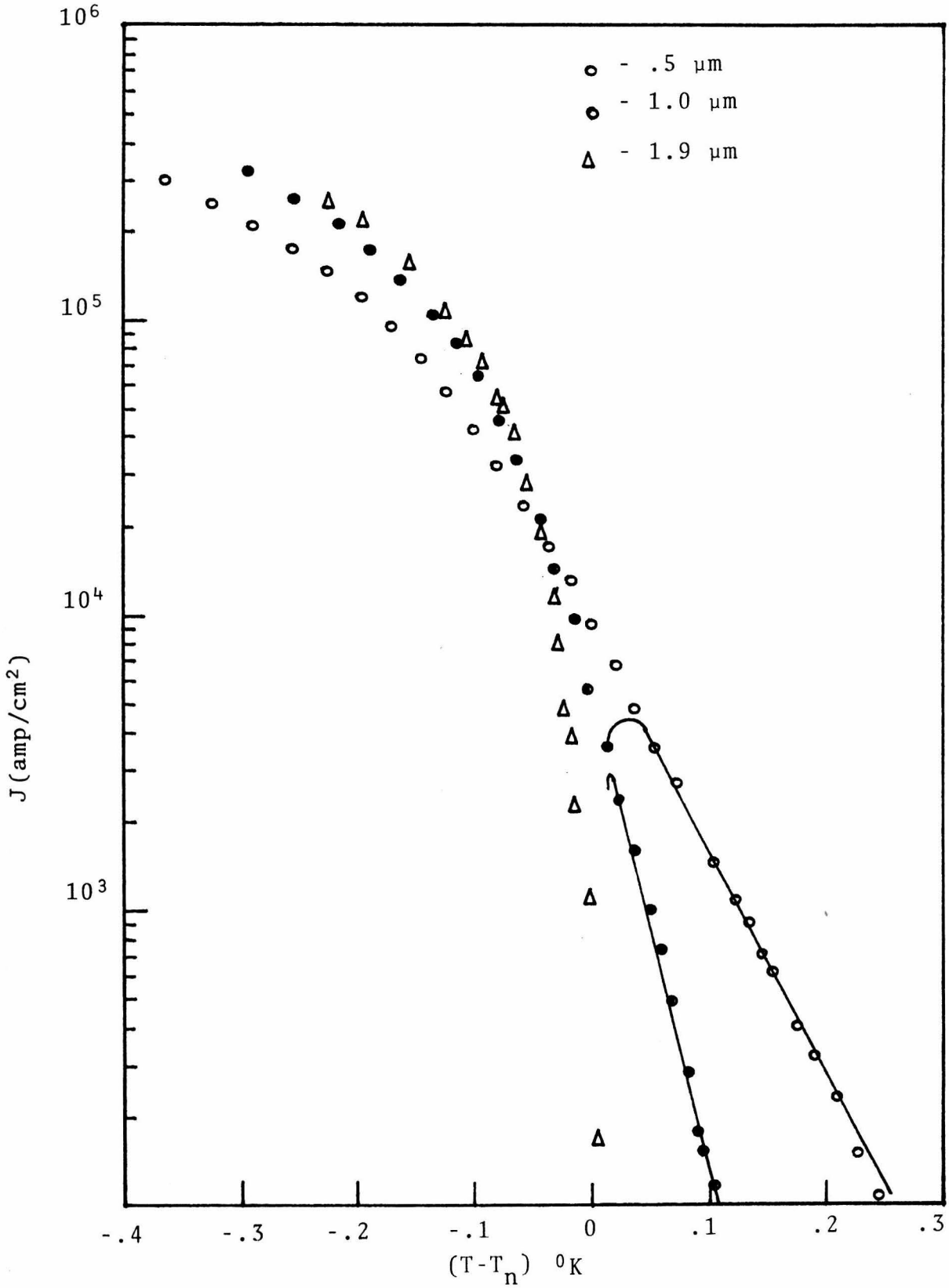

10^6
10^5
10^4
10^3
J_c (amp/cm^2)
○ - .5 μm
● - 1.0 μm
Δ - 2.0 μm
-.3
-.2
-.1
0
.1
.2
.3
(T-T_n) °K

Figure 15 - Critical Current Density vs Temperature for a set of these anodized bridges on a Tantalum/Titanium film. The bridge transition temperature are approximately $1.2^{0}K$ below the film transition temperature.


10^6
10^5
10^4
10^3
J (amp/cm^2)
- .5 μm
- 1.0 μm
- 1.9 μm
-.4
-.3
-.2
-.1
0
.1
.2
.3
(T-T_n) ^0K

3) Comparison of anodized and ion implant bridges showed no difference in the critical current behavior with respect to bridge length. The only observed difference was that the anodized bridges were seen to have larger critical densities than ion implant samples of the same length.

For the critical current density observed above T_n, the bridge should be adequately modeled as two superconductors coupled by a strip of normal metal. The observed supercurrent would then be due to the diffusion of Cooper pairs through the normal metal. The first presentation of the behavior of the pair potential, Δ, at an S-N interface, which was expanded to include an S-N-S junction was by DeGennes.[18] The physics is essentially that a pair formed in the superconductor diffuses into the normal region and decays exponentially with distance into the normal region. DeGennes argued that the lifetime of the pair in the normal region is roughly the time necessary for the thermal energy, kT, to break the pair, $\sim h/kT$. The spatial extent of this effect is then how far an electron at the Fermi velocity, v_f, can travel, or (hv_f/kT), and characterizes the rate of decay of the pair potential in the normal material. For the work here, where the normal metal is 1) a superconductor above the transition temperature, T_n and 2) a dirty metal such that the lifetime of the paired state is foreshortened by mean free path (1) effects, the decay length has been examined theoretically and found to be[19]

$$\xi_n = \left(\frac{hv_F l}{6\pi kT}\right)^{1/2} \left(1 + \frac{2}{\ln(T/T_n)}\right)^{1/2} \qquad (2.5.5)$$

In all subsequent discussions, $\xi_n(T)$ will be defined as the characteristic decay length of the pairs in the normal material.

The model proposed by DeGennes for the situation of an S-N interface was used to describe boundary conditions of the pair potential, Δ, at an interface. (This point will be considered again later). The transition temperature of layered super-normal films as a function of relative film thickness seems to be adequately described by this model. For the situation of an S-N-S structure, DeGennes obtained a critical current which varied sinusoidally with phase - exactly as the Josephson result. However, the critical current density,[14] j_c, was predicted to vary as $(\Delta T)^2$. The prediction seems to be observed for the case where N is a normal metal that does not go superconducting - however, for the case of a superconductor above its transition temperature, T_n, as in these experiments, it is not observed. It should be pointed out, though, that the DeGennes model does not consider the decay of the pair potential inside the normal material - instead it is handled as an extension of the tunneling problem of Josephson.

The decay of the pair potential within the bridge normal region was proposed by Aslamazov and Larkin[20] (AL) and was dealt with in a GL formalism. Their basic premise was that the wavefunction in an S-N-S structure (where the normal region is a superconductor above the transition temperature, T_n) could be described as a linear superposition of the two separate wavefunctions emanating from each superconductor, that is

$$\Psi = \psi_1 + \psi_2 = \psi_1 e^{i\phi_1} + \psi_2 e^{i\phi_2} \qquad (2.5.6)$$

ψ_1 and ψ_2 were seen to vary as simple decaying exponentials and the quantum mechanical phases, ϕ_1, and ϕ_2, were assumed to be position independent. Applying the usual quantum mechanical current operator, AL showed that the critical current from this wavefunction should vary proportionally to the sine of the phase difference and that the temperature dependence of the critical current density prefactor should then be proportional to

$$j_c \propto \left(\frac{T_s - T}{T_s}\right)\left(\frac{T-T_n}{T_n}\right)^{\frac{1}{2}} \exp\left(\frac{-L}{\xi_n}\left(\frac{T-T_n}{T_n}\right)^{\frac{1}{2}}\right) \sin(\Delta\phi) \qquad (2.5.7)$$

While the temperature dependence predicted by AL is not observed, the importance of the AL model lies in its prediction of the critical current density being proportional to the sine of phase difference and therefore offers a general explanation for Josephson-like phenomena in any weak link.

Thus, for the critical current density above T_n, no theory has previously been available for the dirty limit ($1 << \xi_0$) that incorporated any or all of the experimental features previously discussed. One would expect that any theoretical model for the critical current density above T_n should depend on the decay length of pairs in the normal material and the magnitude of the order parameter, ψ, at the S-N interface.

Recently, Likharev and Yakobson[21] (LY) have presented a

steady state model of weak links - in particular, for the case of a variable thickness bridge. It should be noted that there is nothing physically new in the model proposed by LY. Quantitatively, a similar, if not the same model, has been proposed by others. What is relevant about this model is that an actual theoretical prediction has been attempted in a GL formalism. Comparison of the LY model and experiment shows an interesting result. It would seem that for most bridges examined, the LY model approximately predicts the temperature dependence of the critical current density above T_n, however, the theoretical value of the critical current density is at least an order of magnitude larger than what is experimentally observed. A closer examination into the assumptions made in this model will show where the problem lies.

The principal assumption of the LY analysis is that the pair potential, Δ, in the main film adjacent to the bridge is equal to the equilibrium value, Δ_s. This assumption has been justified specifically for the case of variable thickness bridges, however, such an assumption is not warranted in the experimental case discussed here. For the samples in this study, Δ in the main film near the bridge edge is depressed below Δ_s due to proximity effects. Aside from the assumption on the magnitude of the order parameter at the boundary, the LY model should adequately describe the exponential critical behavior of proximity effect bridges if the magnitude of the order parameter can be determined at the boundary. The question of boundary effects in superconductors and at super-norm-

al interfaces has previously been discussed by DeGennes[18] and others[22] in connection with the proximity effect in layered films. What has been attempted here is to extend the LY model to describe the exponential critical current density behavior of proximity effect bridges using the correct boundary conditions as described by DeGennes. The comparison of theory and experiment is felt to be particularly meaningful in that all experimental parameters have been measured, that is, there are no adjustable parameters in the theoretical model discussed here. What will follow is a discussion first of the boundary conditions at a S-N interface, application of a corrected version of the LY model for predicting the exponential critical current density of proximity effect bridges and a comparison between theory and experiment.

2.5.3 Boundary Conditions at an S-N Interface

A complete discussion of the boundary conditions at an S-N interface has been given by DeGennes[18] and Werthamer,[22] among others. The technique for handling the problem of an interface begins with the linear integral self consistency equation due to Gor'kov and assumes that the coupling of the electrons can be approximated by a point interaction. This is a good approximation since the range of the exact interaction is of the order of a Fermi wavelength, $\sim 10A^0$ (Anderson and Morel).[23] In the dirty limit, $1 << \xi_0$, the only region considered in this work, these approximations are readily justified. DeGennes has shown that the boundary conditions for a dirty supercon-

ductor are

$$\frac{\Delta(x)}{NV} \qquad \text{continuous at a metallic interface}$$

$$\frac{D}{V}\frac{d\Delta(x)}{dx}$$

where N in the density of states at the Fermi level, V is the interaction potential and D, the diffusion constant is $1/3v_f l$. An actual derivation of the boundary conditions will not be included here as it is somewhat long and complex and no new insight into the present problem can readily be gained by such an exercise. The interested reader is referred to the references cited above.

The physics behind these boundary conditions becomes apparent once the quantity $\Delta(x)/V$ is identified. According to Gor'kov's formulation of the microscopic theory, $\Delta(x)/V$ is defined as the condensation amplitude $F(x)$ and can be related to the probability amplitude of finding two electrons in the condensed state at point x. $|F(x)|^2$ is seen to be the probability of finding such a pair. Therefore, the boundary condition at the interface may be reexpressed as

$$\frac{F_n(0)}{N_n} = \frac{F_S(0)}{N_S} \tag{2.5.8}$$

and implies that the fraction of electrons paired in each material at x=0 is identical. The second boundary condition may then be expressed as

$$D_n \left.\frac{d F_n(x)}{dx}\right|_{x=-0} = D_s \left.\frac{d F_s(x)}{dx}\right|_{x=+0} \qquad (2.5.9)$$

The second boundary condition reduces to a diffusion equation on both sides of the interface with the number of pairs being conserved across the S-N interface.

Before proceeding, the DeGennes boundary conditions will be expressed in terms of more easily measurable quantities. From the BCS theory, it can be shown that the transition temperature, T_s, of a superconductor can be expressed as

$$T_s = 1.14\ \theta_D \exp\ (-1/NV) \qquad (2.5.10)$$

where θ_D is the Debye temperature of the material and N and V have been previously defined. Solving for the product, NV, one obtains

$$NV = \frac{1}{\ln\left(\frac{1.14\theta_D}{T_s}\right)} \qquad (2.5.11)$$

Therefore, the first boundary condition can be rewritten for the case where both materials are superconductors (and where one of them is a superconductor above its transition temperature, T_n) as

$$\Delta_n(-0)\ln\left(\frac{1.14\theta_{Dn}}{T_n}\right) = \Delta_s(+0)\ln\left(\frac{1.14\theta_{Ds}}{T_s}\right) \qquad (2.5.12)$$

where θ_{Ds} and θ_{Dn} are the Debye temperatures of the super and

normal metals, respectively. As can be seen, Δ is not necessarily continuous at the S-N interface.

The second DeGennes boundary condition can be considered using the relation 2.3.1 between the resistivity, the density of states at the Fermi level, N, and the diffusion constant, D. Rewriting 2.3.1, one has

$$\frac{1}{\rho} = \frac{2}{3} e^2 N v_F l = 2e^2 N D \qquad (2.5.13)$$

This relation and expression 2.5.11 allows the second boundary condition to be written as

$$\frac{1}{\rho_n} \ln \left[\frac{1.14\theta}{T_n} D_n\right] \left.\frac{d\Delta_n(x)}{dx}\right|_{x=-0} = \frac{1}{\rho_s} \ln \left[\frac{1.14\theta}{T_s} D_s\right] \left.\frac{d\Delta_s(x)}{dx}\right|_{x=+0} \qquad (2.5.14)$$

It is seen that the slope of Δ is not necessarily continuous at the S-N interface.

There is one other "boundary" condition which should be discussed before proceeding - even though it is merely an extension of those considered here. It was shown in Chapter 1 that the order parameter, ψ, is proportional to the energy gap, Δ. However, as has been mentioned, ψ is a complex number and can be expressed as having a phase, that is $\psi = \psi_0 e^{i\phi}$. Therefore, the pair potential, Δ, is complex and the only way that boundary condition 2.5.12 can be satisfied is that

$$\phi_s = \phi_n \qquad (2.5.15)$$

where ϕ_s and ϕ_n are the phases in the super and normal material, respectively. Also, since the pairs in the normal metal are present by virtue of diffusion and since no gradient term in the phase exists in the superconductor, it can be shown by application of 2.5.14 that no gradient term in the phase should exist in the normal material. Therefore, in the model examined here, the phase of the order parameter as it passes through an S-N interface and decays in the normal material will be considered independent of position, that is, a constant.

The approach of the remaining portion of this section will be to employ the asymtotic solutions of the GL equations for the order parameter in the super and normal regions. Since the order parameter in the superconducting film is depressed near the normal metal, the DeGennes boundary conditions will be used to determine the value of the order parameter in both the super and normal materials at the interface.

At this point it is worth commenting on the use of the GL equation for a normal metal and the existence of $\Delta(x)$ in the normal material. As was shown in Chapter 1, the GL free energy was expanded in terms of ψ near the transition temperature, T_c. No restriction was made whether one was considering above or below the transition temperature, T_n. The equilibrium value above T_n was shown to be $|\psi|^2=0$, however, that discussion did not include the existence of superconductivity in the normal material by diffusion from another superconductor. Therefore, the existence of $\Delta(x)$ in the normal material is a consequence of pair diffusion and will be described in

the following sections using GL formalism.

The first area to be considered is the solution of the GL equation for the case of an S-N interface. The asymptotic behavior of $\psi(x)$ far from the boundary in each material is first considered. The behavior of ψ near the S-N interface is then obtained by matching the asymtotic solutions of ψ in the super and normal material using the DeGennes boundary conditions.

Consider the case of a S-N interface, Figure 16a, where in this case the normal material, N, is a superconductor above its critical temperature, T_n. The behavior of the order parameter within each material can be described by the GL differential equation (1.13)

$$\xi^2_{s/n} \nabla^2 f \pm f - f^3 = 0 \qquad (2.5.16)$$

where f, the normalized wave function, is $f = \psi/\psi_\infty$ and ψ_∞ is defined in 1.8. The upper sign in 2.5.16 is used in the superconducting material ($T < T_s$) while the lower sign is used in the normal material ($T > T_n$).

The characteristic length of the problem, $\xi_{s/n}$, needs some explanation. Within the superconducting material, ξ_s, is the coherence length as discussed previously. However, within the normal material, ξ_n, will refer to the decay length of pairs which have diffused in from S, as considered in expression 2.5.5.. The pair decay length, ξ_n, in the normal material can be rewritten in terms of the coherence length for the same

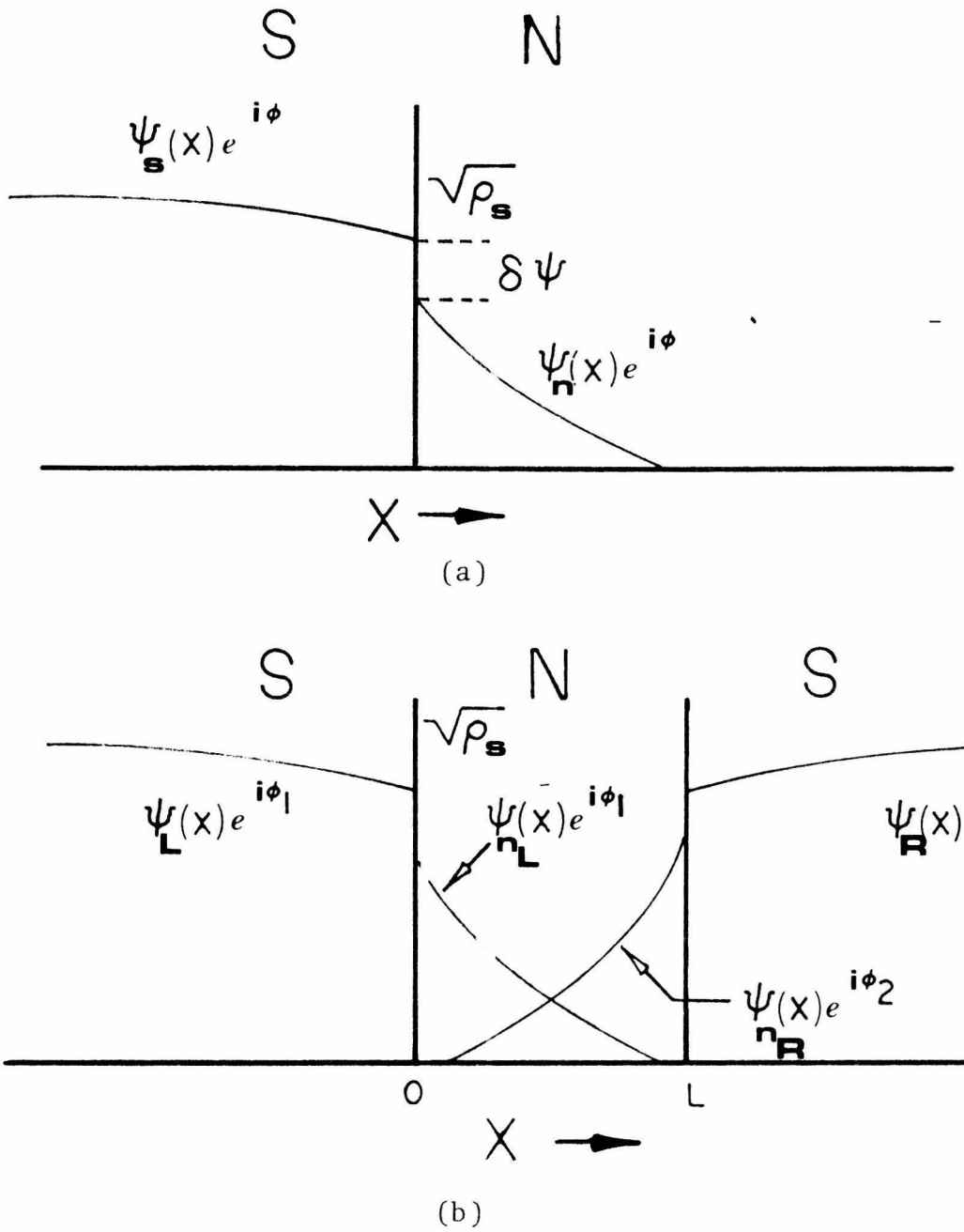


Figure 16 -(a) Variation of ψ at an S-N interface (not to scale).

(b) Variation of ψ in an S-N-S bridge. Note the superposition of the two wavefunctions (not to scale).

material when superconducting, as

$$\xi_n(T) = .898\ \xi_n(0) \left(\frac{T_n}{T-T_n} \right)^{\frac{1}{2}} \qquad (2.5.17)$$

The length, $\xi_n(0)$, is the coherence length for the metal (superconductor above its transition temperature) at $T=0^0K$ and will be considered in subsequent discussions.

Equation 2.5.16 will first be solved for the case of the superconducting material ($x<0$ - Figure 16a) when f assumes the values

$$f = f_0 \qquad x = 0$$
$$f \to 1 \qquad x \to -\infty$$

The behavior of f as $x \to -\infty$ describes the asymptotic behavior of f as one moves away from the interface. The value f_0 at $x = 0$ is a dummy variable and will be used to match the boundary conditions into N at the interface. Multiplying 2.5.16 by f and integrating, the first integral is obtained

$$-\xi_s^2 f_s'^2 - f_s^2 + \frac{f_s^4}{2} = \text{const.} \qquad (2.5.18)$$

In order to satisfy the limiting behavior of f as $x \to -\infty$, the constant must be taken equal to $-\frac{1}{2}$. Therefore,

$$-\xi_s^2 f_s'^2 = \tfrac{1}{2}(1-f_s^2)^2 \qquad (2.5.19)$$

which can readily be integrated. The appropriate solution is

$$f_s = -\tanh\left(\frac{x}{\sqrt{2}\xi_s(T)} + C \right) \qquad (2.5.20)$$

where

$$C = \tanh^{-1}(f_0) \qquad (2.5.20b)$$

In the normal material (x>0)(Figure 16a), the appropriate limiting behavior on f_n is

$$f_n = A = \frac{\psi_n(x=0)}{\psi_{n\infty}} \qquad x = 0$$

$$f \to 0 \qquad x \to \infty$$

where $\psi_{n\infty}$ is defined as $|\psi_{n\infty}|^2 = -\alpha_n/\beta_n$. $\psi_{n\infty}$ acts simply as a scale factor in the normal material. As in the previous solution, A will denote the value of f_n at the interface and will be used to match the boundary conditions at the interface.

As before, multiplying through 2.5.16 by f' and upon integrating, the first integral is obtained

$$\xi_n^2 f_n'^2 - f_n^2 - \tfrac{1}{2} f_n^4 = \text{const.} \qquad (2.5.21)$$

In order to satisfy the limiting behavior of f_n as

$x \to \infty$, the constant must be taken equal to zero. Therefore

$$\xi_n f_n' = f_n (1+f_n^2/2)^{\frac{1}{2}} \tag{2.5.22}$$

which can readily be integrated. Upon application of the remaining boundary condition, the final expression for f_n within the normal region becomes

$$f_n = \frac{A\ 4\ (1 + \sqrt{1 + A^2/2})\ e^{-x/\xi_n}}{2\ (1 + \sqrt{1 + A^2/2})^2 - A^2 e^{-2x/\xi_n}} \tag{2.5.23}$$

At this particular point, it will become more convenient to work in terms of ψ_s and ψ_n rather than the normalized wavefunctions f_s and f_n. This is easily accomplished since $\psi_s = \psi_{s\infty}\ f_s(x)$ and $\psi_n = \psi_{n\infty} f_n(x)$ and will be used in all subsequent discussions.

The two asymptotic solutions will now be used in conjunction with the DeGennes boundary conditions to determine the value of ψ_s and ψ_n at the interface. Since the boundary conditions have been determined in terms of the energy gap, Δ, they will be reexpressed in terms of the order parameter, ψ, by expression 1.3.5. Applying the first boundary condition to the two wavefunctions at the interface, one finds that

$$\frac{\lambda_s(0) T_s^{\frac{1}{2}}}{(NV)_s} \psi_s(0) = \frac{\lambda_n T_n^{\frac{1}{2}}}{(NV)_n} \psi_n(0) \tag{2.5.24}$$

Solving for $\psi_n(0)$, one obtains

$$\psi_n(0) = \psi_s(0) \quad \frac{\lambda_s(0)}{\lambda_n(0)} \quad \frac{(NV)_n}{(NV)_s} \left(\frac{T_s}{T_n} \right)^{\frac{1}{2}} \tag{2.5.25}$$

and identifying $\psi_s(0) = \psi_{s\infty} \tanh C$ this can be rewritten

$$\psi_n(0) = \psi_{s\infty} \quad \frac{\lambda_s(0)}{\lambda_n(0)} \quad \frac{(NV)_n}{(NV)_s} \left(\frac{T_s}{T_n} \right)^{\frac{1}{2}} \tanh C \tag{2.5.26}$$

The second boundary condition can be written

$$\frac{\lambda_s(0) T_s^{\frac{1}{2}}}{\rho_s (NV)_s} \left. \frac{d\psi_s(x)}{dx} \right|_{x=-0} = \frac{\lambda_n(0) T_n^{\frac{1}{2}}}{\rho_n (NV)_n} \left. \frac{d\psi_n(x)}{dx} \right|_{x=+0} \tag{2.5.27}$$

and taking the derivative of expressions 2.5.20 and 2.5.23 and using 2.5.26, $\psi_n(0)$ can be eliminated from 2.5.27. What has been done is to eliminate $\psi_n(0)$ leaving an expression which must be solved for the value of C. This expression can be rearranged so that one is left with

$$\sinh 2C \left\{ 1 + \frac{1/2 \left(\frac{\psi_{s\infty}}{\psi_{n\infty}} \frac{\lambda_s(0)}{\lambda_n(0)} \frac{(NV)_n}{(NV)_s} \frac{T_s^{\frac{1}{2}}}{T_n^{\frac{1}{2}}} \tanh C \right)^2}{1 + \sqrt{1 + 1/2 \left(\frac{\psi_{s\infty}}{\psi_{n\infty}} \frac{\lambda_s(0)}{\lambda_n(0)} \frac{(NV)_n}{(NV)_s} \frac{T_s^{\frac{1}{2}}}{T_n^{\frac{1}{2}}} \tanh C \right)^2}} \right\}$$

$$= \sqrt{2} \frac{\rho_n}{\rho_s} \frac{\xi_n}{\xi_s} \tag{2.5.28}$$

which must be solved numerically for the value of C. Once C

is determined, the values of $\psi_s(0)$ and $\psi_N(0)$ can be found. It should be pointed out that C is a function of temperature since both $\psi_{s\infty}$ and $\psi_{N\infty}$ are functions of T. As was mentioned in Chapter 1, $\psi_{s\infty}$ is proportional to the energy gap deep within the superconducting material. If the superconducting material is near its transition temperature, T_s, combining 1.3.2 and 1.3.5 one finds that $\psi^2_{s\infty}$ is

$$\psi^2_{s\infty} = \frac{K^2}{T\lambda^2_s(0)} T_s \frac{8}{7\zeta(3)} (\pi k_B T_s)^2 \left(\frac{T_s - T}{T_s} \right) \qquad (2.5.29)$$

while at temperatures $T << T_s$, using 1.3.3, $\psi^2_{s\infty}$ is

$$\psi^2_{s\infty} = \frac{K^2}{T\lambda^2_s(0)} T_s (1.76kT_s)^2 \qquad (2.5.30)$$

For the normal material $\psi^2_{n\infty}$ is defined as $-\alpha_n/\beta_n$, however, since the sign of α_N changes above T_N, one can write near T_N that

$$\psi^2_{n\infty} = \frac{K^2}{T\lambda^2_n(0)} T_n \frac{8}{7\zeta(3)} (\pi k_B T_n)^2 \left(\frac{T - T_n}{T_n} \right) \qquad (2.5.31)$$

For the case of both the super and normal material being near their respective transition temperatures, the expression for $(\psi_{s\infty}/\psi_{N\infty})^2$ can be written as

$$\left(\frac{\psi_{s\infty}}{\psi_{n\infty}} \right)^2 = \left(\frac{\lambda^2_n(0)}{\lambda^2_s(0)} \right) \left(\frac{T_s - T}{T - T_n} \right) \qquad (2.5.32)$$

while if the superconductor is at a temperature $T << T_s$ then

$$\left(\frac{\psi_{s\infty}}{\psi_{n\infty}}\right)^2 = .330 \quad \frac{\lambda_n^2(0)}{\lambda_s^2(0)} \left(\frac{T_s}{T-T_n}\right) \tag{2.5.33}$$

These expressions are used in the determination of the value of C for each temperature considered. The value of $(NV)_n$ and $(NV)_s$ are calculated using 2.5.11.

The final expression for the order parameter, $\psi_n(x)$, in the normal metal is then

$$\psi_n(x) = \psi_{n\infty} \frac{4B\,(1 + \sqrt{1 + B^2/2})\, e^{-x/\xi_n(T)}}{2\,(1 + \sqrt{1 + B^2/2})^2 - B^2 e^{-2x/\xi_n}} \tag{2.5.34}$$

where B is defined as

$$B = \frac{\psi_{s\infty}\, \lambda_s(0)(NV)_n\, T_s^{\frac{1}{2}}}{\psi_{n\infty}\, \lambda_n(0)(NV)_s\, T_n^{\frac{1}{2}}} \tanh C \tag{2.5.35}$$

2.5.4 Calculation of the Critical Current of a Proximity Effect Bridge - $T > T_N$

Once the behavior of the wavefunction, ψ, has been determined across an S-N interface, it is fairly straightforward to extend these findings to the case of an S-N-S structure, at least in a linear approximation. As has been discussed, within the normal bridge region the order parameter, ψ_N, decays exponentially. As a first approximation, it will be assumed that the bridge length, L, is $>> \xi_N(T)$ so that the

cubic terms in the GL differential equation (1.13, 2.5.16) can be ignored and the problem linearized. This model will treat the bridge as the superposition of an S-N and N-S boundary separated by a normal metal of length, L. (Figure 16b). The wavefunction in the normal bridge, ψ_B, will be a linear combination of the wavefunctions from each bounding superconductor, that is,

$$\psi_B = \psi_n(x) + \psi_n(L - x) \exp(i\phi) \tag{2.5.36}$$

where ϕ is the relative phase difference between the two superconductors. Applying the quantum mechanical current operator to ψ, one is left with the expression for the supercurrent

$$J_S = \frac{e\hbar}{m\xi_n} \psi_{n\infty}^2 \left[\frac{8B^2}{\left(1 + \left(1 + B^2/2\right)^{1/2}\right)^2} \right] \exp(-L/\xi_n) \sin\phi \tag{2.5.37}$$

where B is defined as 2.5.35. The prefactor to this expression can be normalized in terms of the critical current when the bridge itself is superconducting ($T < T_N$). In that case, the simple GL theory predicts that the critical current density for a thin film can be written as (See section 2.4)

$$J_{GL} = .898\ (2/3\sqrt{3})\ (e\hbar\psi_{n\infty}^2/m\xi_n) \tag{2.5.38}$$

so that the final expression for the critical current density may be written as

$$J_c = (.898)\ (3\sqrt{3}/2)\ J_{GL}(T)\left[\frac{8B^2}{\left(1 + (1 + B^2/2)^{\frac{1}{2}}\right)^2}\right] \quad X$$

$$\exp\ (-L/\xi_n(T))\ \sin\ \phi \qquad (2.5.39)$$

This expression is consistent with the work of others in that J_c is proportional to $\sin\phi$ and agrees with the findings of Ganz[24] who showed that in the zero voltage state, J_s, was proportional to $\sin\ \phi$.

In the next section a comparison will be made between this prediction and experimental measurements. A comparison will be made with bridges of various resistivities and lengths Both expressions 2.5.32 and 2.5.33 will be used for the cases of a superconducting film near and far from its transition temperature, T_s. It should be emphasized that the comparison between this result and experiment is particularly meaningful since expression 2.5.39 has no adjustable parameters - all of the bridge and film parameters have been determined.

2.5.5 Comparison of Theoretical and Experimental Results

Two limits will be considered in this analysis: one where the transition temperature of the bridge, T_N, and the film, T_s, are approximately identical ($T_N \gtrsim T_s$), second when $T_N << T_s$. The expression for the bridge critical current density where T_N is near T_s with all the temperature dependences included is, combining 2.5.39 and 2.5.32

$$J_c = (.898)\ \frac{3\sqrt{3}}{2}\ J_{GL}(0)\left(\frac{T-T_n}{T_n}\right)^{3/2} \quad X$$

$$\left[\frac{8\left(\frac{T_s-T}{T-T_n}\right)\left(\frac{NV_n}{NV_s}\right)^2\ \frac{T_s}{T_n}\ \tanh^2 C}{\left(1+\left(1+\tfrac{1}{2}\left[\left(\frac{T_s-T}{T-T_n}\right)\left(\frac{NV_n}{NV_s}\right)^2\ \frac{T_s}{T_n}\ \tanh^2 C\right]\right)^{\frac{1}{2}}\right)^2}\right] \quad X$$

$$\exp\left(\frac{-L}{.898\ \xi_n(0)}\left(\frac{T-T_n}{T_n}\right)^{\frac{1}{2}}\right) \qquad (2.5.40)$$

whereas the temperature dependence when $T_n << T_s$

$$J_c = (.898)\ \frac{3\sqrt{3}}{2}\ J_{GL}(0)\left(\frac{T-T_n}{T_n}\right)^{3/2} \quad X$$

$$\frac{8\ (.330)\left(\frac{T_s}{T-T_n}\right)\left(\frac{NV_n}{NV_s}\right)^2\ \frac{T_s}{T_n}\ \tanh^2 C}{\left(1+\left(1+\tfrac{1}{2}\left[.330\left(\frac{T_s}{T-T_n}\right)\left(\frac{NV_n}{NV_s}\right)^2\frac{T_s}{T_n}\ \tanh^2 C\right]\right)^{\frac{1}{2}}\right)^2} \quad X$$

$$\exp\left(\frac{-L}{.898\ \xi_n(0)}\left(\frac{T-T_n}{T_n}\right)^{\frac{1}{2}}\right) \qquad (2.5.41)$$

In both expressions, C is calculated from 2.5.28. All other terms are measured parameters. $J_{GL}(0)$ is determined from the critical current density behavior for $T < T_n$ where the temperature dependence is $\Delta T^{3/2}$. This point will be considered in more detail in the next section. As previously mentioned, $\xi_n(0)$, $\xi_s(0)$, L, T_n and T_s have been determined and are contained in Tables 1-4.

One observation here on the determination of the terms containing NV. For the materials studied, the Debye temperature are those as found in any standard reference text.[25] To this author's knowledge, there is no way of determining the Debye temperature of a layered film, therefore a spatial ave-

rage employing the relative film thicknesses and Debye temperatures was used.

The theoretical and experimental results are shown in Figures 12 through 15 and, as can be seen, the agreement is excellent in all cases. The general behavior of the critical current density outlined at the beginning of this section is readily predicted by this model. A comparison is made between similar bridges (same film same length - different bridge transition temperatures). The bridge with the lower transition temperature, T_n, is observed to have a narrower temperature region above T_n in which critical current can be measured. This is easily understood since the coherence length is always smaller for the lower temperature samples - thus, the effective bridge length, $L/\xi_n(0)$ is always larger for the low temperature bridge. Stated another way, the lower temperature bridge behaves as if it were longer. The differences in the critical current density behavior of the anodized and ion implant bridges can likewise be explained by the differences in the coherence lengths.

The entire model described in this section is for the temperature region, $T > T_n$. As T approaches T_n, the model described here breaks down. The approximation of employing the linear superposition of two wavefunctions is no longer valid. The pair decay length, ξ_n, becomes comparable with the bridge length, L, and the cubic terms in the GL differential equation can no longer be ignored. Also there is a change in the form of the asymptotic wavefunction above and below

T_n (as seen in the solutions 2.5.20 and 2.5.25). This particular temperature area has been approached via numerical calculations by other authors[2] (different models) but was not attempted here since it was felt no new insight into the problem could readily be gained. The next area to be examined is the critical current density behavior of a proximity effect bridge for $T < T_n$.

2.5.6 Critical Current of a Proximity Effect Bridge, $T < T_n$

As T decreases below T_n, the critical current density for all but the longest bridges is seen to vary more slowly with respect to temperature (See Figures 12 through 15). The general features of the bridge critical current vs temperature for a typical set of bridges, plotted $I_c^{2/3}$ vs T, is shown in Figure 11. Below the bridge transition temperature, T_n, the bridge critical current as a function of temperature is seen to approach the limiting behavior of a superconducting film strip with $J_c \propto ((T_n-T)/T_n)^{3/2}$. For the temperature region $T < T_n$, the magnitude of the quantum interference effects (B field modulation, rf response) observed diminishes for the shorter bridges and is almost totally absent in the longer structures. In light of this behavior, it is assumed that for $T < T_n$, the two superconductors, S are coupled by a weaker ($T_n < T_s$) intrinsically superconducting strip. For such a situation, the critical current should be adequately described by a 1-dimensional GL calculation similar to that already made. From the derivation in section 2.4, the expression for

the critical current density prefactor, $J_{GL}(0)$ is dependent only on the coherence length, $\xi_n(0)$, and the penetration depth, $\lambda_n(0)$, of the bridge region and is given as

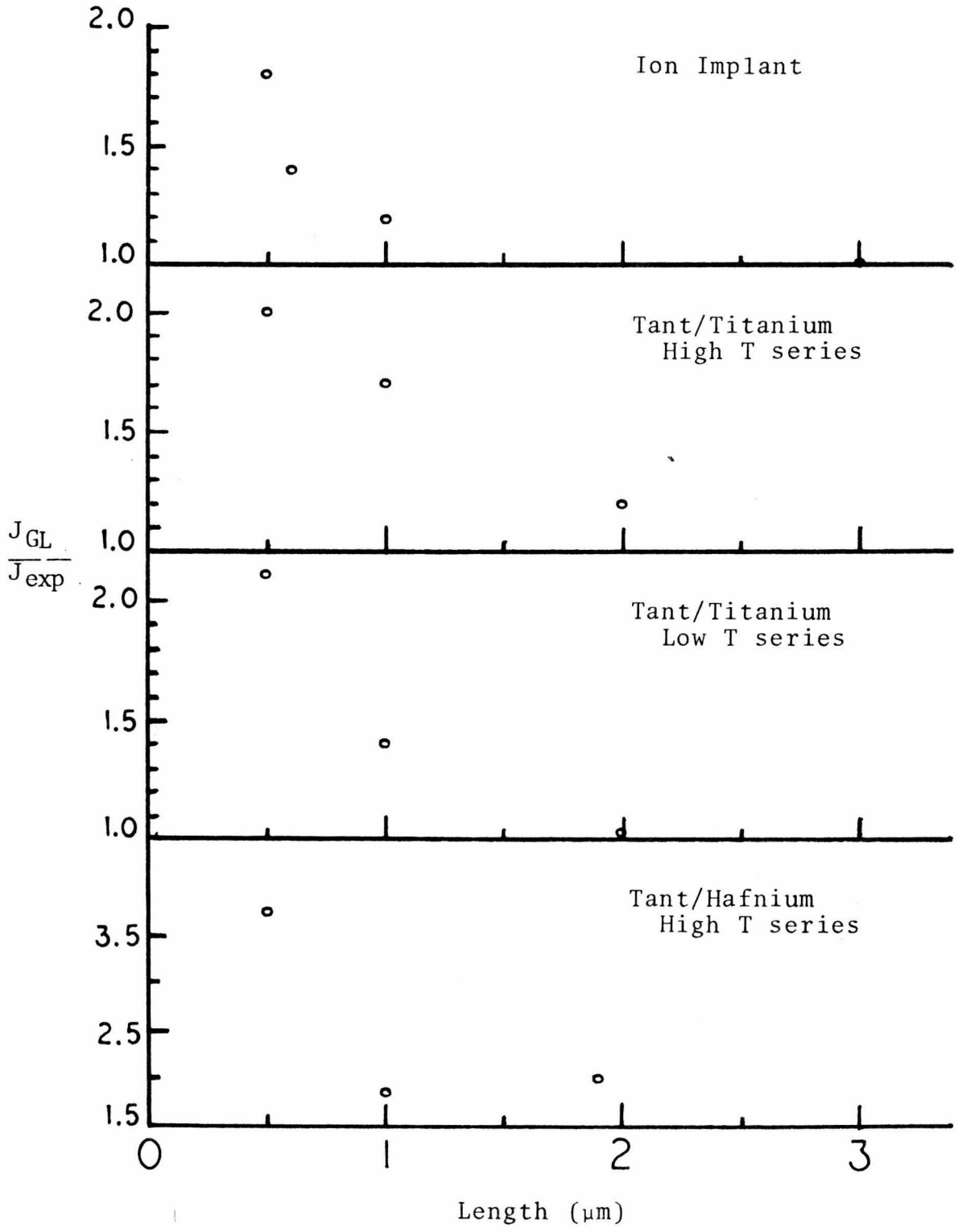
$$J_c(T) = \frac{c\phi_0}{12\sqrt{3}\pi^2 \xi_n(0)\lambda_n^2(0)} \left(\frac{T_n - T}{T_n}\right)^{3/2} = J_{GL}(0)\left(\frac{T_n - T}{T_n}\right)^{3/2} \quad (2.5.42)$$

This model of the critical current density of a proximity effect bridge is based on the destruction of the superconducting state when the critical current is attained. Inherent to this sort of reasoning is that both superconductors are strongly coupled by the superconducting bridge region, that is, the model of the two superimposed wavefunctions postulated earlier no longer applies. The diminished quantum interference effects observed in the temperature region, $T < T_n$, would seem to correlate with this

The bridge critical current density when $T < T_n$ and varies as $(\Delta T)^{3/2}$ has been calculated using expression 2.5.42 and the values $\xi_n(0)$ and $\lambda_n(0)$ from Tables 1-4. Comparison between the experimentally determined current density prefactor, $J(0)_{exp}$, and the one determined theoretically is plotted as a function of bridge length, L, in Figure 17.

For the Ta/Ti anodized and Ta ion implant samples the longest bridges agree quite well with the GL prediction. However, the shorter bridges show critical current densities much less (by about a factor of 2) than theoretically predicted. The Ta/Hf samples show the same characteristic behavior of large deviations between theory and experimental critical current density values for short samples, with this devia-

Figure 17 - Variation in J_{GL}/J_{exp} vs bridge length for the four sets examined. J_{GL} is calculated using expression 2.5.42 and the values of $\xi(0)$ and $\lambda(0)$ from Tables 1 through 4.


Ion Implant
Tant/Titanium
High T series
Tant/Titanium
Low T series
Tant/Hafnium
High T series
$\frac{J_{GL}}{J_{exp}}$
2.0
1.5
1.0
2.0
1.5
1.0
2.0
1.5
1.0
3.5
2.5
1.5
0
1
2
3
Length (μm)

tion being reduced as the bridge length is increased. However, even the longest bridges show a deviation by a factor of $\cong 2$. This behavior is believed to be attributed to the high resistivity of the Hf bottom film (Figure 2a). One might reasonably argue that few pairs diffuse into the Hf and that for the Ta/Hf films, the proper physical description would be that of a superconducting sheet (Ta) over a normal metal (Hf) film. If this is the case, then, a current running through the film, would pass only in superconducting Tantalum film with the Hafnium bottom film acting as a normal shunt. In order to further pursue this point, tests were run on a set of Ta/Hf bridges of the same length but of various bridge thicknesses. These results are compared with the GL predictions and are shown in Figure 18. As can be seen, as the Ta film thickness is diminished the discrepancy is seen to increase. No similar behavior is observed in the Ta/Ti samples and it is concluded that for the case of the Ta/Hf film samples, the current flows only through the superconducting Ta film with the Hf film acting as a normal shunt. The difference therefore observed in the longer Ta/Hf samples is due to not knowing the effective thickness, t^*, of the current sheath and should be independent of bridge length.

It would seem that the shorter bridges exhibit critical current densities smaller than theoretically expected. This result for shorter bridges is somewhat unexpected since one might intuitively expect that the pair density in the center of the shorter bridges (Figure 19) would be larger (due to

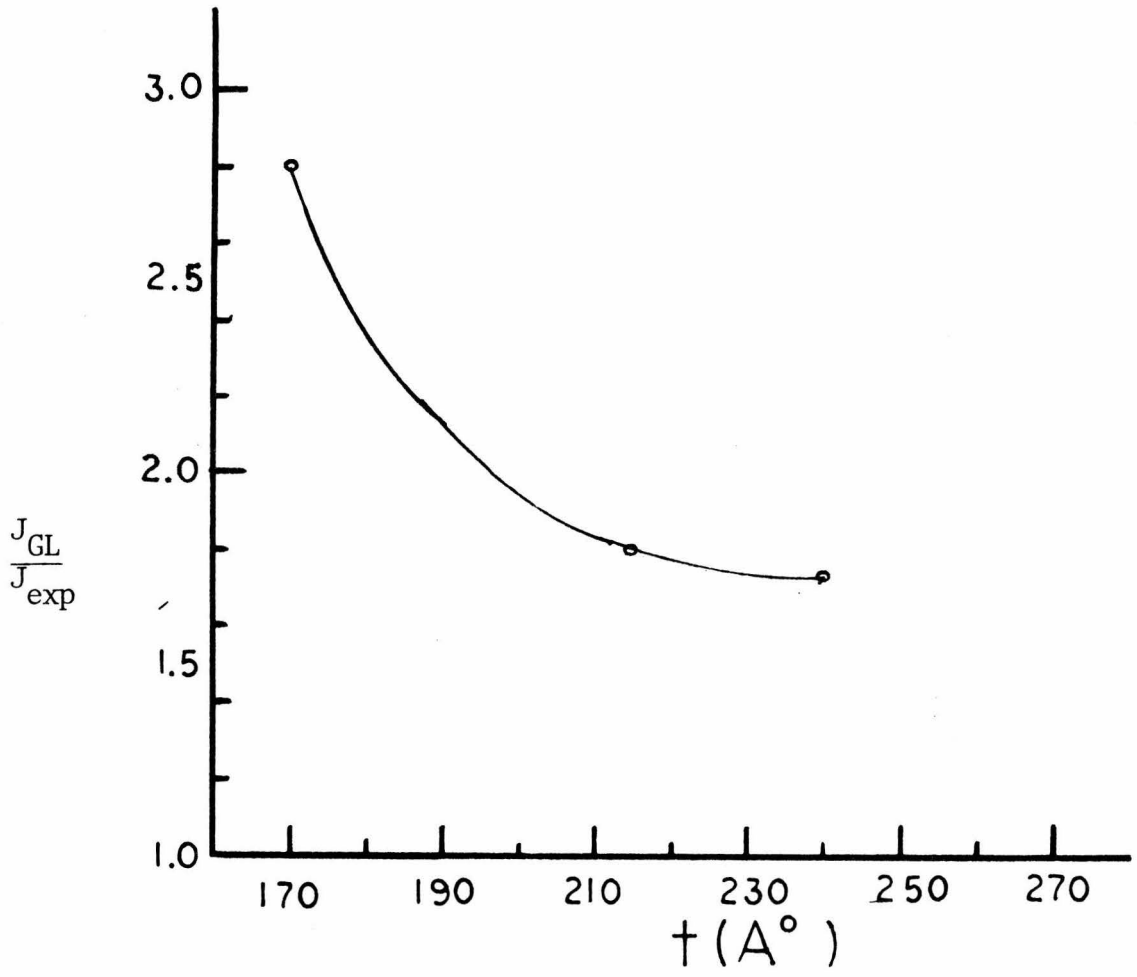


Figure 18 - J_{GL}/J_{exp} vs Film thickness, t, for a Tantalum/Hafnium bridge of length 1.1 μm. Note that as t decreases, the deviation increases. No corresponding behavior was observed on the Ta/Ti sets.

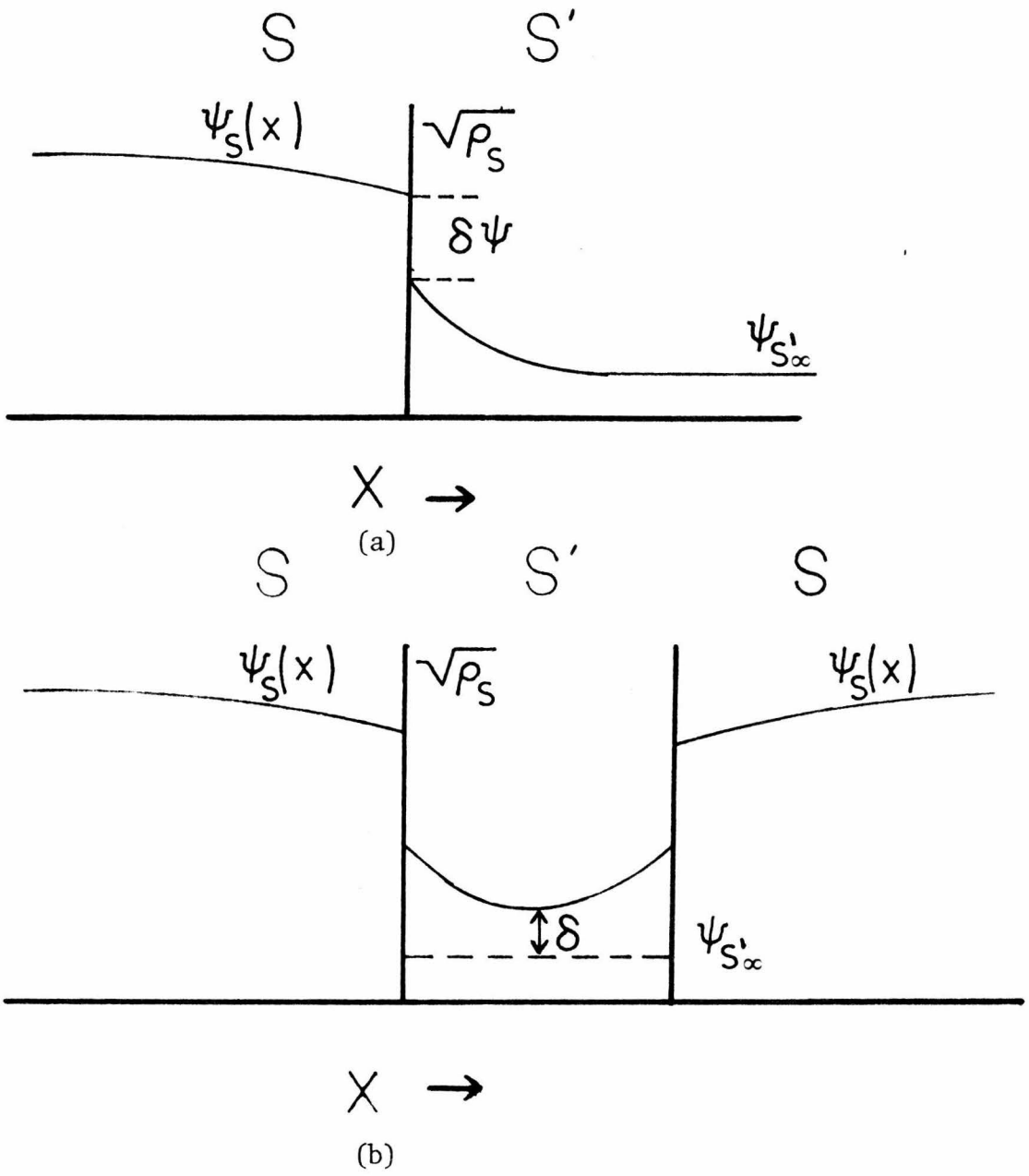


Figure 19 - (a) Behavior of ψ at an S-S' Interface.

(b) Behavior of ψ in an S-S'-S bridge. Note that if the bridge is sufficiently short, one would expect to see an excess number of pairs, δ, in the bridge center.

diffusion from the stronger superconductor) than in the case of a longer sample. One might then argue that a larger pair density implies a larger critical current density, which is not experimentally observed.

It should be noted that the same difference between the theoretically and experimentally determined critical current density is also observed when $T > T_N$. In expressions 2.5.40-41, the critical current density scale factor, $J_{GL}(0)$, used in the comparison of theory and experiment for $T > T_N$ is determined from the critical current density data for $T < T_N$.

2.5.7 Behavior of the Order Parameter with Two Boundaries

The experimental results outlined here indicate that the measured critical current density both above and below the transition temperature, T_N, is smaller than one would expect theoretically. In the temperature regime $T > T_N$, the basic postulate is that ψ, the order parameter, is a linear superposition of wavefunctions, each emanating from an S-N interface. However, the effect of the second N-S boundary on either wavefunction was never considered. Likewise, for $T < T_N$, the critical current density was calculated without regard to the effect of the boundaries. It is suggested that the observed deviation between the present theory and experiment is a direct result of the second boundary and its effect on the behavior of the order parameter, ψ. Other situations exist (in optics, for instance) in which the behavior of some physical variable is radically different for the case of

one and two boundaries.

As an example of this point, consider the elementary quantum mechanical problem of a beam of particles incident from the left on a barrier of height V_0 such that $E < V_0$. Two cases will be considered and compared, one in which the barrier is of infinite width and one in which the barrier is of some finite width, a (Figure 20a/b). For the single barrier problem, the Schrodinger equation (with $\hbar = \sqrt{2}$, $m = 1$) is

$$\nabla^2\psi + V\psi = E\psi \tag{2.5.43}$$

where the potential is $V = 0$ for $x < 0$ and $V = V_0$ for $x > 0$. Defining $k_1 = \sqrt{E}$ for the region $x < 0$ and $k_2 = \sqrt{V_0 - E}$ for $x > 0$, the solution of 2.5.43 is

$$\begin{aligned} \psi_I &= e^{ik_1x} + B_0e^{-ik_1x} && x < 0 \\ \psi_I &= C_0e^{-k_2x} && x > 0 \end{aligned} \tag{2.5.44}$$

which can be solved for B_0 and C_0 upon application of the usual boundary conditions (ψ and ψ' continuous at $x = 0$). It is obvious that the Schrodinger equation is just a linearized form of the GL equation and for the case considered here it is analogous to the behavior of the order parameter at an S-N interface. For the region $x > 0$, the probability of a particle being at a distance $a/2$ inside the barrier is

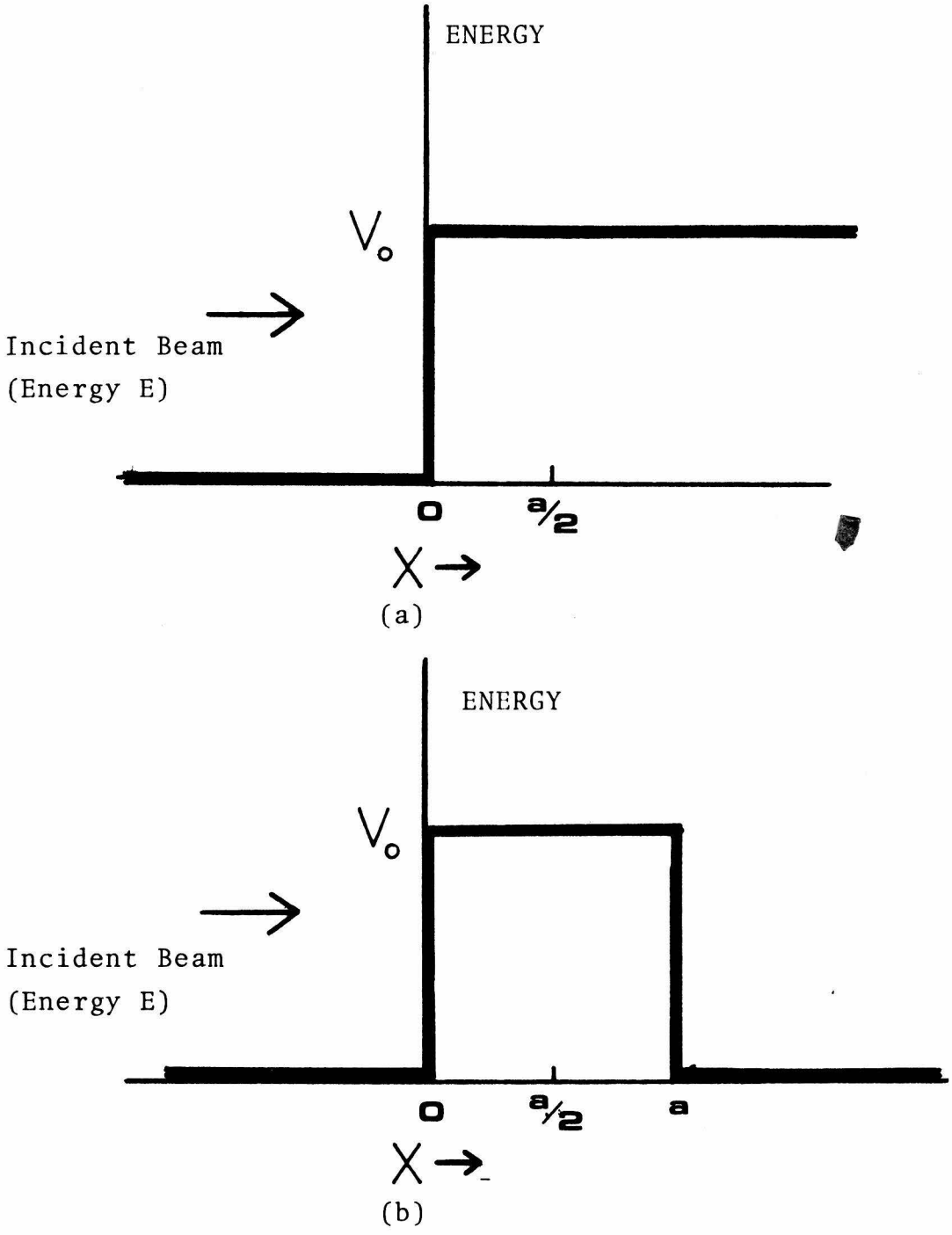


Figure 20 - (a) Beam of particles with energy, E, incident from left on barrier of height V_0, and infinite width such that $E < V_0$. (b) Beam of particles with energy, E, incident from left on barrier of height V_0 and width a, such that $E < V_0$.

$$|\psi_I \ (x = a/2)|^2 = \frac{4k_1^2 \ e^{-k_2 a}}{k_1^2 + k_2^2} \qquad (2.5.45)$$

The probability of a particle being inside the barrier falls off exponentially, which is similar to the solution of the GL equation for an S-N interface (See Section 2.5.3).

This result will be compared to the solution of a problem in which two boundaries are present, in this case that of a barrier of finite width, a (analogous to a bridge when $T > T_N$). As will be shown here, the probability of a particle being inside the barrier is different than in the case of a single boundary. Depending upon certain conditions (to be specified later), it can be either greater or less than the case of a single boundary. As before, one must solve the Schrodinger equation (2.5.43), only in this case the potential, V, is nonzero only when $0 < x < a$. The solution to 2.5.43 can be written as

$$\begin{aligned} \psi_{II} &= e^{ik_1 x} + Be^{-ik_1 x} && x < 0 \\ \psi_{II} &= Ce^{-k_2 x} + De^{+k_2 x} && 0 < x < a \\ \psi_{II} &= Ee^{ik_1 (x-a)} && x > a \end{aligned} \qquad (2.5.46)$$

The region of interest here is $0 < x < a$, since the probability of a particle being at $x = a/2$ will be compared with the one boundary solution. It is interesting to note that ψ_{II} for this region is expressed in a form equivalent to a wave emanating from the left boundary and that of one emanating

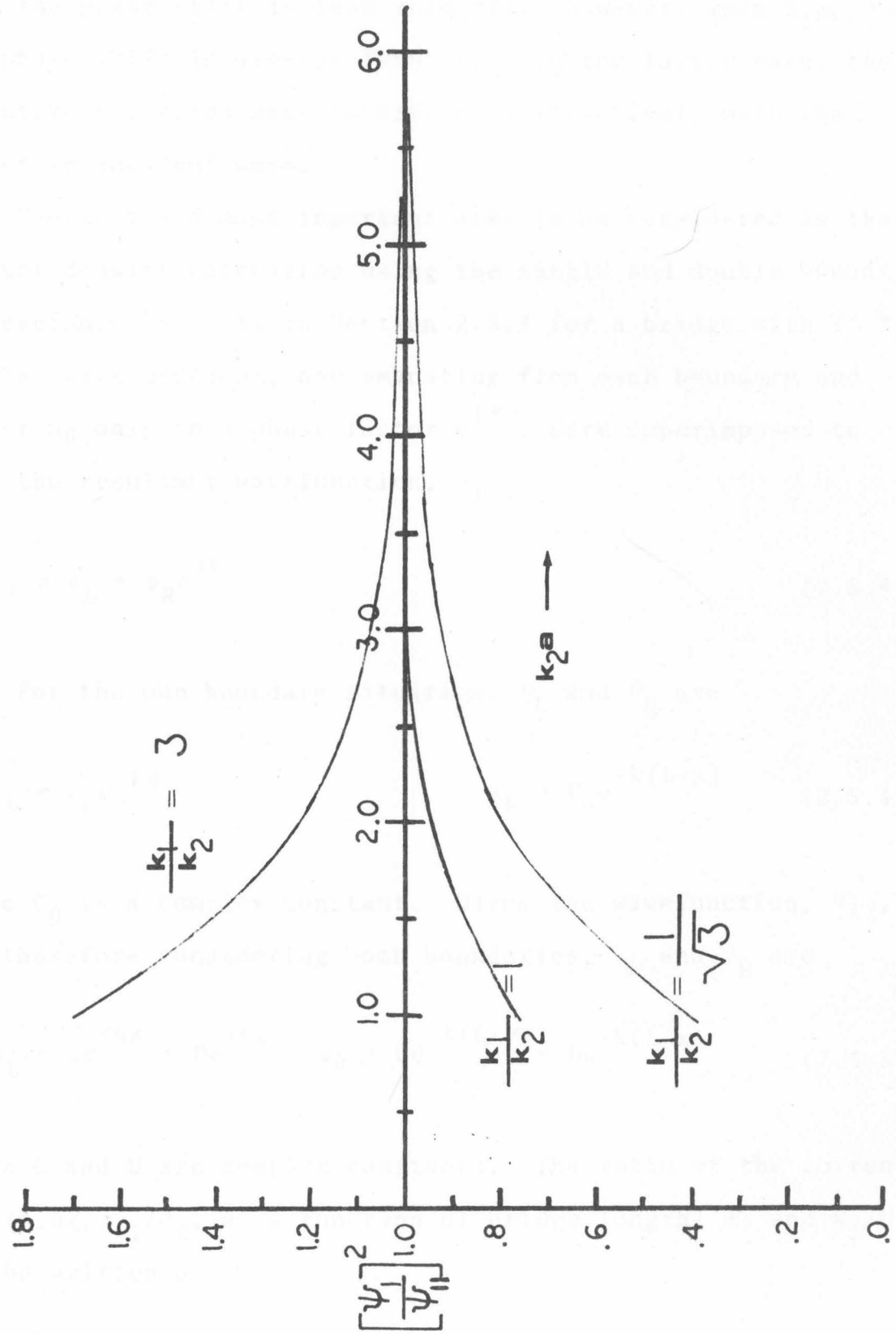
(through reflection) from the right. A solution for $|\psi_{II}|^2$, evaluated at x = a/2, is

$$|\psi_{II}\ (x=a/2)|^2 = \frac{2k_1^2}{(k_1^2 + k_2^2)\cosh k_2 a + (k_1^2 - k_2^2)} \qquad (2.5.47)$$

Figure 21 shows $|\psi_1/\psi_{II}|^2$ as a function of barrier length, a, for various values of k_1/k_2. When $|\psi_1/\psi_{II}|^2 = 1$, then the probability of finding a particle at x = a/2 for the single and double boundary is identical. When $|\psi_1/\psi_{II}|^2 < 1$, then the probability of finding a particle at x = a/2 is greater for the two boundary situation. However, when $|\psi_1/\psi_{II}|^2 > 1$, then the probability of finding a particle at x = a/2 is less for the two boundary case. Figure 21 shows that when $k_1/k_2 < 1$ the probability of finding a particle at x = a/2 is always greater in the two boundary situation. However, when $k_1/k_2 > 1$, the probability of finding a particle at x = a/2 is always smaller in the two boundary case. Stated another way, when $k_1/k_2 > 1$, any attempt to calculate the probability $|\psi_{II}(x)^2|^2$ or the transmission function using the single boundary probability, $|\psi_I|^2$, (as in the case of trying to superimpose S-N interface) will always lead to a result which is too large.

The behavior $|\psi_I/\psi_{II}|^2 > 1$ when $k_1/k_2 > 1$ can be understood by noting that, in effect, the wave reflected from the far (right) boundary interferes destructively with the incoming wave from the left. A solution of 2.5.46 for the constants C and D shows that the wave from the right boundary has

Figure 21 - $|\psi_I/\psi_{II}|^2$ as a function of barrier length, k_2a, for various values of k_1/k_2.


6.0
5.0
4.0
3.0
2.0
1.0
1.8
1.6
1.4
1.2
1.0
.8
.6
.4
.2
.0
$\left[\frac{\psi_1}{\psi_{1i}}\right]^2$
$k_2a \longrightarrow$
$\frac{k_1}{k_2} = 3$
$\frac{k_1}{k_2} = 1$
$\frac{k_1}{k_2} = \frac{1}{\sqrt{3}}$

a phase shift which is a function of k_1/k_2. When $k_1/k_2 < 1$, then the phase shift is less than $\pi/2$. However, when $k_1/k_2 > 1$, the phase shift is greater than $\pi/2$. In the latter case, the effective reflected wave interferes destructively with the effective incident wave.

The last and most important area to be considered is the current density calculated using the single and double boundary wavefunctions. As in Section 2.5.4 for a bridge with $T > T_N$, the two wavefunctions, one emanating from each boundary and differing only in a phase factor $e^{i\phi}$, were superimposed to form the resultant wavefunction, ψ_T

$$\psi_T = \psi_L + \psi_R e^{i\phi} \tag{2.5.48}$$

For the one boundary situation, ψ_L and ψ_R are

$$\psi_L = C_0 e^{-kx} \qquad \psi_R = C_0 e^{-k(L-x)} \tag{2.5.49}$$

where C_0 is a complex constant. Using the wavefunction, ψ_{II}, and therefore considering both boundaries, ψ_L and ψ_R are

$$\psi_L = Ce^{-kx} + De^{+kx} \qquad \psi_R = Ce^{-k(L-x)} + De^{+k(L-x)} \tag{2.5.50}$$

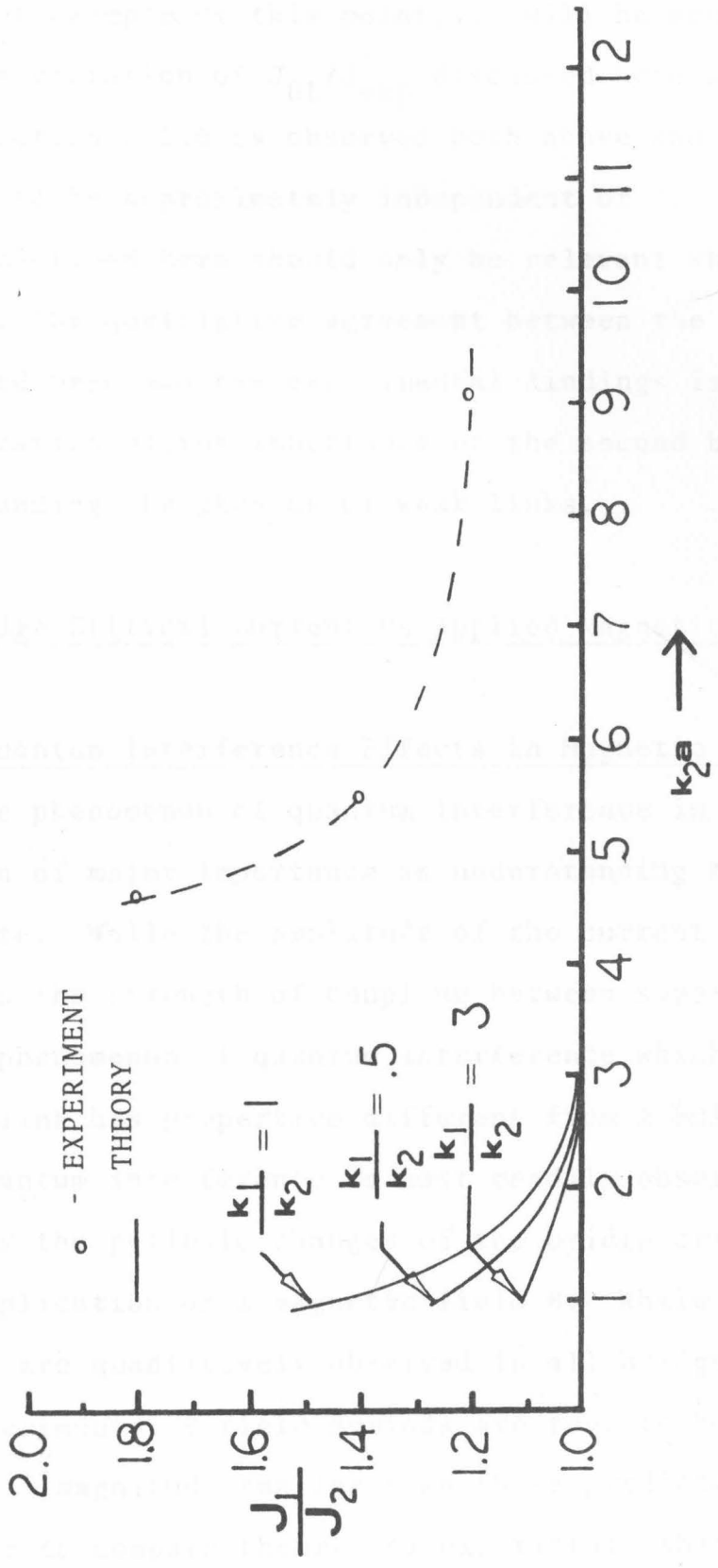
where C and D are complex constants. The ratio of the current densities, J_1/J_2, as a function of bridge length, a, and k_1/k_2 can be written as

$$\frac{J_1}{J_2} = \frac{4\left(\sinh^2 k_2 a + 4\left(\frac{k_1/k_2}{1 + k_1^2/k_2^2}\right)^2\right)e^{-2k_2 a}}{\left(1 - e^{-2k_2 a}\right)} \qquad (2.5.51)$$

and is plotted in Figure 22. As expected, the calculation using the one boundary wavefunction always predicts a current which is too large, that is, $J_1/J_2 > 1$. What is somewhat unexpected is that $J_1/J_2 > 1$ independent of whether k_1/k_2 is greater or less than 1. In all cases, as $k_2 a$ increases, J_1/J_2 is seen to approach one.

Comparison of this rather crude, highly linearized model to the physical situation of a weak link needs some examination. The simple model described here predicts that the theoretical critical current, J_1, calculated using a wavefunction, ψ_I, which considers only one boundary, will be larger than the experimentally determined value. The deviation will diminish as the bridge length increases. As an example of this point, Figure 22, shows the one boundary wavefunction critical current, J_{GL}, normalized with respect to the experimental critical current, J_{exp}, for set I, the Tantalum Ion implant bridges, plotted as a function of $k_2 L$, where $k_2 = 1/\xi_N$. The bridge critical current is evaluated at $\Delta T = .13^0 K$ from the bridge transition temperature, T_N. As can be seen, while the linearized model and J_{GL}/J_{exp} for set I show a similar trend, comparison of the two would seem to indicate that the bridges should have a decay length, ξ_N~5 times larger than presently determined. The deviation between theory and experiment is felt

Figure 22 - J_1/J_2 as a function of barrier length, k_2a, for various values of k_1/k_2. Also shown is J_{GL}/J_{exp} for Set 1, the Ta Ion implant bridges evaluated at $\Delta T = .13^0K$ from T_n


2.0
1.8
1.6
1.4
1.2
1.0
$\frac{J_1}{J_2}$
1
2
3
4
5
6
7
8
9
10
11
12
k_2a
° - EXPERIMENT
— THEORY
$\frac{k_1}{k_2} = 1$
$\frac{k_1}{k_2} = .5$
$\frac{k_1}{k_2} = 3$

to be due to the highly linear nature of the model used. As a further example of this point, it will be mentioned again that the variation of J_{GL}/J_{exp} discussed here and in the previous section 2.5.6 is observed both above and below T_N and appears to be approximately independent of T. The linear model described here should only be relevant when $T > T_N$. However, the qualitative agreement between the linear theory presented here and the experimental findings is felt to be an indication of the importance of the second boundary in understanding the physics of weak links.

2.6 Bridge Critical Current vs Applied Magnetic Field

2.6.1 Quantum Interference Effects in Magnetic Fields

The phenomenon of quantum interference in magnetic fields has been of major importance in understanding the superconducting state. While the amplitude of the current of a weak link reflects the strength of coupling between superconductors, it is the phenomenon of quantum interference which indicates that a weak link has properties different from a bulk superconductor. Quantum interference is most readily observed in weak links by the periodic changes of the bridge critical current upon application of a magnetic field B. While these modulation effects are quantitively observed in all bridges studies here, the experimental B field periods are seen to be between 1 and 2 orders of magnitude smaller than those predicted by theory. In order to compare theory and experiment, this section is

intended as an introduction to quantum interference effects in magnetic fields. As will be shown, quantum interference in magnetic fields stems directly from the requirement of gauge invariance.

In the previous section, for $T > T_N$, the critical current density, J_c, was shown to be proportional to sin $(\Delta\phi)$. In the absence of a magnetic field or voltage, $\Delta\phi$ is just the phase difference between the superconductors. In order to calculate the effect of a magnetic field on the behavior of a proximity effect bridge, two pieces of information are necessary. First, gauge invariance requires that the phase, ϕ, and vector potential, $\vec{A}$, be related by

$$\vec{A}' = \vec{A} + \vec{\nabla}\chi(x)$$
$$\phi = \phi_0 + \frac{2e}{\hbar}\chi(x) \qquad (2.6.1)$$

Second, the phase in the normal material is fixed by the boundary condition on the S-N interface (See Section 2.5.3). With this information, it is easy to show what the phase difference, $\Delta\phi$, is across a proximity effect bridge upon application of a magnetic field. Consider the bridge shown in Figure 1. If in S_1 at $x = 0$, $\phi = \phi_1$, and in S_2 at $x = L$, $\phi = \phi_2$, then the phase difference (with no magnetic field, $\vec{A} = 0$) is simply $\Delta\phi = \phi_2 - \phi_1$. If one were to perform a gauge transformation on the system, then, in S_1 at $x = 0$, $\phi_1' \rightarrow \phi_1 + \frac{2e}{\hbar}\chi_1(0)$, in S_2 at $x = L$, $\phi_2' \rightarrow \phi_2 + \frac{2e}{\hbar}\chi_1(L)$ and $\vec{A}' \rightarrow \vec{A} + \vec{\nabla}\chi$. It is easy to see, then, that gauge invariance requires that $\Delta\phi$ be

$$\Delta\phi = \phi_2' - \phi_1' + \frac{2e}{\hbar}\int_0^L A' \, dl \qquad (2.6.2)$$

which can be generalized for the case in which a magnetic field is present to be

$$\Delta\phi = (\phi_2 - \phi_1) + \frac{2e}{\hbar}\int_0^L A \, dl \qquad (2.6.3)$$

Defining j_0 as the prefactor to the sine term in expression 2.5.40-41 and explicitly expressing the phase term, the current density is

$$J_s = j_0 \sin\left(\Delta\phi + \frac{2e}{\hbar}\int_0^L A \, dl\right) \qquad (2.6.4)$$

In the presence of a magnetic field, the current through the bridge is found by integrating expression 2.6.4 across the width of the bridge, that is

$$I_s = j_0 t \int_{-w/2}^{w/2} \sin\left(\Delta\phi + \frac{2e}{\hbar} B_a L \, y\right) dy \qquad (2.6.5)$$

where B_a is the magnetic field applied perpendicular to the plane of the bridge, and t is the bridge thickness. The integration is simple and the final expression for the supercurrent as a function of a magnetic field is

$$I_s = j_0 tw \left(\frac{\sin\left(\frac{2e}{h} BL^* w\right)}{\frac{2e}{\hbar} B L^* w} \right) \sin \Delta\phi \qquad (2.6.6)$$

The maximum zero voltage current is written as[26,27]

$$I_c = I_0 \frac{\sin(2\pi n \phi_Q)}{(2\pi n \phi_Q)} \qquad (2.6.7)$$

Note that the modulation of the critical current has a periodicity of one flux quantum, $\phi_Q = h/2e$. Figure 23 shows the critical current as a function of applied magnetic field, B_a, for a typical proximity effect bridge of w = 25 μm and L = .5 μm. The most obvious observation is that the B field period is seen to be much less than ϕ_Q, in this case, ~ .025 ϕ_Q. It has been suggested (Notarys 1971)[28] that this effect is due to a distortion of the magnetic field by the surrounding superconducting film which concentrates the field in the bridge region. If this hypothesis is correct, then the B field period would be a strong function of the external film geometry.

This section will concentrate on two aspects of the B field modulation of the bridge critical current. The first area investigated is the effect of magnetic shielding by the surrounding superconducting film on the observed B field periodicity of the bridge. The second aspect investigated will be to compare bridges of differing length, composition, and fabrication for differences in the critical current modulation by a magnetic field.

2.6.2 The Effect of Film Geometry on Magnetic Field Period

In order to directly observe the effect of the demagnetization of the superconducting film on the behavior of a proxi-

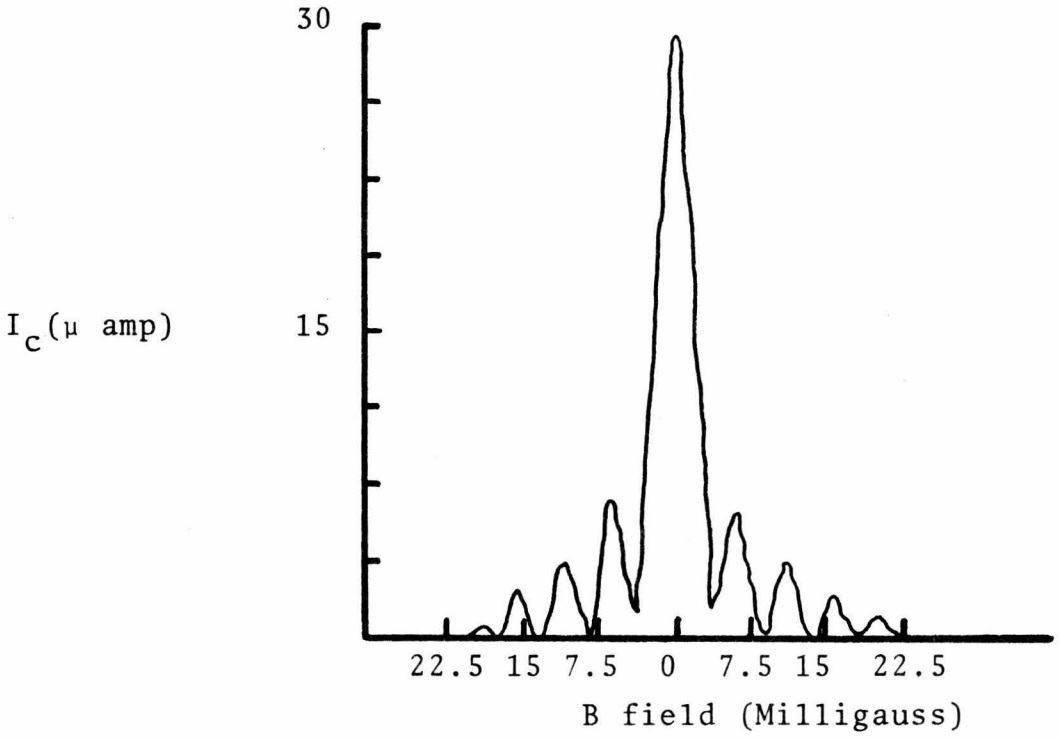
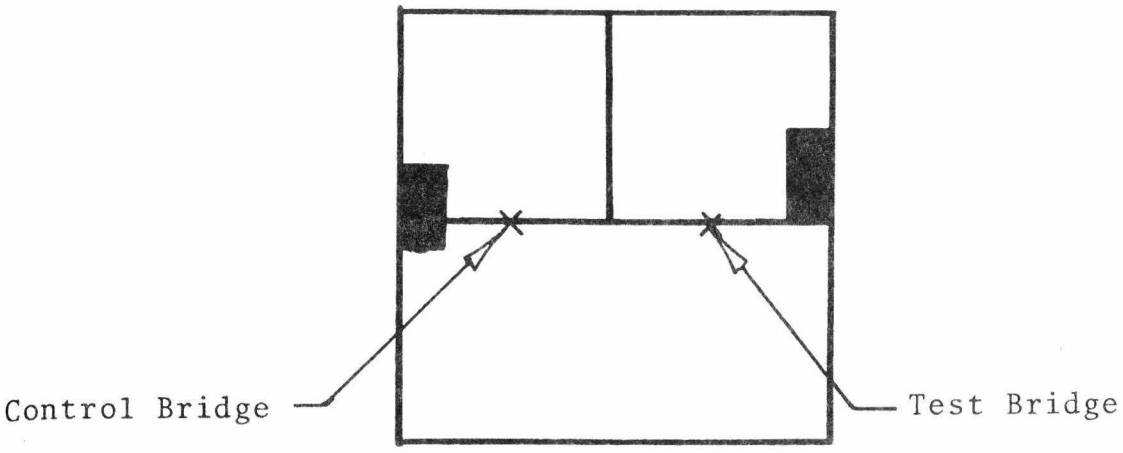


Figure 23 - Critical current as a function of applied magnetic field, B. The bridge, BS-14, is .5 μm x 25 μm. One should expect a period of 185 Mg while the observed period is approximately 5 mg.

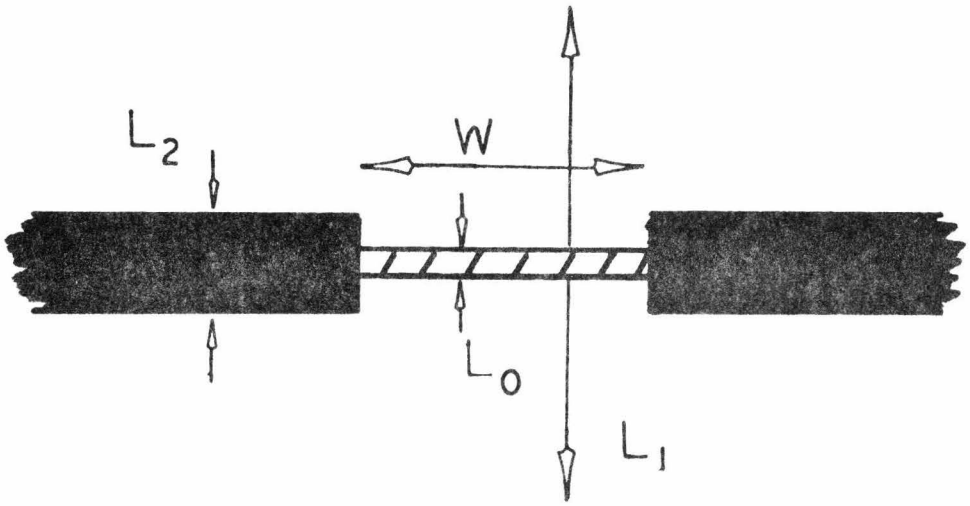
mity effect bridge, two bridges were placed on the same film in similar geometric surroundings. One of the bridges had the surrounding film geometry modified while the other bridge's surroundings remained unchanged. The B field period for each bridge was then recorded. Throughout these tests, the unmodified control bridge period was never observed to change. However, the test bridge period was observed to be a strong function of external film geometry.

Figure 24a shows test and control bridges with surrounding film geometry. The bridges were constructed by standard photolithographic-anodization techniques on a 1 inch square Nb/Ta film (156A^0 Nb/184A^0 Ta). The magnetic field was applied from a D.C. coil located around the superconducting film. The field from the coil was determined by first calculating its value at the film plane and then comparing with measurements made with a superconducting magnetometer. Agreement was found to be within 5%. In order to insure that the B field from the coil was uniform and did not affect the experimental results, the test bridges and film were moved and reoriented above the field coil and the periodicity of each bridge was remeasured. In no case was a difference in the B field period ever recorded. Therefore, for this test, the applied field was considered uniform across the film.

A generalized geometry of the test (control) bridge and external film geometry is outlined in Figure 24b. The dimension L_0 refers to the bridge length, L_2 to the film cutout dimension adjacent to the bridge and L_1 to the dimension over



(a)



(b)

Figure 24 - (a) TBS-10 A and B with surrounding film geometry. Dark lines and regions are where there is no film material. (b) Generalized film geometry of bridge and surrounding superconducting film.

which magnetic flux is shielded from the film. A further discussion on the determination of L_1 will be considered later. The first set of modifications to the external film geometry of the test bridge involved changing the bridge cutout width, L_2, and are shown in Figure 25. As can be seen, two types of cutout were used in this study. Figures 25a, b, d, f will be referred to as the square cutouts while Figures 25c and e will be referred to as the T-cutouts. The B field period for both bridges was recorded after each film modification and observed to be independent of temperature for small critical currents ($I_c < 100\mu$ amp) and small magnetic field (typically less than ~20 complete B field periods). The B field period for the control bridge was observed to be .42 milligauss regardless of the film modifications made to the test bridge. The resultant changes in the B field period as a function of modifications to the film cutout width, L_2, are shown in Figure 26. These data demonstrate one curious point: the B field period is not a simple function of the cutout width L_2, as can be seen by comparison of the square and T cutouts at 48 and 125μm. The B field period would appear to be more than a simple function of the local film geometry surrounding the bridge.

In order to insure that the B field period was a property of the surrounding film geometry of the test bridge and not a function of the film thickness, a 1 μm thick superconducting shield of Indalloy 11 (95% Pb, 5% In) was evaporated over the entire sample. The Indalloy film was then chemically etched so as to remove the shield from those regions which

Figure 25 - Test Bridge with Modification of Cutout Dimension, L_2.

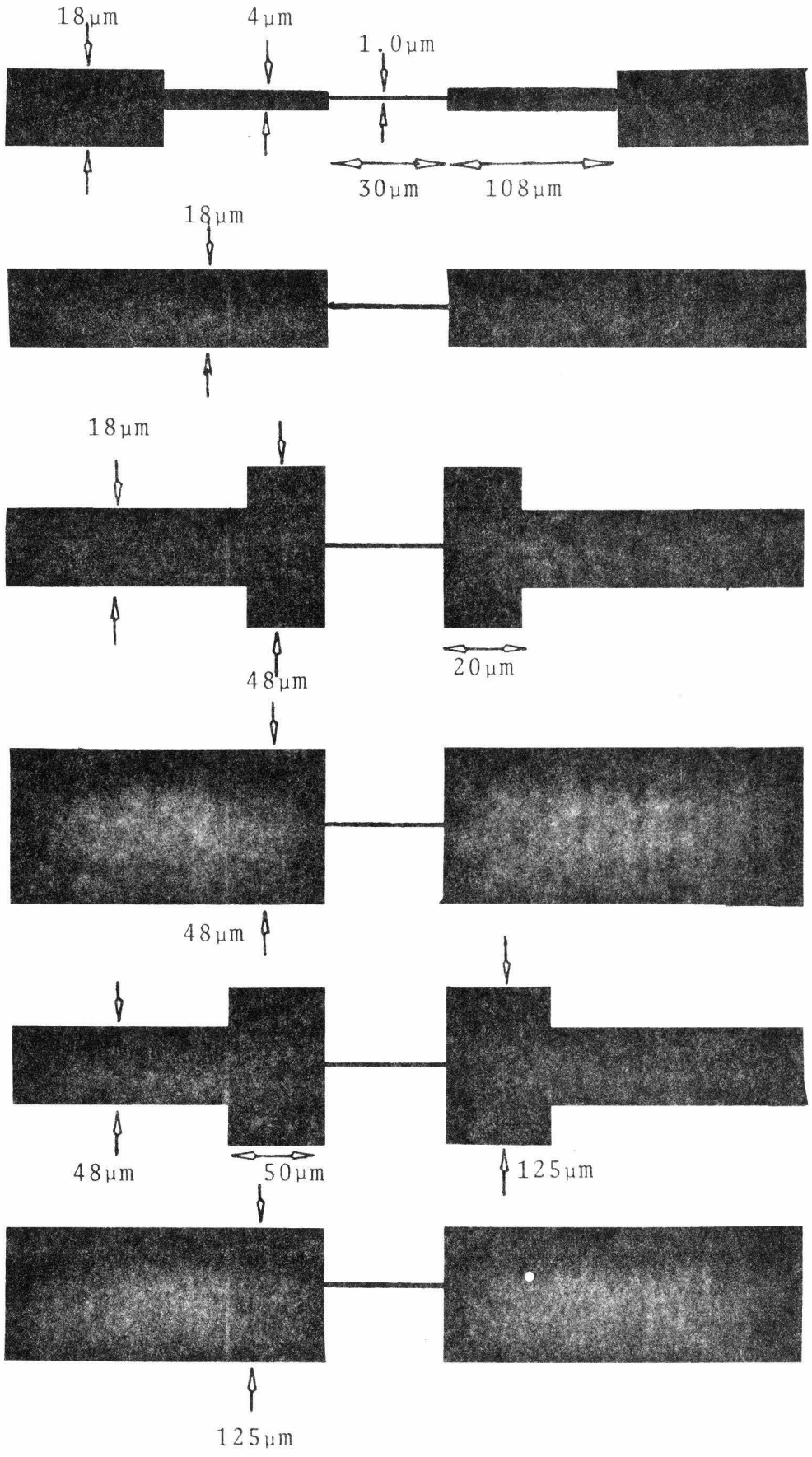
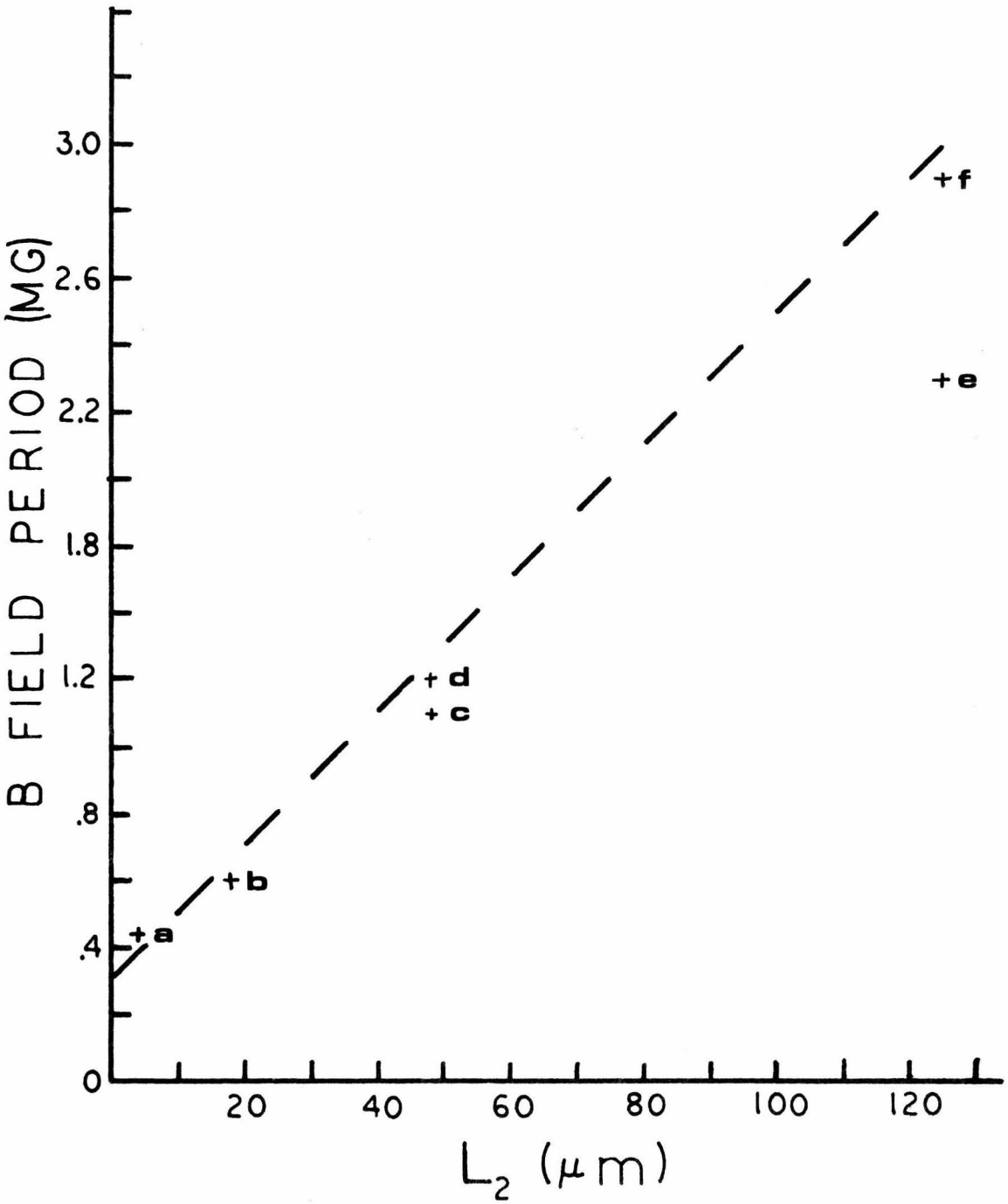

18μm
4μm
1.0μm
30μm
108μm
18μm
18μm
48μm
20μm
48μm
48μm
50μm
125μm
125μm

Figure 26 - Magnetic Field Period, B_p as a function of bridge cutout dimension, L_2. Points a, b, d, f refer to the square cutouts while points c and e are the T cutouts of Figure 25.


B FIELD PERIOD (MG)
3.0
2.6
2.2
1.8
1.2
.8
.4
0
20
40
60
80
100
120
L_2 (μm)
+a
+b
+c
+d
+e
+f

previously had the superconducting film removed, that is, the shield masked the existing film. The B field period was then rechecked and found to be unchanged for both test and control bridges. This indicates that the effect is not due to flux penetration into the film. The Indalloy shield was then removed entirely.

The final set of modifications to the external film geometry of the test bridge involved changing the film dimension, L_1 (Figure 24b). As before, the B field period was recorded for both bridges after each film modification (See Figure 27). The B field period as a function of the cutout dimension L_1 for the test bridge is shown in Figure 28. As can be seen the B field period again appears to be a strong function of the external film geometry.

One last remark about these data. As has been mentioned, the B field periods reported here were taken for small applied fields and, to within experimental error (± .05 MG), appear to be constant in this limit. For all geometries investigated, however, as the applied field is increased there appears a threshold level at which the B field periodicity was observed to increase, that is, the B field periodicity then becomes a function of the applied field. This effect was observed in all samples and geometries investigated.

2.6.3 Discussion of Results

The experiments discussed in the previous section describe the use of proximity effect bridges as magnetometers to determine the influence of the surrounding film geometry on

Figure 27 - TBS-10A - Film modification of L_1 (not to scale).

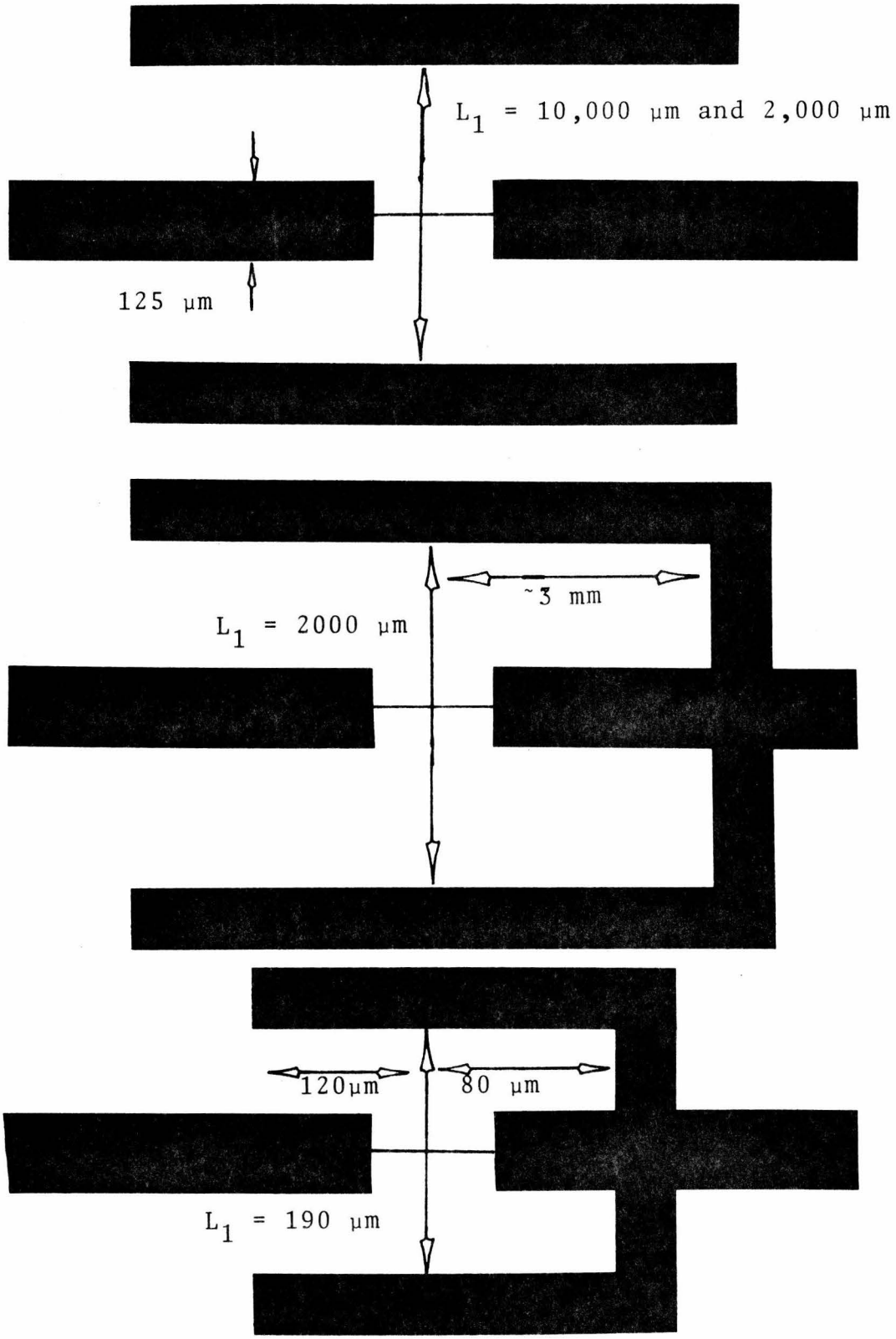
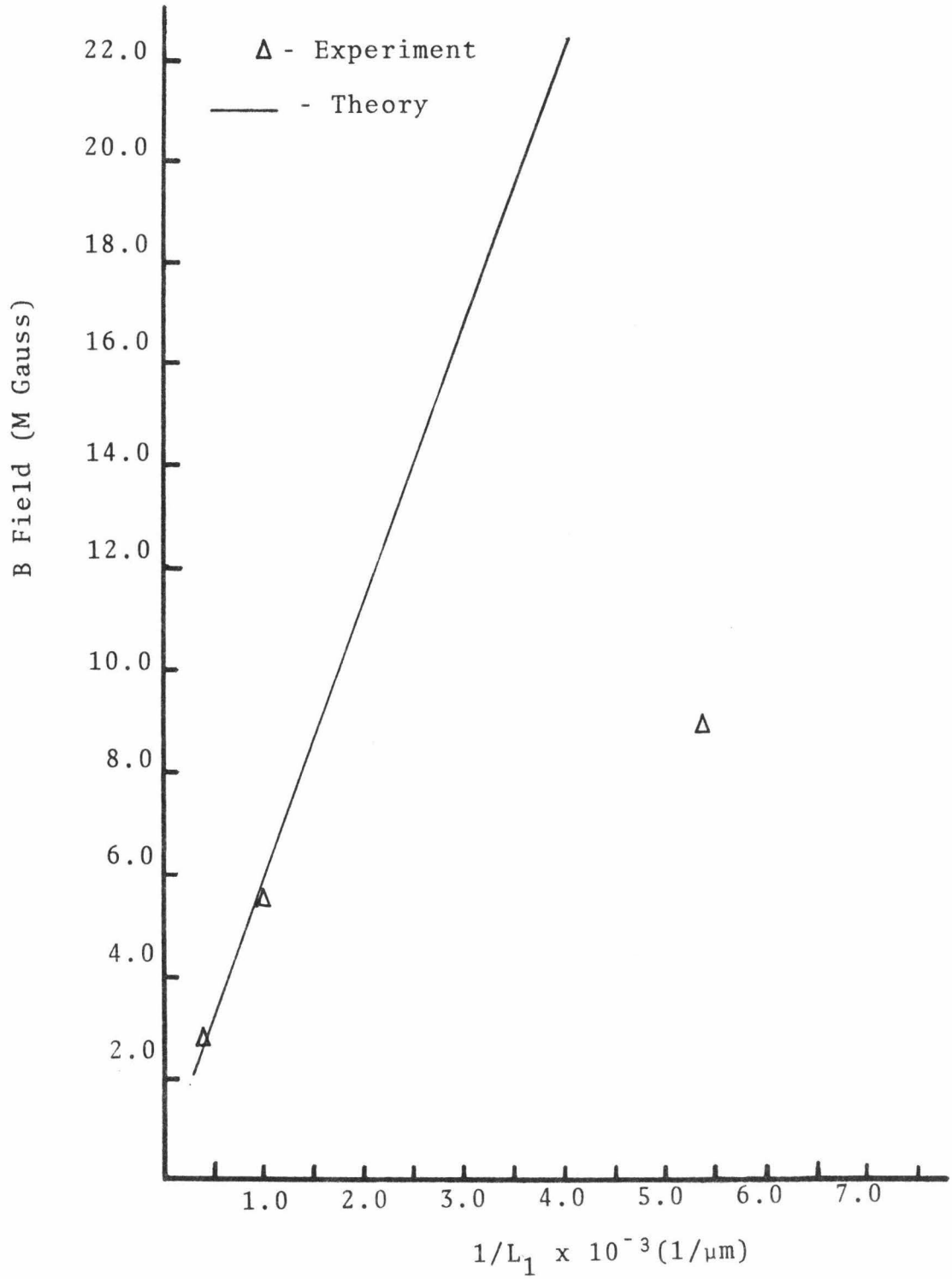

L_1 = 10,000 μm and 2,000 μm
125 μm
L_1 = 2000 μm
~3 mm
120μm
80 μm
L_1 = 190 μm

Figure 28 - B field period, B_p, as a function of film dimension $1/L_1$.


Δ - Experiment
——— - Theory
B Field (M Gauss)
22.0
20.0
18.0
16.0
14.0
12.0
10.0
8.0
6.0
4.0
2.0
1.0
2.0
3.0
4.0
5.0
6.0
7.0
1/L1 x 10-3(1/μm)

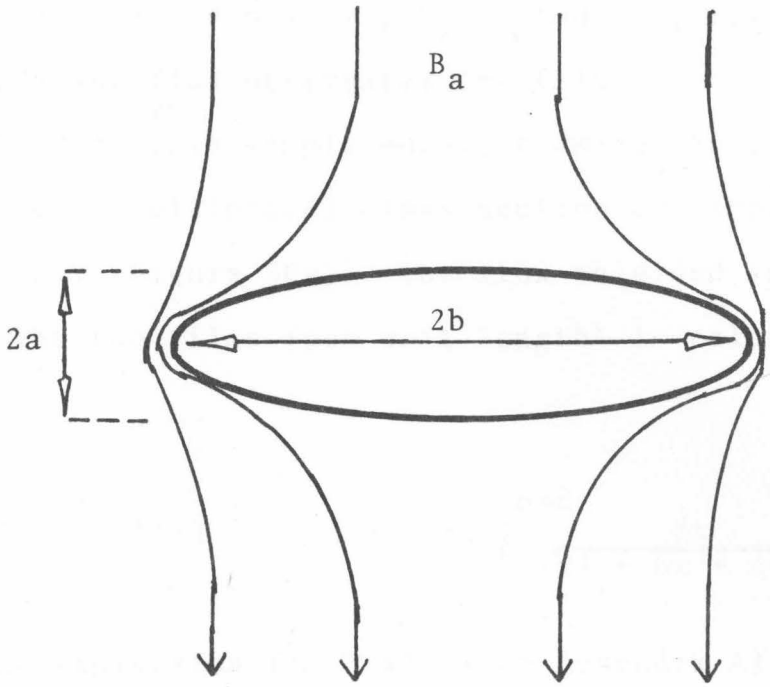
the flux present in the bridge. Ideally, an analysis of this work should begin with Maxwell's and London's equations and consider the shielding of the magnetic field by the superconducting film. While numerical calculations of the demagnetization of the superconducting film can be made for each specific film geometry, some general arguments permit an approximate solution for simple geometries. Therefore, in this section a simple model is proposed which, while not intended to be rigorous, does describe the salient features of the observed B field periodicity.

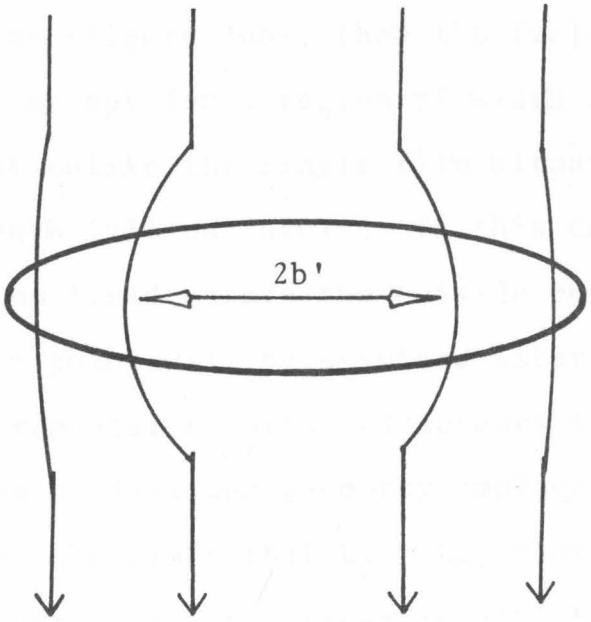
The first topic to be discussed is the general features of the shielding of the magnetic field from superconducting thin films and how the film dimension L_1 is determined.

Consider the simple situation shown in Figure 29 of a strip superconductor of elliptical cross section with width 2b and thickness 2a. If a B field, B_a, is applied perpendicular to the strip and the strip length, L, is much greater than the width, 2b, then the field should be shielded out in the narrowest direction, that is, to the nearest edge. The field will be excluded as long as the field at the film edge, B_e, is less than H_{c1}. If B_0 were to exceed H_{c1}, the field would penetrate the film except for a region of width 2b', where the field is excluded (Figure 29b). The field at the film edge, B_e, has been considered in Appendix A and shown to be

$$B_e = (1 + b/a)\, B_a \qquad (2.6.8)$$

Figure 29 - (a) A superconducting film of elliptical cross section of width 2b and thickness 2a. A magnetic field applied perpendicular to the film is shielded from the film as long as the field at the edge, B_e, is less than H_{c1}.
(b) The same superconducting film but B_e has exceeded H_{c1} at the edge and the field has penetrated the film. The B field is still excluded from a region of width 2b' near the film center.


B_a
2a
2b


2b'

One can see that as $b/a \to \infty$, B_e exceeds H_{c1} for even the smallest fields and flux penetrates the film.

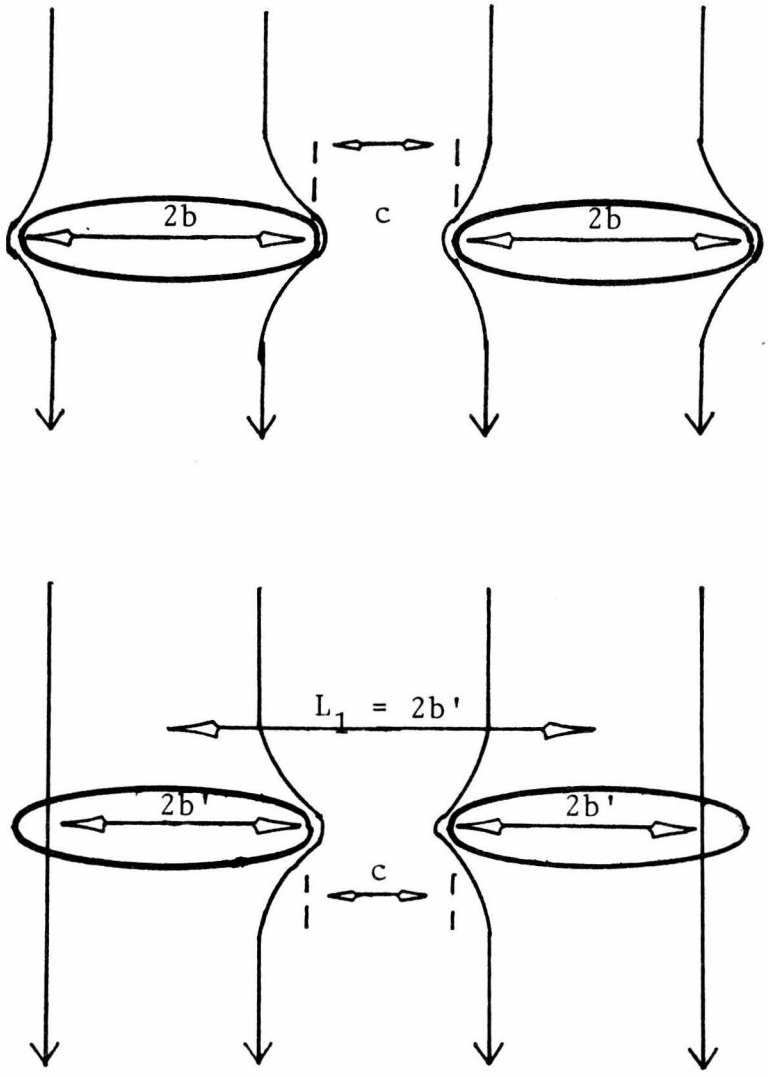
Extending this simple model, examine the case where identical films of elliptical cross section are separated by some dimension, c (Figure 30a). The flux shielded into the gap between the two films (per unit length) is calculated as

$$\Phi = 2\int_0^{b+c} B(x)\,dx = 2(a+b)B_a \int_0^{b+c} \frac{dx}{\sqrt{x^2 + bx + a^2}} \qquad (2.6.9)$$

where the expression for B(x) (from Appendix A) for a single film has been used. Note, that B_e at the inside edges still must be less than H_{c1}. However, if $B_e > H_{c1}$ at the outside edges of two films (Figure 30b), then the field should penetrate both films except for a region of width 2b' in each film. Note, that unlike the single film situation, the flux does not enter each film uniformly. In this case it is suggested that the field enters the outside edge of each film first. This point will be examined later in the discussion of the experimental results and appears to be substantiated.

Consider the bridges and geometry employed in this study and in particular the limit that $L_2 \to L_0$, that is, the cutout dimension, L_2, approaches the bridge length, L_0. This is similar to the situation described by 2.6.9 where B_a is identifield as B_p and b is b'. Expression 2.6.9 is used to determine L_1 for the first set of tests. Note that L_1 in these tests is identified as 2b' in the previous discussions. The

Figure 30 - (a) Two identical superconducting films of elliptical cross section of width 2b and separation c. A magnetic field applied perpendicular to the film is shielded from both films as long as the field at the edge, B_e, is less than H_{c1}. (b) The same superconducting films but B_e has exceeded H_{c1} at the outside film edges and flux has penetrated the films. The B field is still excluded from a region of width 2b' in each film, however, the B field does not enter the films uniformly.


2b
c
2b
$L_1 = 2b'$
2b'
2b'
c

intercept of the B vs L_2 in Figure 26 as $L_2 \rightarrow L_0$ is B_0=.3 milligauss. Using expression 2.6.9, this corresponds to a value of L_1 = 2200 μ. Once L_1 has been determined, a description of the magnetic field between the two films must be found.

For the modifications of the bridge cutout dimension, L_2, the length L_1 does not change. The effective B field, B_{eff}, between the two main films is modeled to be constant between the two main superconducting films enhanced by a factor of $\sim L_1/L_2$ over the applied field, B_a. Near the bridge, the effective magnetic field, B_{eff} has two areas to be shielded to, out either side of the film or into the bridge (Figure 31). Therefore, near the bridge the magnetic field within the area outlined in Figure 31 is expelled into the bridge. Thus, the flux in the bridge region is

$$\Phi = B_{eff} \frac{w^2}{2} = B_a \, (L_1/L_2) \frac{w^2}{2} \qquad (2.6.10)$$

Solving for B_a and identifying this as the measured B field period, B_p, (when $\Phi = \phi_Q$, one flux quantum), this expression is combined with the intercept B_0 when $L_2 \rightarrow L_0$ to give the B field period as a function of surrounding film geometry (that is, L_1 and L_2).

$$B_p = B_0 + \phi_Q \, (L_2/L_1)(2/w^2) \qquad (2.6.11)$$

From this expression, it is obvious that B_p should vary linearly with the cutout dimension L_2 and invesely with L_1.

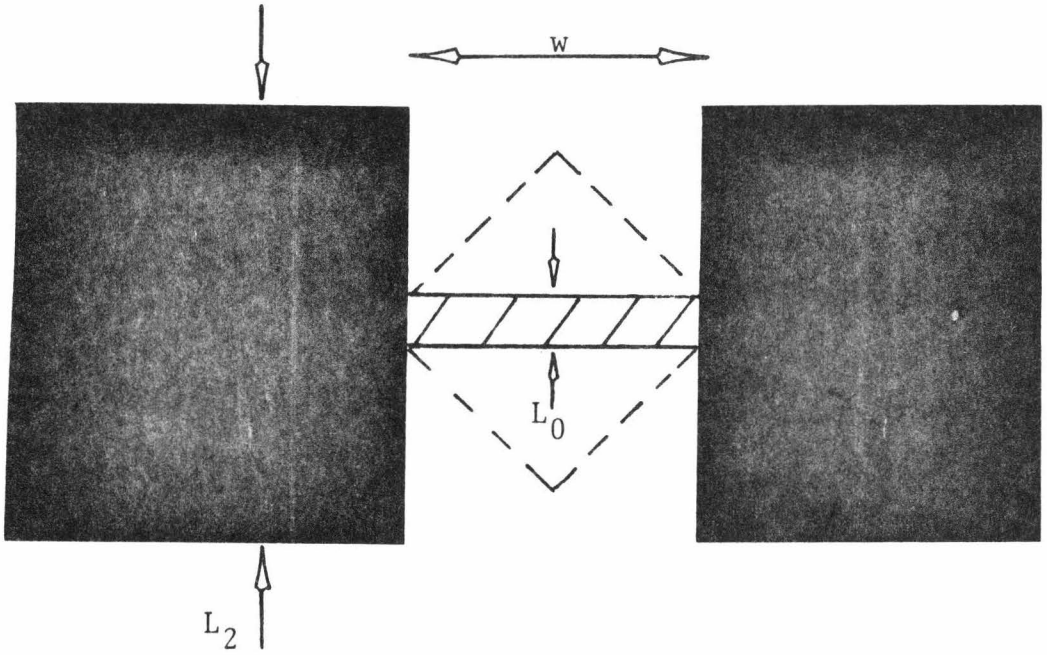


Figure 31 - The effective area of the bridge is outlined in the above figure and modeled to be $w^2/2$. Since the leads to the bridge are superconducting, the magnetic field is modeled to be shielded to the nearest edge. Therefore, the flux in the bridge is $\Phi = B_{eff}\, w^2/2$.

A comparison between expression 2.6.11 and experiment as a function of the cutout dimension, L_2, is seen in Figure 26. The theoretical B field period, B_p, is seen to closely approximate the experimental data for the square cutout geometry.

The experiments on the film dimension, L_1, need some discussion. Expression 2.6.11 indicates that the B field period, B_p, should vary inversely with L_1. The film length, L_1, was first modified so that $L_1 = 1000\,\mu$, and is shown in Figure 27a. No change in the B field period was observed. One would not expect to observe a change in the B field period since there is no way for the flux to enter the anodized (normal) region unless $B_e > H_{c1}$. When the geometry was modified so that the normal region extended to an edge (Figute 27b), a change B_p was observed. The change indicated a response that varies inversely as L_1. The last cut (Figure 27c) also showed an increase in period, but not as large as anticipated. It should be pointed out, however, that unlike the other modifications made, the last film cut did not preserve the one-dimensionality of the bridge with respect to the surrounding geometry. A similar result was observed earlier in a comparison between the T shaped and square cutouts.

One last remark on the final observation in these experiments. The applied B field at the inside film edge, B_e, in all of these discussions is modeled never to exceed H_{c1}. If the B field is increased such that $B_e > H_{c1}$ at the inside edges of the films, one would expect that the B field period would increase since not all of the B field is being expelled

from the superconducting films into the cutout region.

As has previously been mentioned, for all bridges and geometries investigated, application of a large enough B field results in an increase in the observed periodicity, B_p, which is in agreement with the proposed model.

2.6.4 Critical Current vs Applied Magnetic Field - Comparison between Bridges

The general features for two typical bridges of the critical current as a function of applied magnetic field for two different lengths is shown in Figures 32-33. The degree of modulation in the sets of bridges studied was seen to decrease as the bridge length increased and as T_N/T_F decreased. No significant difference was seen between anodized bridges on different film materials or between anodized and ion implant samples. All samples exhibited the usual diffractionlikebehavior. The loss of critical current modulation as a function of increasing critical current has been examined for the case of wide Josephson Junctions[29] and attributed to shielding currents in the junction itself. While a similar loss of critical current modulation with increasing critical current is observed, it is the opinion of the author that the mechanism here is entirely different. Since the modulation of the critical current by a B field is a direct result of the gauge invariance of the phase, for the critical current to be sensitive to the phase, it must be proportional to sin ϕ and, has been dis-

Figure 32 - Percent modulation of the critical current as a function of the applied magnetic field, B, for the .5 μm BS-24 bridge for various critical currents.

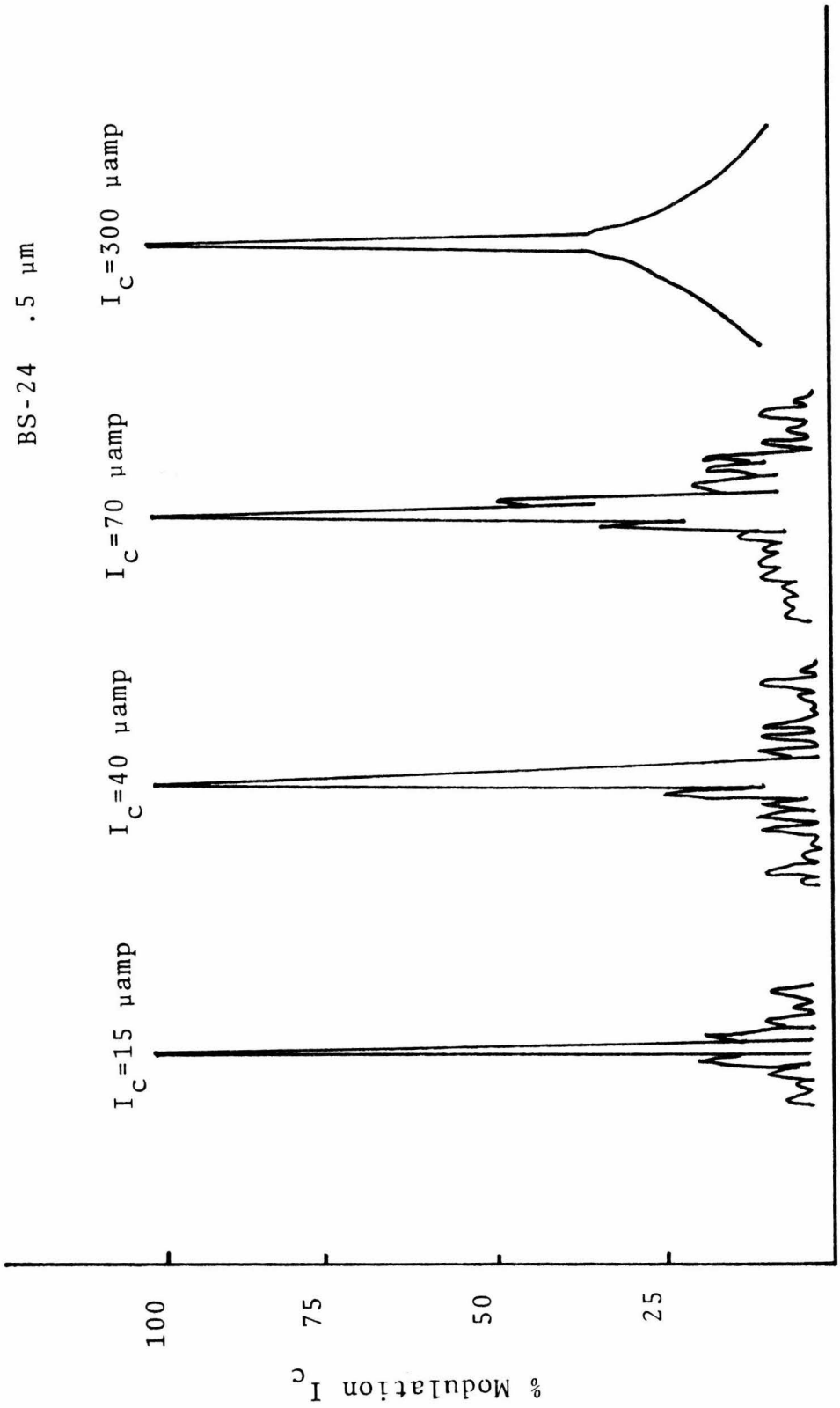
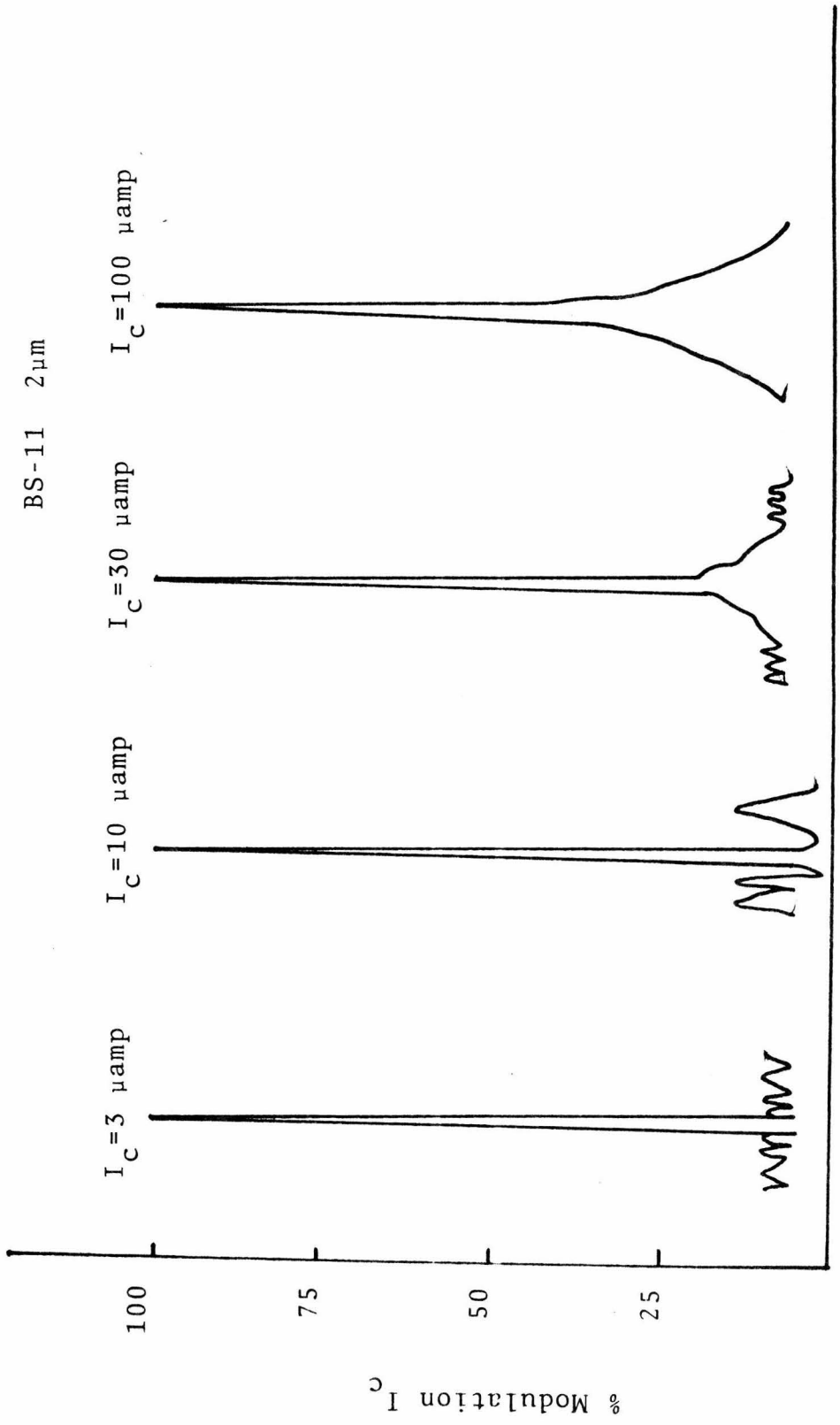

BS-24 .5 µm
I_c=15 µamp
I_c=40 µamp
I_c=70 µamp
I_c=300 µamp
100
75
50
25
% Modulation I_c
B Field →

Figure 33 - Percent modulation of the critical current as a function of the applied magnetic field, B, for the 2.0 μm BS-11 bridge for various critical currents.


BS-11 2μm
I_c=3 μamp
I_c=10 μamp
I_c=30 μamp
I_c=100 μamp
100
75
50
25
% Modulation I_c
B Field →

cussed in the previous section, should only occur when $T > T_N$. Below the bridge transition temperature, T_N, the critical current is seen to vary as the gradient of the phase, that is, $I_c \propto \nabla\phi$. Therefore, the loss of critical current modulation as a function of increasing critical current (decreasing temperature) is a natural consequence of the critical current becoming proportional to $\nabla\phi$. Proof of this point is not possible (or very difficult at best) by observing the behavior of the B field modulation as a function of temperature.

III. R.F. RESPONSE OF PROXIMITY EFFECT BRIDGES

3.1 Introduction

The preceding discussion has dealt with the steady state (equilibrium) properties of proximity effect bridges. In this chapter, one of the nonequilibrium properties, the rf response, will be investigated. The usual method employed in analyzing the rf response of weak links is to combine the phase dependent supercurrent, $I_s = I_p \sin \Delta\phi$, with the Josephson relation[1]

$$\frac{d}{dt}(\Delta\dot{\phi}) = \frac{(\mu_1-\mu_2)}{\hbar} = \frac{2eV}{\hbar} \qquad (3.1.1)$$

which relates the time evolution of the phase difference to the chemical potential difference $(\mu_1-\mu_2)$ between the two superconductors. While expression 3.1.1 has been justified for a Josephson (tunneling) junction, it has never explicitly been justified for the case of a weak link where the wavefunction and chemical potential are position dependent. Therefore, it seems reasonable to digress for a moment and consider the validity of 3.1.1 before employing it in the analysis of the rf response of proximity effect bridges.

Consider the case of a tunnel junction. The time dependence of the wavefunction in each respective superconductor is given by

$$\frac{d\psi}{dt}_{L,R} = \frac{-i\mu}{\hbar}_{L,R}\,\psi_{L,R} = i\dot{\phi}_{L,R}\,\psi_{L,R} \qquad (3.1.2)$$

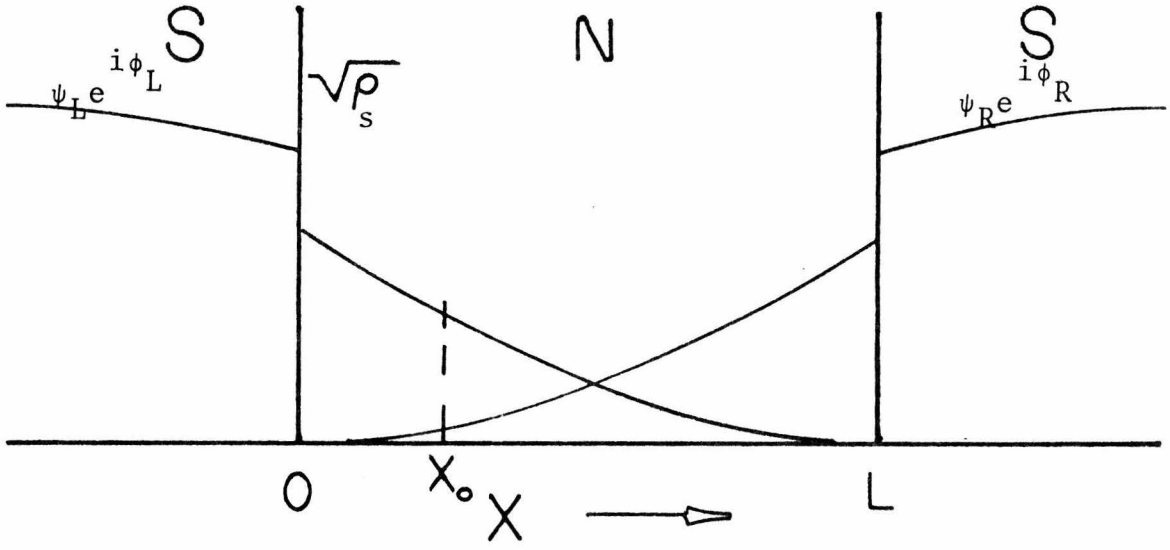
where the subscripts L and R denote the left and right superconductors. For a tunnel junction, the chemical potential in each superconductor is independent of position and the time evolution of the phase difference, $\Delta\phi$, is given by 3.1.1.

The physical situation for a proximity effect bridge is somewhat more complex. In figure 1 , the bridge is modeled to behave as two overlapping wavefunctions, $\psi_n = \psi_R e^{i\phi_R} + \psi_L e^{i\phi_L}$. In the equilibrium case ($\mu_L=\mu_R$), the two phase concept for ψ_n implies that when a supercurrent flows a pair in the bridge transfers between state L and R at some position x_0. If the superconductors are driven out of equilibrium ($\mu_L \neq \mu_R$), the chemical potential, μ, in the bridge region becomes a function of position. Since the chemical potential at x_0 is identical for both ψ_L and ψ_R, by expression 3.1.2 one would not expect to have a second Josephson relation (3.1.1) since $d(\phi_L-\phi_R)/dt$ is identically zero. A model of the type described here would predict dc quantum interference effects but would forbid ac quantum interference effects. This does not correspond with the experimental situation since ac quantum interference effects are observed in proximity effect bridges.

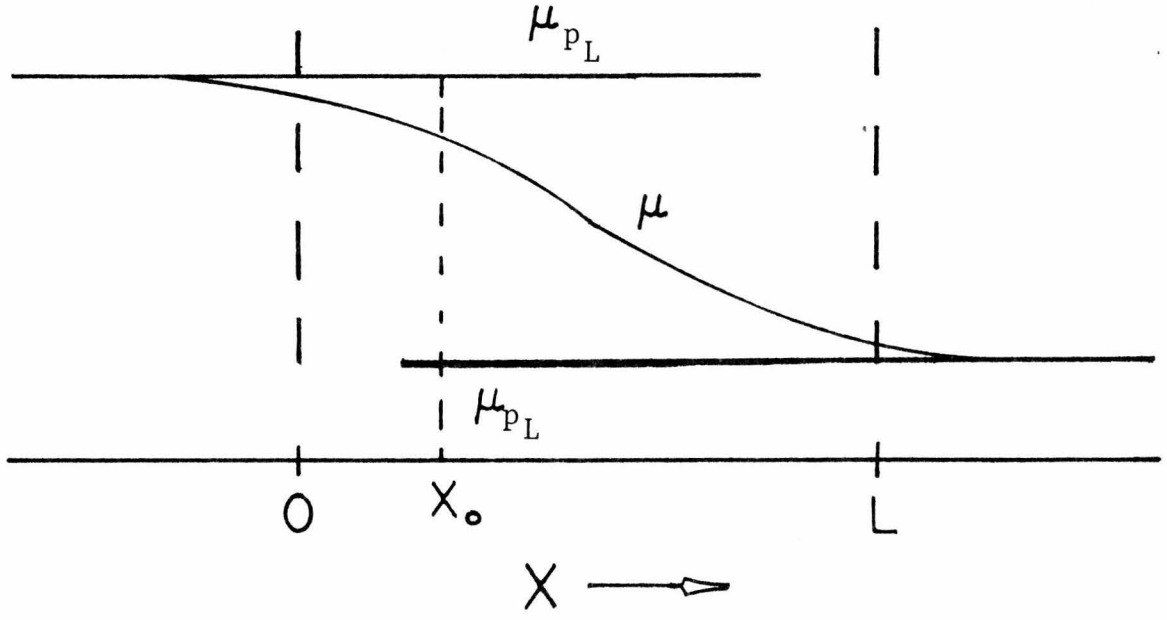
This difficulty can be overcome by expanding upon the model presented in the last chapter for the behavior of the phase of the wavefunction on both sides of an S-N interface. In the steady state, the phase in both the super and normal materials was assumed to be continuous ($\phi_S(-0)=\phi_n(+0)$ at the interface and that no phase gradients existed in either material

Figure 1 - (a) Proximity Effect Bridge in which the wavefunctions in the normal region is modeled as a linear superposition of overlapping wavefunctions, $\psi_n = \psi_{Rn} e^{L\phi R} + \psi_{Ln} e^{1\phi L}$.

(b) Pair and chemical potential distribution in a proximity effect bridge in the non-equilibrium case.


S
N
S
$\psi_L e^{i\phi_L}$
$\sqrt{\rho_s}$
$\psi_R e^{i\phi_R}$
0
X_o
X
L

(a)


μ_{p_L}
μ
μ_{p_L}
0
X_o
L
X

(b)

($\nabla\phi_s = \nabla\phi_n = 0$). For the nonequilibrium case, the time evolution of the phase in the superconductor, $\dot{\phi}_s$, is independent of position even when a gradient in the chemical potential, $\nabla\mu_s$, exists. The time dependence of the wavefunction, ψ_s, in the superconductor is found to be

$$\frac{d\psi_s}{dt} = -i\frac{\mu_p\psi_s}{\hbar} = i\dot{\phi}_s\psi_s \qquad (3.1.3)$$

where μ_p is defined as the pair potential and is independent of position. Far away from the S-N boundary where the chemical potential is constant, $\mu_p=\mu_s$.

The assumption is now made that in the nonequilibrium case the phase at an S-N interface is continuous, that is $\phi_s(-0)=\phi_n(0)$. If no phase gradients exist in the normal material, the time evolution of the phase in the normal material is then $\dot{\phi}_s=\dot{\phi}_n$. The concept of a pair potential that does not vary spatially has been investigated experimentally and appears to be justified.[2]

Thus, for Figure 1b, where the superconductors are not in equilibrium, the time evolution of $(\phi_L - \phi_R)$ is

$$\frac{d}{dt}(\phi_L - \phi_R) = \frac{\mu_{p_L} - \mu_{p_R}}{\hbar} = \frac{(\mu_L - \mu_R)}{\hbar} = \frac{2eV}{\hbar} \qquad (3.1.4)$$

Note that while 3.1.4 gives the same final result as 3.1.1, the assumptions behind it are entirely different. The behavior, as predicted by 3.1.4, appears to be in agreement with

the experimentally observed ac quantum interference effects in proximity effect bridges.

The work discussed here describes investigations into the behavior of the phase dependent supercurrent, I_s ($=I_p \sin \Delta\phi$), for the nonequilibrium situation. Previous studies[3] have indicated that the prefactor term, I_p, varies from approximately $I_p \sim I_c$ to $I_p \sim .2I_c$. I_p has also appeared to be frequency and temperature dependent. This study was undertaken in an attempt to determine the amplitude and functional dependence of I_p. In order to have some framework to compare the rf response, the experimental results are related to the resistivity shunted junction (RSJ)[4] model of a weak link. For the RSJ model, the supercurrent is modeled as $I_s = I_p \sin \Delta\phi$, where the prefactor term, I_p is independent of frequency and equal to the critical current, I_c, of the weak link.

3.2 Resistivity Shunted Junction (RSJ) Model

Changes in the I-V characteristics of weak links induced by low levels of microwave radiation have been extensively analyzed in the literature by the resistively shunted junction (RSJ) model. In the RSJ representation, the weak link is replaced by an ideal Josephson element (with a sinusoidal current-phase relation of $I_s = I_c \sin \Delta\phi$) shunted by a normal resistor, R. The weak link is current biased since the impedance of the entire circuit used in these studies is much greater than the impedance of the bridge itself. The total current, I_T, through the bridge is assumed to be a linear combination of super and

normal components and is written as

$$I_T = \frac{V}{R} + I_s \qquad (3.2.1)$$

where V is the voltage and R is the resistance of the bridge. Expression 3.2.1 is used to calculate the size of rf induced step widths on the bridge I-V curves when the link is irradiated at microwave frequencies.

Consider a bridge which is irradiated with microwave radiation of frequency ω_μ. Since the impedance of the link is small compared to the rest of the test circuit, this is equivalent to impressing a current $I_\mu \sin \omega_\mu t$ across the bridge. The time dependent voltage, V(t) developed across the bridge is

$$V(t) = R(I + I_\mu \sin \omega_\mu t - I_s(t)) \qquad (3.2.2)$$

where I is the bias current. This can be rewritten, including the time dependence of the supercurrent term as

$$V(t) = R(I + I_\mu \sin \omega_\mu t - I_c \sin (\phi_0 + \int V(t)dt)) \qquad (3.2.2b)$$

The problem of calculating the step size of a weak link reduces to obtaining the time average supercurrent, I_s, through the bridge using 3.2.2. The width of the rf induced step on the I-V curve of a weak link has been calculated using 3.2.2 and found[4,5] to be

$$\Delta I_n = 2I_c J_n \left(\frac{2eI_\mu R}{\hbar\omega_\mu}\right) = 2I_c J_n \left(\frac{V_{RF}}{V_\mu}\right) \qquad (3.2.3)$$

where $I_\mu R \equiv V_{RF}$ and $\hbar\omega/2e \equiv V_\mu$.

In the limit where $2eI_c R/\hbar\omega_\mu << 1$, computer solution (Russer, 1972)[6] of expression 3.2.2 indicates that the step widths given by 3.2.3 are valid up to the limit $I_c R = \hbar\omega_\mu/2e = V_\mu$. When $V_\mu < I_c R$, the sensitivity and maximum step size decreases. This point has experimentally been verified in the low frequency (~1 GHz) limit for various types of weak links.

3.3 R.F. Response of a Proximity Effect Bridge As a Function of Frequency, Temperature and Applied R.F. Power.

Investigations of the rf response of bridges were made for applied microwave radiation between 1 GHz and 10 GHz. Since all of the experimental results were compared with a supercurrent assumed to vary as sin ($\Delta\phi$), the temperature range investigated was limited to the region $T > T_n$. The reason for limiting this study to the temperature range $T > T_n$ is obvious when one considers that when $T < T_n$, the bridge behaves as two superconductors connected by a third superconductor with $I_s \propto \nabla\phi$. Experimentally, these two temperature regions could be distinguished by the onset of hysteresis in the I-V curve of the bridge (Figure 2). When T decreased below T_n, hysteresis was observed in the I-V curve of all bridges in this study.

In this study, the maximum size of the rf induced steps was compared with the bridge critical current as a function of bridge length, frequency, temperature and applied rf power.

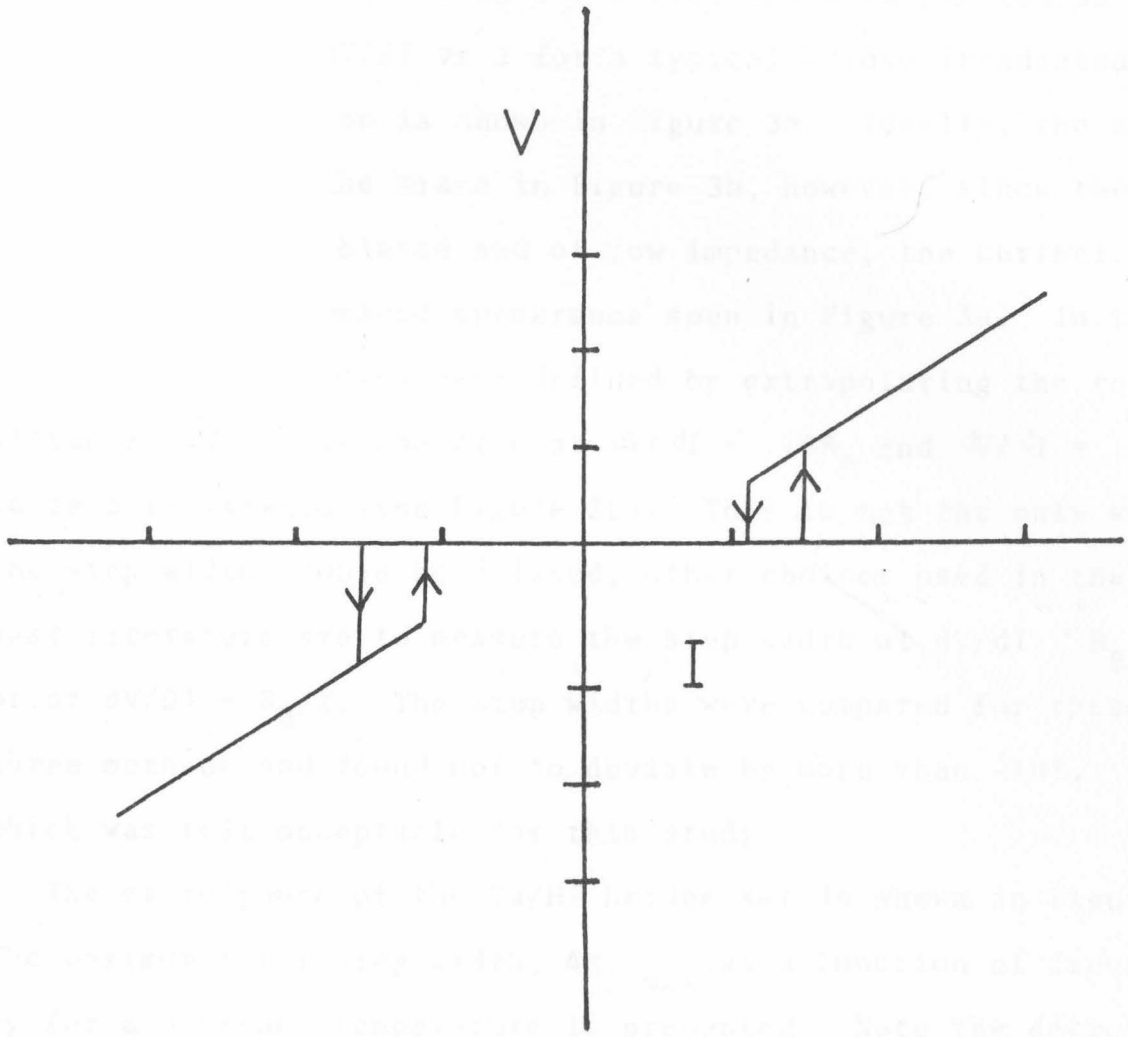


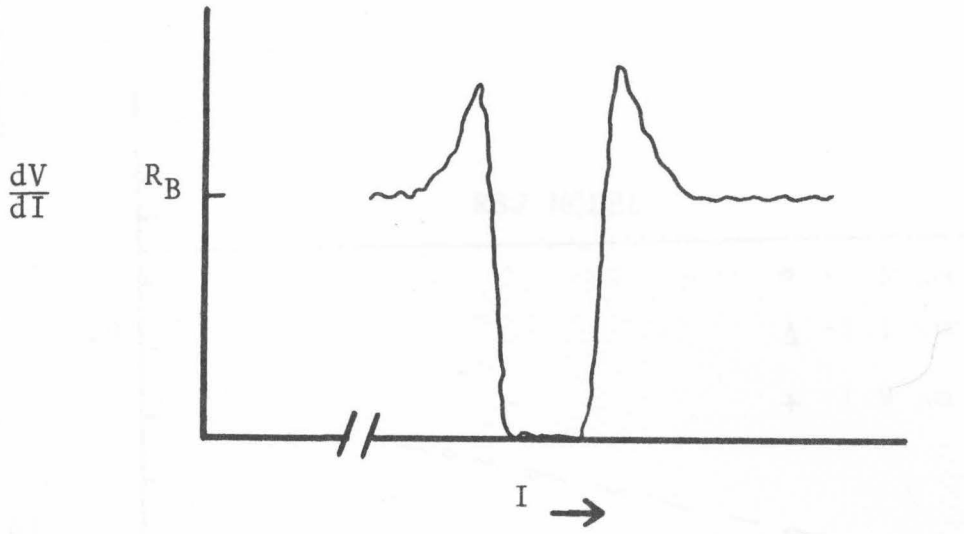
Figure 2 - I-V curve of a bridge exhibiting hysteresis. The onset of hysteresis was always observed at or slightly below T_n for all bridges in this study.

Tests were run employing the bridges examined in Chapter 2.

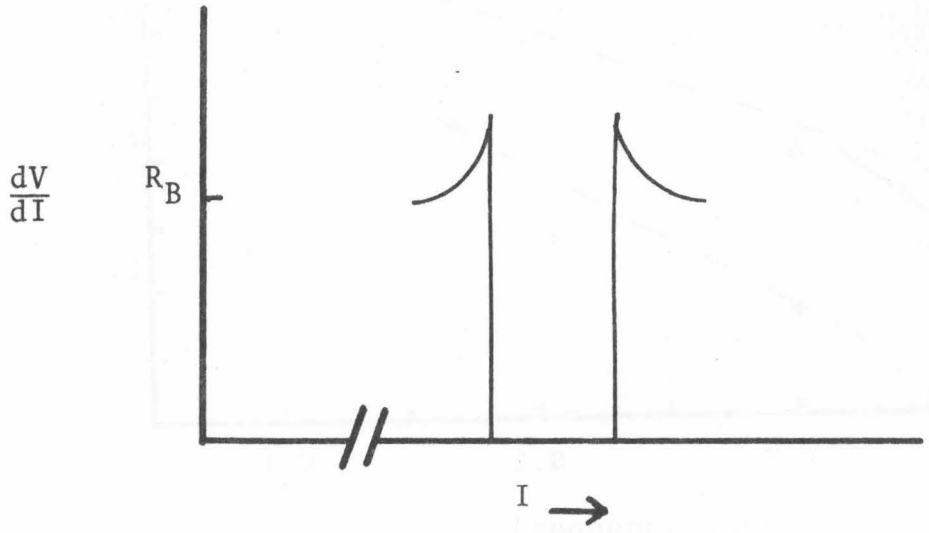
The actual measurement of the step widths is made by looking at the derivative of an I-V curve, which is plotted as dV/dI vs I. The dV/dI vs I for a typical bridge irradiated with 4 GHz radiation is shown in Figure 3a. Ideally, the step should look like the trace in Figure 3b, however, since the bridge is current biased and of low impedance, the current noise gives the smeared appearance seen in Figure 3a. In this study, the step widths were defined by extrapolating the resistance (dV/dI) of the step at $dV/dI = .75R_B$ and $dV/dI = .25R_B$ to zero resistance (see Figure 3c). This is not the only way the step widths could be defined, other choices used in the past literature are to measure the step width at $dV/dI = R_B$ or at $dV/dI = R_B/2$. The step widths were compared for these three methods and found not to deviate by more than ~10%, which was felt acceptable for this study.

The rf response of the Ta/Hf bridge set is shown in Figure 4. The maximum first step width, $\Delta I_{1\ max}$, as a function of frequency for a constant temperature is presented. Note the decrease in rf response as the bridge length and microwave frequency are increased. The maximum first step width, $\Delta I_{1\ max}$, as a function of temperature is seen in Figure 5 for the .5 μm bridge and compared with the bridge critical current (No R.F. applied). The step width, $\Delta I_{1\ max}$, appears to be roughly a constant fraction of the critical current, I_c, as a function of temperature. This behavior was characteristic of all samples examined. (The only exception to the above behavior was observed

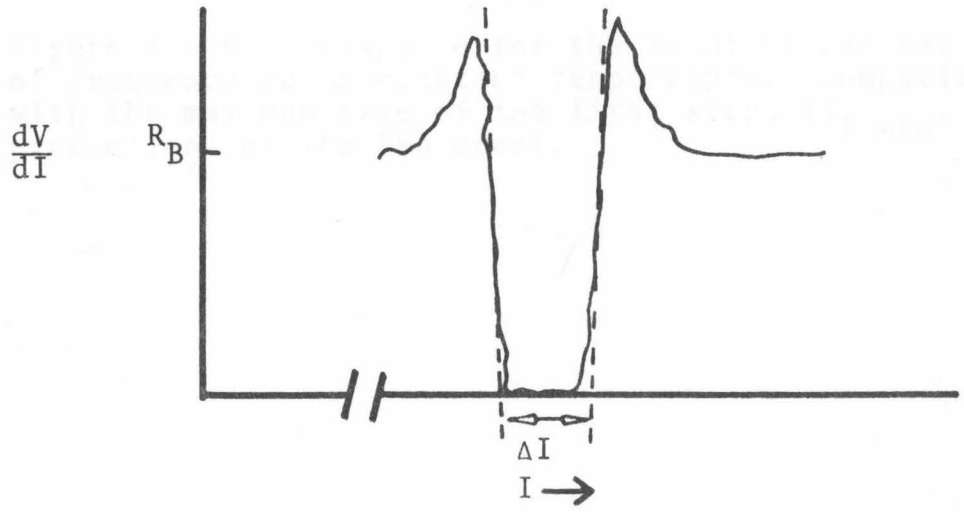
Figure 3 - (a) The dV/dI vs I for a typical bridge irradiated with 4 GHz radiation.
(b) An "ideal" rf step if no noise were present in the system.
(c) For this study, the step width, ΔI, was defined by extrapolating the dV/dI of the step at .75 R_B and .25 R_B to zero resistance.



(a)



(b)



(c)

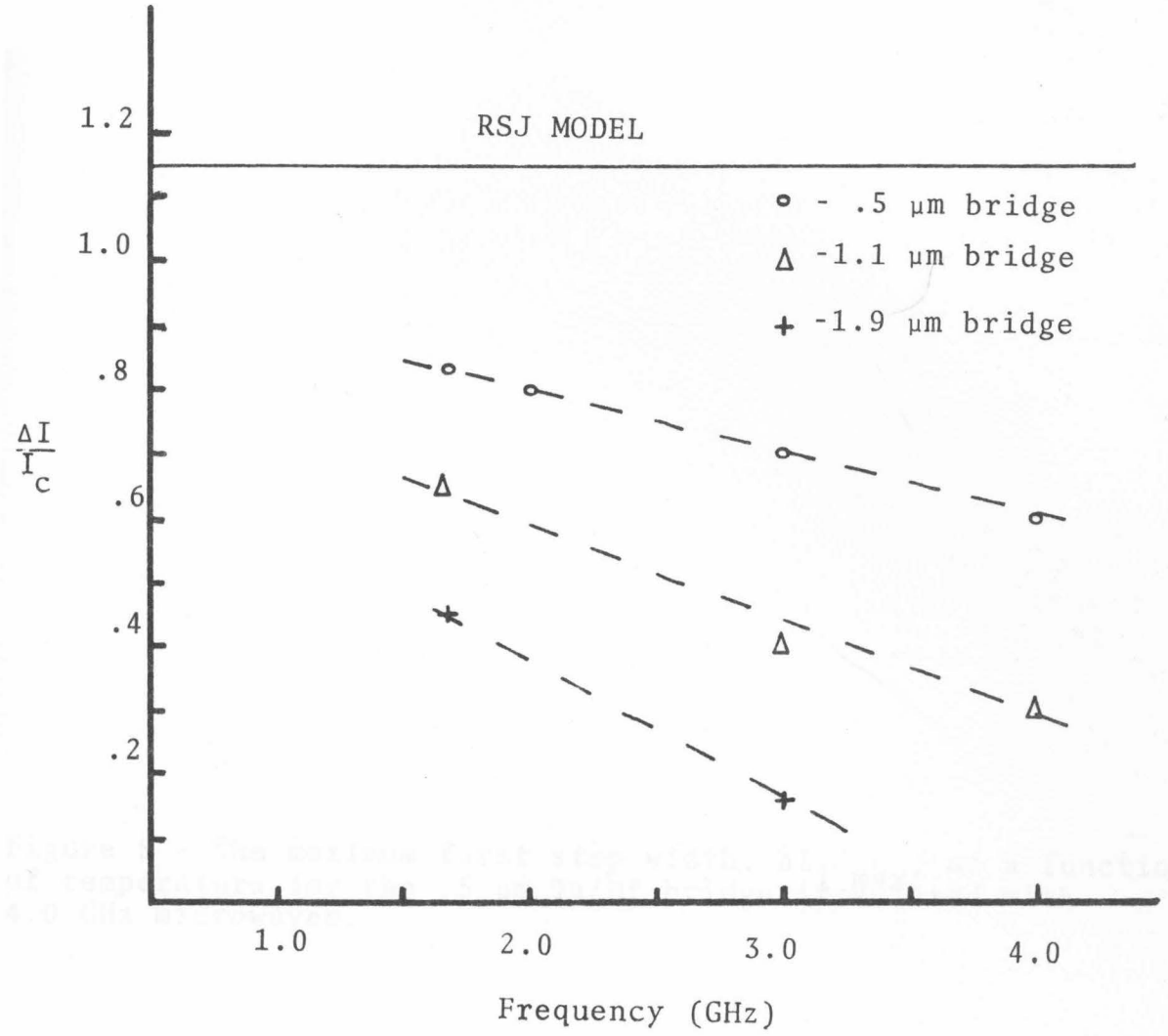
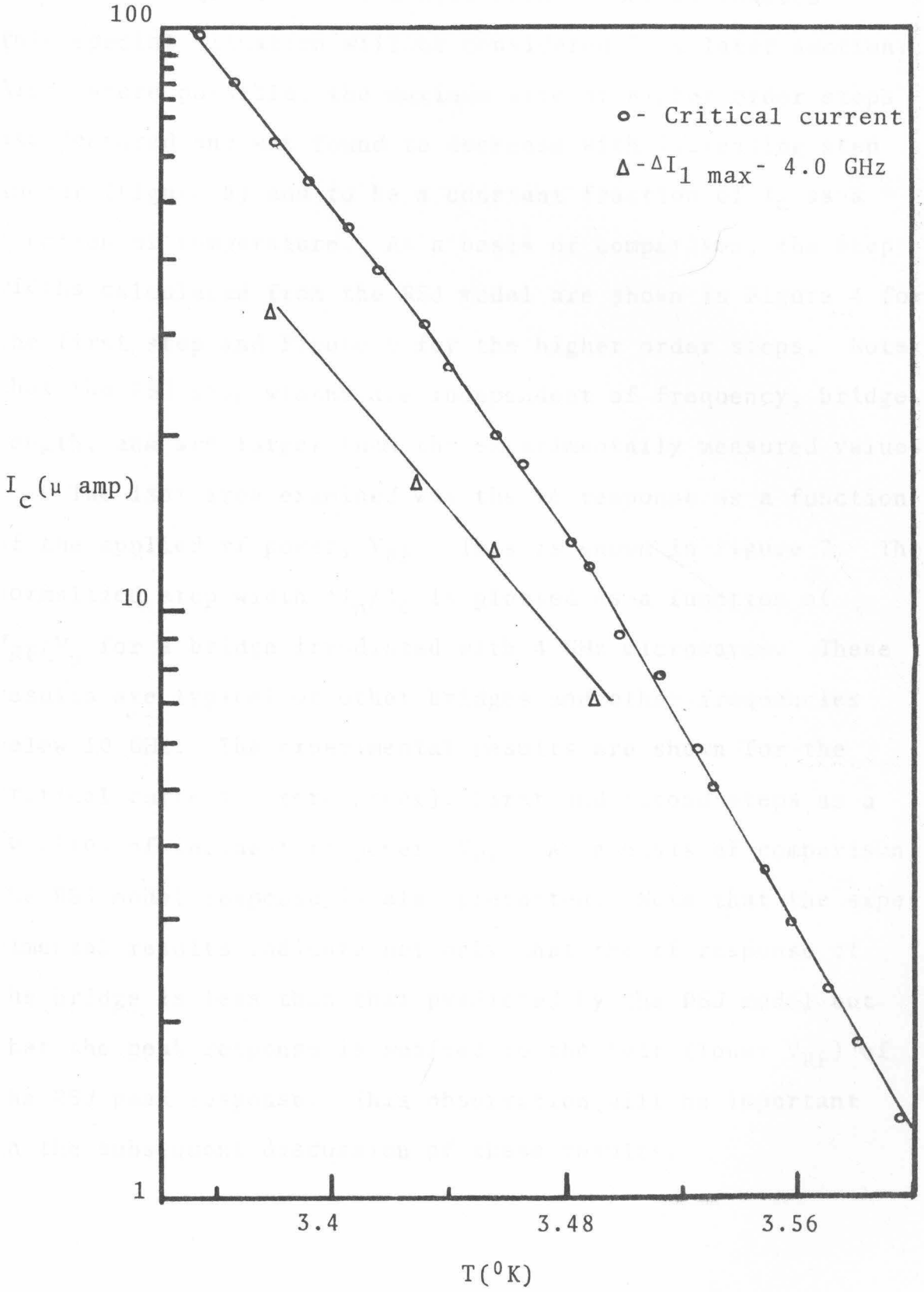


Figure 4 - R.F. response for the Ta/Hf bridge set as a function of frequency for a constant temperature. Comparison is made with the maximum size of the first step, $\Delta I_{1\ max}$, with the predictions of the RSJ model.

Figure 5 - The maximum first step width, $\Delta I_{1\,max}$, as a function of temperature for the .5 μm Ta/Hf bridge irradiated with 4.0 GHz microwaves.


100
10
1
o- Critical current
Δ-ΔI1 max- 4.0 GHz
Ic(μ amp)
3.4
3.48
3.56
T(°K)

when the bridges were irradiated with 10 GHz microwaves. This special situation will be considered in a later section. Also, where possible, the maximum size of higher order steps was measured and was found to decrease with increasing step number (Figure 6) and to be a constant fraction of I_c as a function of temperature. As a basis of comparison, the step widths calculated from the RSJ model are shown in Figure 4 for the first step and Figure 6 for the higher order steps. Note that the RSJ step widths are independent of frequency, bridge length, and are larger than the experimentally measured values.

The last area examined was the rf response as a function of the applied rf power, V_{RF}. This is shown in Figure 7. The normalized step width $\Delta I_n/I_c$ is plotted as a function of V_{RF}/V_μ for a bridge irradiated with 4 GHz microwaves. These results are typical of other bridges and other frequencies below 10 GHz. The experimental results are shown for the critical current (zero order), first and second steps as a function of incident rf power, V_{RF}. As a basis of comparison, the RSJ model response is also presented. Note that the experimental results indicate not only that the rf response of the bridge is less than that predicted by the RSJ model but that the peak response is shifted to the left (lower V_{RF}) of the RSJ peak response. This observation will be important in the subsequent discussion of these results.

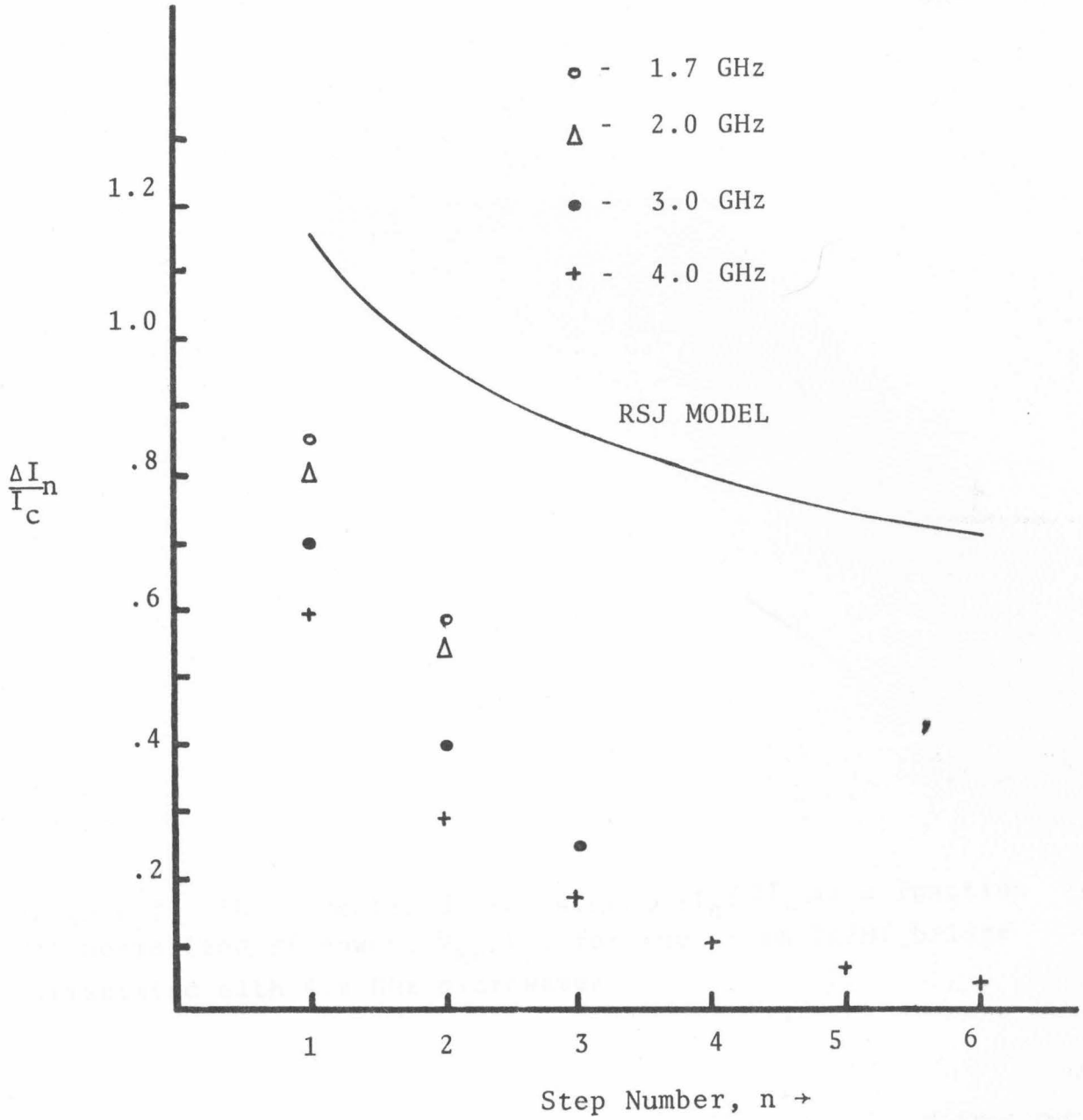
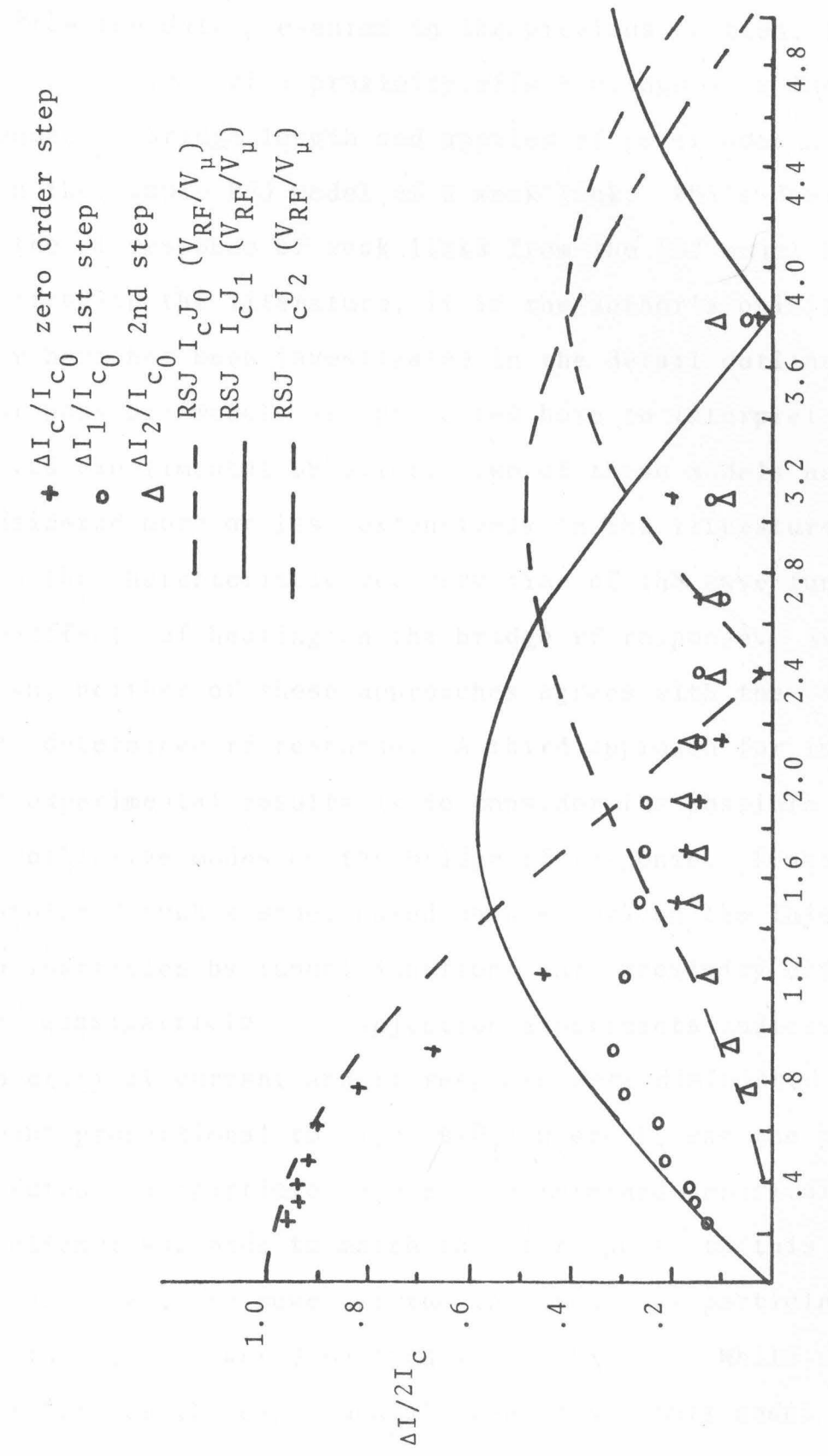


Figure 6 - The maximum width for the nth step, ΔI_n as a function of step number for the .5 μm Ta/Hf bridge. Higher order steps are shown at 1.7, 2.0, 3.0, and 4.0 GHz. Comparison is made with the RSJ model (solid line).

Figure 7 - The normalized step width, $\Delta I_n / 2I_c$, as a function of normalized rf power, V_{RF}/V_μ, for the .5 μm Ta/Hf bridge irradiated with 4.0 GHz microwaves.


$\Delta I_c/I_{c_0}$ zero order step
$\Delta I_1/I_{c_0}$ 1st step
$\Delta I_2/I_{c_0}$ 2nd step
RSJ I_cJ_0 (V_{RF}/V_μ)
RSJ I_cJ_1 (V_{RF}/V_μ)
RSJ I_cJ_2 (V_{RF}/V_μ)
$\Delta I/2I_c$
1.0
.8
.6
.4
.2
.4
.8
1.2
1.6
2.0
2.4
2.8
3.2
3.6
4.0
4.4
4.8
V_{RF}/V_μ

3.4 Discussion of Results

From the data presented in the previous section, the observed rf response of a proximity effect bridge as a function of frequency, bridge length and applied rf power does not agree with the simple RSJ model of a weak link. While deviations in the rf response of weak links from the RSJ model have been reported in the literature, it is the author's opinion that they have not been investigated in the detail outlined here. Four possible models are presented here to interpret the observed experimental behavior. Two of these models have been considered more or less extensively in the literature and deal with the characteristic recovery time of the wave function and the effects of heating on the bridge rf response. As will be shown, neither of these approaches agrees with the experimentally determined rf response. A third approach for interpreting the experimental results is to consider the possible effects of collective modes on the bridge rf response. Franson recently postulated such a model based on his work on the injection of quasiparticles by tunnel junctions into proximity effect bridges. The quasiparticle injection experiments indicated that the critical current and rf response were diminished by an amount proportional to $\exp(-\beta\sqrt{P_I})$ where P_I was the power of injected quasiparticles and β is determined empirically. An attempt was made to match the rf response to this model by replacing P_I, the power of the injected quasiparticles, with P_T, the total power developed in the bridge. While some agreement between the experimental results and this model was found

it was felt that this model still did not adequately describe the experimental situation.

A fourth model is introduced which describes the behavior of the wavefunction in a normal material when the chemical and pair potential differ. An expression, based on this model, seems to adequately describe the measured rf results.

The first model considered is based on the characteristic recovery time of the wavefunction. The RSJ τ model is derived from the time dependent Ginzburg-Landau theory.[7] The characteristic relaxation time, τ, in this model is temperature dependent and varies as $\tau = \tau_0/(1 - T/T_n)$. Unfortunately, this model cannot be solved in closed form and must be handled by computer. Figure 8 shows the rf response of a weak link predicted by the RSJ τ model as a function of temperature and is based on the computer simulation by Clarke and Lindelof. These predictions are compared with the experimentally determined step widths for a typical bridge. As a function of decreasing temperature, the RSJ τ model predicts that the maximum step width, ΔI_n, should first increase and then decrease. The increase in the rf response is attributed to the critical current increasing so that $V_\mu < I_c R$, and was included in the discussion of expression 3.2.3.

The behavior predicted by the RSJ τ model was never observed in any of the bridges in this study. It is this deviation between theory and experiment which suggests that the observed

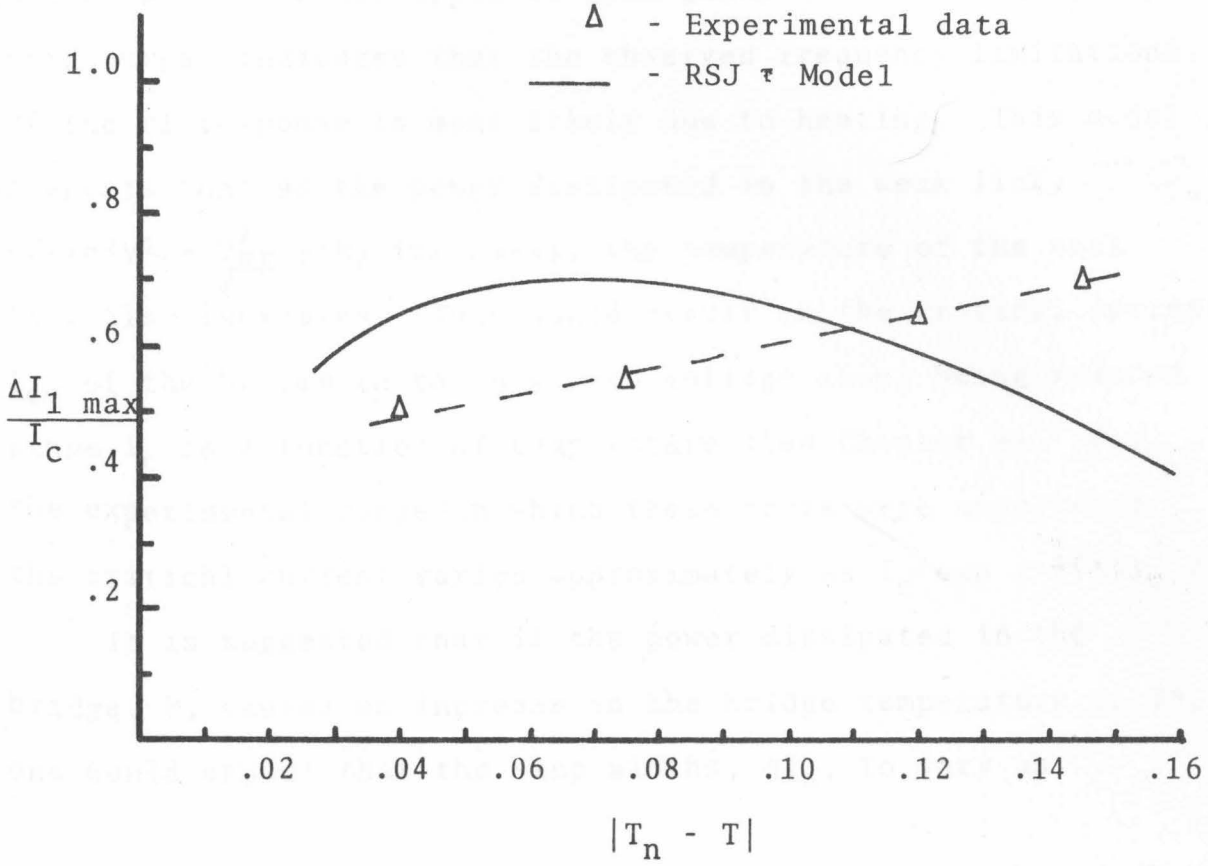


Figure 8 - Comparison of the RSJ τ model of rf response as a function of temperature with a .5 μm Ta/Hf bridge irradiated with 4.0 GHz microwaves. On none of the samples was the rf response seen to increase and then decrease as predicted by the RSJ τ model.

rf response is not dependent on a relaxation time phenomenon.

The second proposed explanation for the reduced rf response often cited in the literature is heating of the bridge. Recent work on other types of weak links (in particular, Daym structures)[8] indicates that the observed frequency limitations of the rf response is most likely due to heating. This model suggests that as the power dissipated in the weak link, $P(=(n^2V^2 + \frac{V_{RF}^2}{2})/R)$ increases, the temperature of the weak link also increases. This would result in the critical current, I_c, of the bridge (in the non-zero voltage case) being reduced since I_c is a function of temperature (See Chapter 2). For the experimental range in which these tests were undertaken, the critical current varies approximately as $I_c \propto \exp(-k(T-T_n)/T_n)$

It is suggested that if the power dissipated in the bridge, P, causes an increase in the bridge temperature to T*, one would expect that the step widths, ΔI_n, to vary as

$$\Delta I_n = 2I_c \exp(-\alpha P)\, J_n(V_{RF}/V\mu) \qquad (3.4.1)$$

where α is dependent on the size of the bridge, the specific heat of the bridge material, the value of k in the expression for the critical current and T_n. It is interesting to observe that expression 3.4.1 not only causes a decrease in the maximum step size as the rf frequency is increased (since, P, the power dissipated in the bridge also increases) but also causes a distortion of step width as a function of applied

rf power with respect to the RSJ model. Note that depending on the value of α, the maximum value of ΔI_n is decreased and shifted to the left of the peak of the RSJ model.

A comparison, however, of the measured step widths as a function of power and step number with expression 3.4.1 leads one to the conclusion that the experimental results cannot be fitted for any choice of α and P. In order to better see this point, the maximum step width, $\Delta I_{n\ max}$, for the first six steps of a bridge irradiated at 4.0 GHz is shown in Figure 9. A fit of 3.4.1 is also shown in Figure 9 and indicates that a simple heating model predicts a bridge rf response which decays much more rapidly than is experimentally observed. A comparison of the coefficient α used in a best fit of the rf data in Figure 9 and α_{SHM} from a simple heating model shows α_{SHM} is an order of magnitude smaller than α. A simple heating model would predict an rf response that would be very close to the RSJ model for the power levels in this experiment. It was concluded, therefore, that the observed rf response could not be explained with a simple heating model.

The third model examined in an attempt to understand the rf response of proximity effect bridges is based on the work of Franson[5] (1976). Recent experiments on the injection of

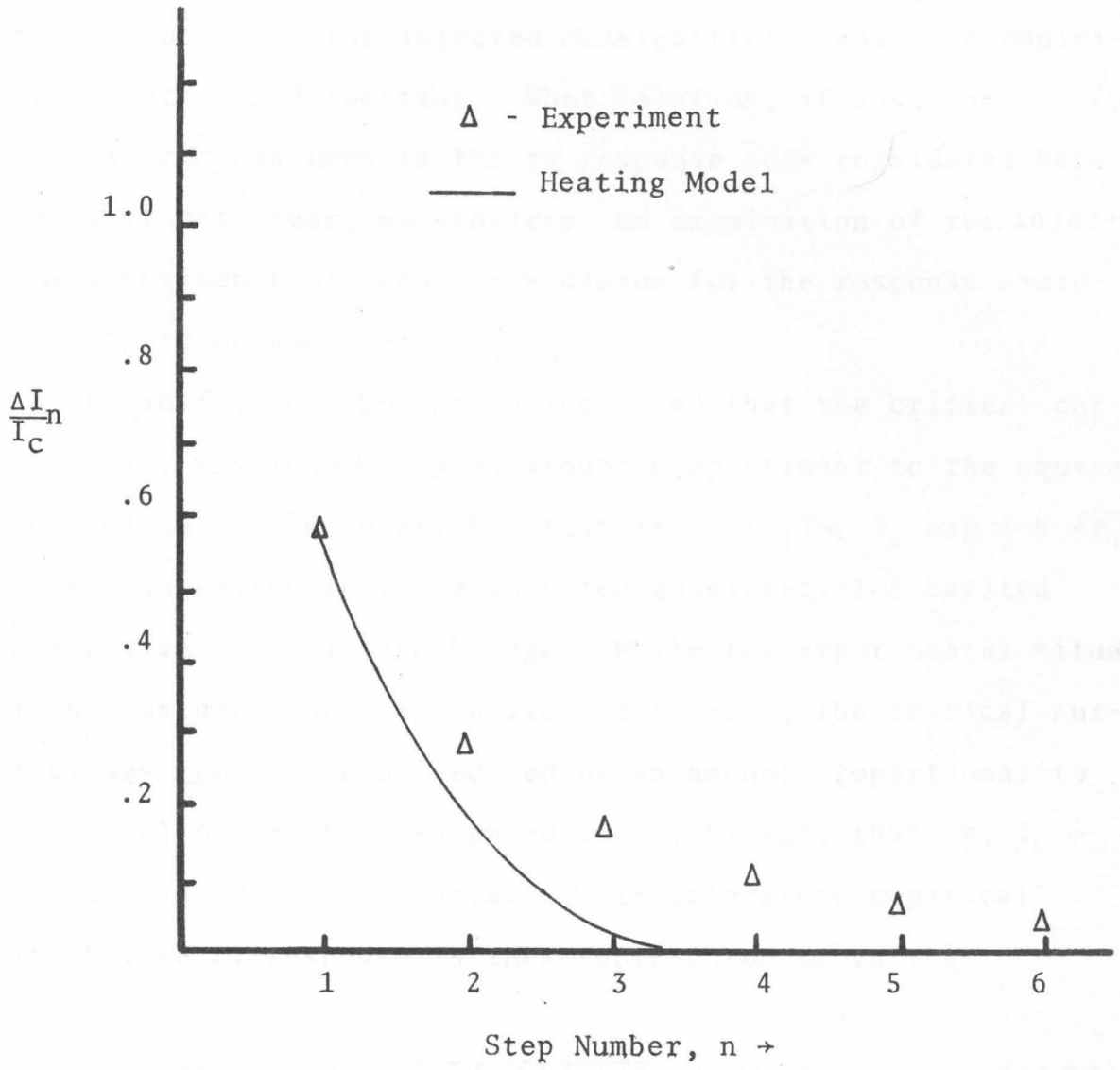


Figure 9 - Comparison of the experimentally determined maximum step widths, $\Delta I_{n\,max}$, as a function of step number and a heating model for the rf response of a bridge. The weak link used in this study was a .5 μm Ta/Hf bridge irradiated with 4.0 GHz microwaves. The value of α in 3.4.1was fitted to maximum of the first step and the subsequent steps were then calculated. A simple heating model of the type predicted by 3.4.1 would predict a bridge response which decays much more rapidly than is experimentally observed.

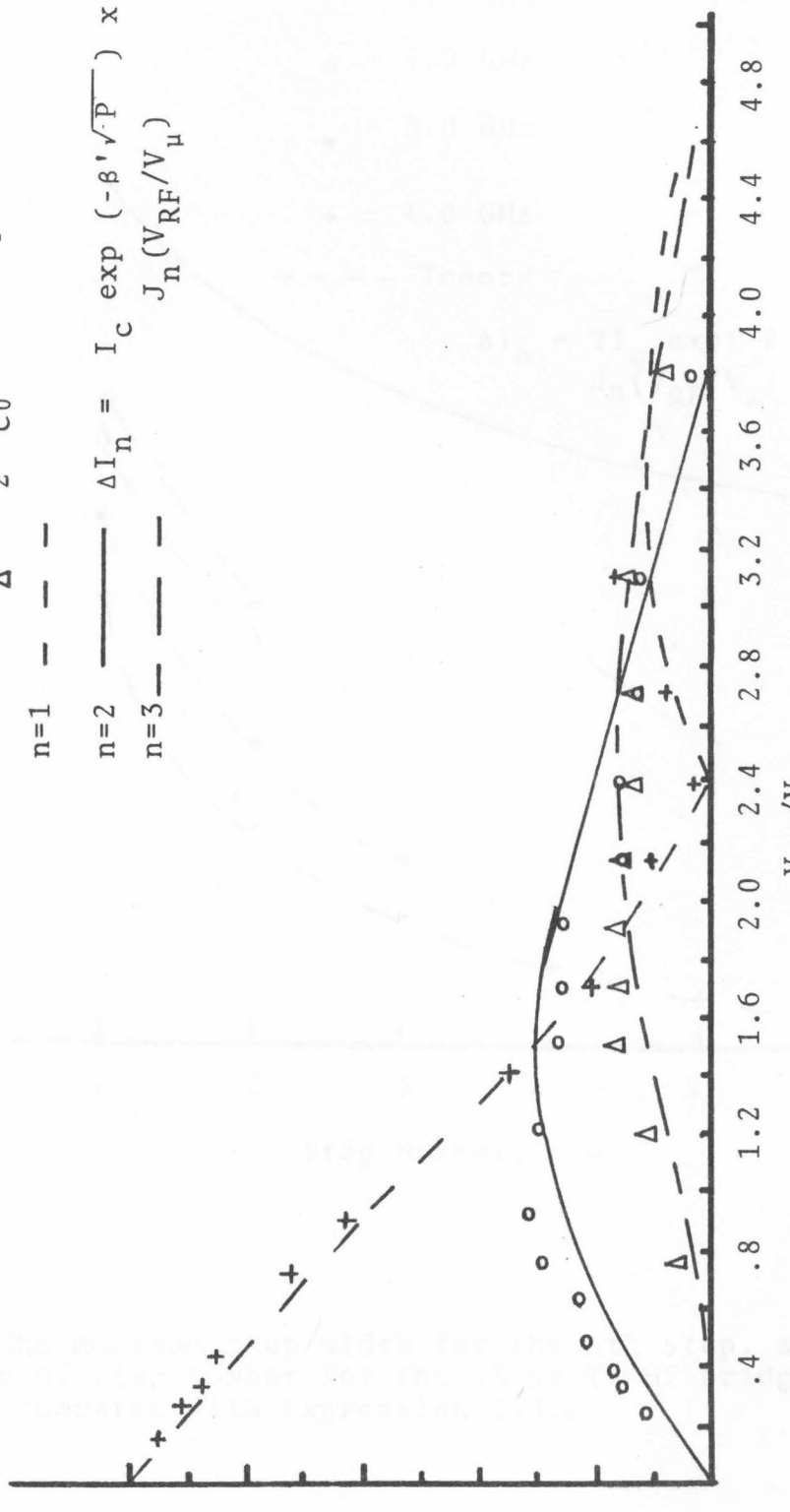
quasiparticles by tunnel junctions into proximity effect bridges resulted in findings that indicated the critical current was reduced by an amount proportional to $\exp(-\beta\sqrt{P_I})$, where P_I was the power of the injected quasiparticles and β an empirically determined constant. What relation, if any, the experiments have to the rf response work considered here is still not clear, nonetheless, an examination of the injection experiments allowed a new avenue for the response measurements to be analyzed.

The injection experiments indicated that the critical current, I_c, was reduced by an amount proportional to the square root of injection power, P_I, that is, $I_c(P_I) = I_c \exp(-\beta\sqrt{P_I})$. It was suggested that the injected quasiparticles excited collective modes in the bridge. While the experimental situation considered here is entirely different, the critical current was assumed to be reduced by an amount proportional to the total power, P, dissipated in the bridge, that is, $I_c = I_c \exp(-\beta\sqrt{P})$. The constant β is determined empirically. The bridge rf response is then represented to vary as

$$\Delta I_n = 2I_c \exp\left(-\beta\sqrt{(n^2V_\mu^2 + \tfrac{1}{2}V_{RF}^2)/R}\right) J_n(V_{RF}/V_\mu) \qquad (3.4.2)$$

where R is the bridge resistance. Comparison of expression 3.4.2 with the experimentally determined rf response for the .5μm Ta/Hf bridge is made in Figures 10 and 11. Expression 3.4.2 is correlated to the step width as a function of the

Figure 10 - The normalized step width, $\Delta I_n/I_c$, as a function of normalized rf power, V_{RF}/V_μ for the .5 μm Ta/Hf bridge irradiated with 4.0 GHz microwaves. These data are compared with expression 3.4.2 where β has been determined empirically.


+ $\Delta I_c/I_{c0}$ zero order step
o $\Delta I_1/I_{c_0}$ 1st step
Δ $\Delta I_2/I_{c0}$ 2nd step
n=1 – – – –
n=2 ———— $\Delta I_n = I_c \exp(-\beta'\sqrt{P}) \times J_n(V_{RF}/V_\mu)$
n=3 — — — —
$\Delta I_n/2I_c$
1.0
.8
.6
.4
.2
.4
.8
1.2
1.6
2.0
2.4
2.8
3.2
3.6
4.0
4.4
4.8
V_{RF}/V_μ

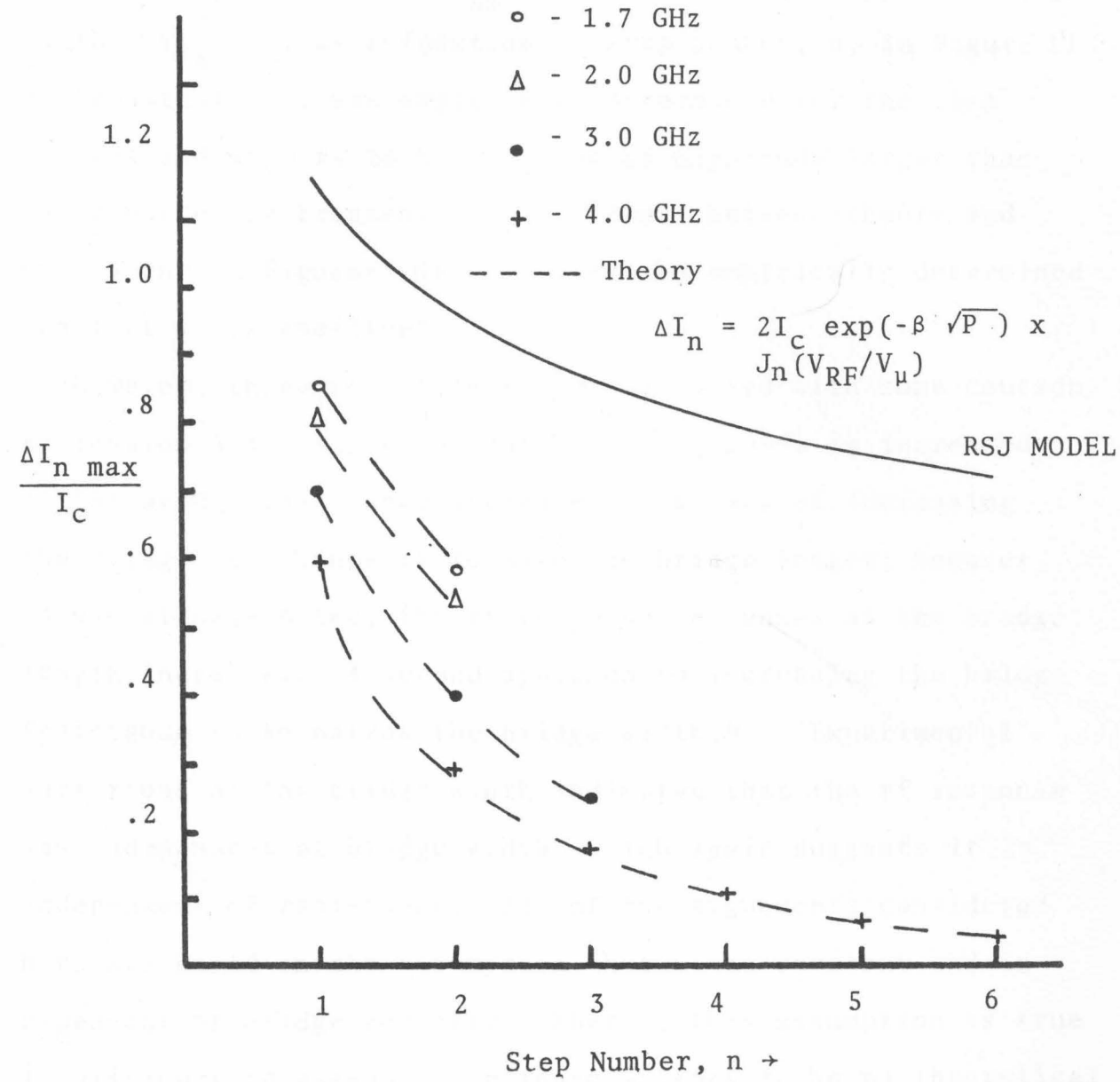


Figure 11 - The maximum step width for the nth step, ΔI_n, as a function of step number for the .5 μm Ta/Hf bridge. These data are compared with expression 3.4.2 .

applied rf power, ΔI_n vs V_{RF} in Figure 10 and the maximum step width, $\Delta I_{n\ max}$, as a function of step number, n, in Figure 11. The constant, β, was empirically determined for the .5μm bridges and appears to be an order of magnitude larger than was reported by Franson. The agreement between theory and experiment in Figures 10 and 11 with the empirically determined constant β is excellent.

However, these results must be considered with some caution. Expression 3.4.2 suggests that the rf response is increased if the bridge resistance increases. One way of increasing the bridge resistance is to make the bridge longer; however, as was already noted, the rf response decreases as the bridge length increases. A second approach to increasing the bridge resistance is to narrow the bridge width, w. Experimental variations of the bridge width indicated that the rf response was independent of bridge width, which again suggests it is independent of resistance. All of the arguements considered here are based on the assumption that β is constant and independent of bridge geometry. Whether this assumption is true is difficult to assess since there appears to be no theoretical understanding for the value of β. The experimental results, however, suggest that the agreement between 3.4.2 and experiment may be fortuitous, and that an entirely different mechanism is responsible for the observed rf response. Since the experimental work considered here does not appear to be dependent on the bridge resistance, it will be concluded that the observed rf response cannot be explained by a model based on

the excitations of collective modes as suggested by 3.4.2. For these reasons a fourth model is presented.

This last model requires that the basic postulates of the RSJ model be examined. The RSJ model is based on a simple two fluid description of the current flowing through the bridge. Implicit in this picture is that the two fluids do not interact, which may be an overly simplistic view of the experimental situation. Therefore, it is proposed that the reduced rf response is a direct result of an interaction between the normal and super currents flowing through the bridge.

In order to better understand the possible nature of the normal-supercurrent interaction, an empirical expression was developed for the rf response of the bridges. This expression is

$$\Delta I_n = 2I_c \exp\left(\frac{-C_0 L}{T}\sqrt{(nV_\mu)^2 + V_{RF}^2/2}\right) J_n\,(V_{RF}/V_\mu) \quad (3.4.3)$$

which is dependent on the dc voltage, $V_\mu (=\hbar\omega/2e)$, the applied rf voltage, V_{RF}, the bridge length, L, and an empirical constant (for this set of bridges) equal to $C_0 = 32.6\ K^0/\text{volt-}A^0$. Expression 3.4.3 is similar to 3.4.2, however, 3.4.3 displays the behavior of the rf response as an explicit function of bridge length, L, applied rf voltage, V_{RF}, and temperature, T. Expression 3.4.3 is compared with the experimental data of the maximum step width, $\Delta I_{n\ max}$, as a function of step number, n, for two bridges of lengths 1.1 μm and 1.9 μm in Figures 12 and 13

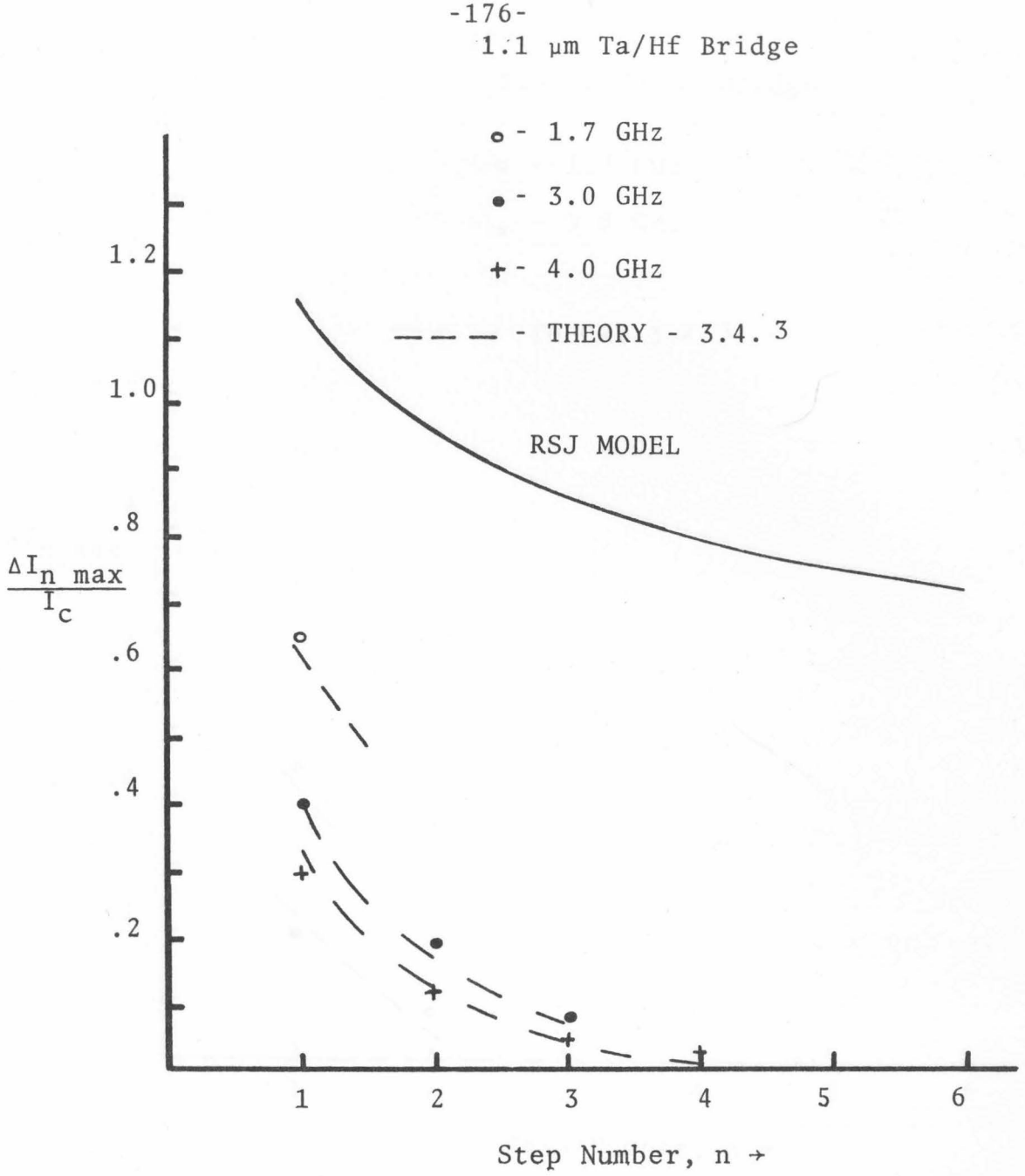


Figure 12 - The maximum step width for the nth step, ΔI_n as a function of step number for the 1.1 μm Ta/Hf bridge. These data arecompared with expression 3.4.3.

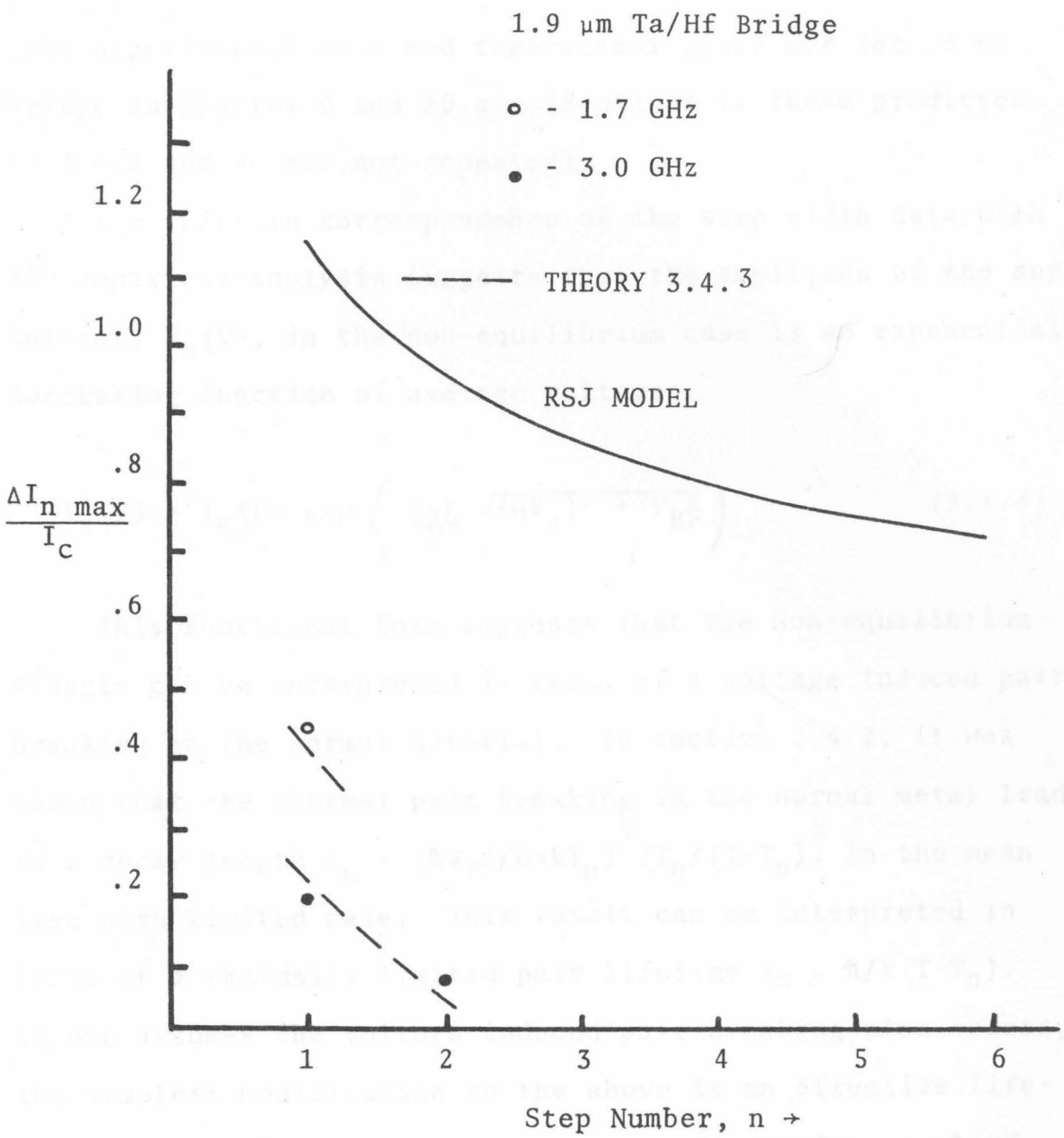


Figure 13 - The maximum step width for the nth step, ΔI_n as a function of step number for the 1.9 μm Ta/Hf BridgeThese data are compared with expression 3.4.3.

(The experimental data and theoretical plots for the .5 μm bridge in Figures 9 and 10 are identical to those predicted by 3.4.3 and so are not repeated).

The relative correspondence of the step width data with the empirical analysis suggests that the amplitude of the supercurrent, $I_s(V)$, in the non-equilibrium case is an exponentially decreasing function of average voltage:

$$I_s(V) = I_c(0) \exp\left(-\frac{C_0 L}{T}\sqrt{(nV_\mu)^2 + V_{RF}^2}\right) \qquad (3.4.4)$$

This functional form suggests that the non-equilibrium effects can be interpreted in terms of a voltage induced pair breaking in the normal material. In section 2.4.2, it was shown that the thermal pair breaking in the normal metal leads to a decay length $\xi_n = (\hbar v_F l/6\pi k T_n)^{\frac{1}{2}} (T_n/(T-T_n))^{\frac{1}{2}}$ in the mean free path limited case. This result can be interpreted in terms of a thermally limited pair lifetime $\tau_n \sim \hbar/k(T-T_n)$. If one assumes the voltage induced pair breaking also occurs, the simplest modification to the above is an effective lifetime $\tau_{eff}^{-1} = \tau_n^{-1} + \tau_V^{-1}$. By dimensional arguments, $\tau_V \sim \hbar/eV$, so that $\tau_{eff} \sim \hbar/(k(T-T_n) + aeV)$, where a is, as yet, an undetermined parameter. The effective decay length with these assumptions is then

$$\xi_n^* = \left(\frac{\hbar v_F l}{6\pi}\right)^{\frac{1}{2}} \left(\frac{1}{k(T-T_n) + aeV}\right)^{\frac{1}{2}} \qquad (3.4.5)$$

If it is further assumed that no other non-equilibrium effects occur to change boundary conditions, an analysis similar to that done in Section 2.5.4 can be done to calculate the nonequilibrium supercurrent density, $J_c^*(V)$. The result is

$$J_c^*(V) = .898\ \frac{3\sqrt{3}}{2}\ J_{GL}(0)\left(\frac{T + \frac{ae\bar{V}}{k_B} - T_n}{T_n}\right)^{3/2} x$$

$$\left\{\frac{8\left(\frac{T_s - T}{T + \frac{ae\bar{V}}{k_B} - T_n}\right)\left(\frac{NV_n}{NV_s}\right)^2 \frac{T_s}{T_n} \tanh^2 C}{\left(1\left(+ 1 + \tfrac{1}{2}\left[\left(\frac{T_s - T}{T + ae\bar{V}/k_B - T_n}\right)\left(\frac{NV_n}{NV_s}\right)^2 \frac{T_s}{T_n} \tanh^2 C\right]\right)^{1/2}\right)^2}\right\} x$$

$$\exp\left(\frac{-L}{.898\ \xi_n}\left(\frac{T + \frac{ae\bar{V}}{k_B} - T_n}{T_n}\right)^{1/2}\right) \qquad (3.4.6)$$

The rf response of the bridges is then

$$\Delta I_n = 2J_c^* A\ J_n\ (V_{RF}/V_\mu) \qquad (3.4.7)$$

where A is the cross sectional area of the bridge. In the range of temperature considered here, the expression simplifies considerably to become similar to the empirical form 3.4.3 if $\bar{V}$ is taken to be $\bar{V} = \sqrt{(nV_\mu)^2 + V_{RF}^2/2}$ and $1/a = 3.35 \pm .3$.

In order to better see this point, expression 3.4.3 which was empirically found to fit the rf response, is compared with 3.4.7. Comparison is also made with the .5 μm bridge rf response (these results are typical of the other bridges in this study) as a function of maximum step width, $\Delta I_{n\ max}$, vs

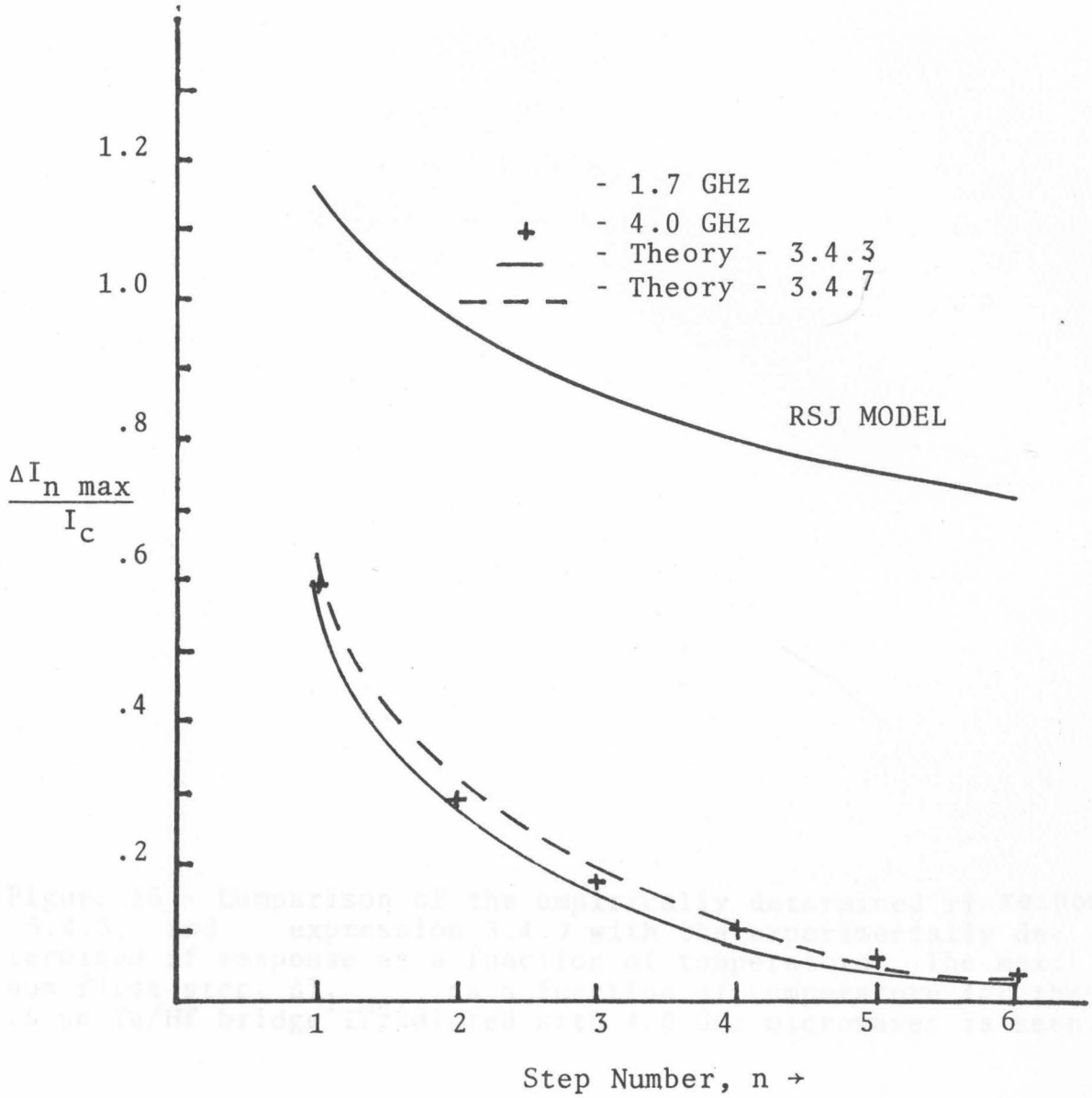
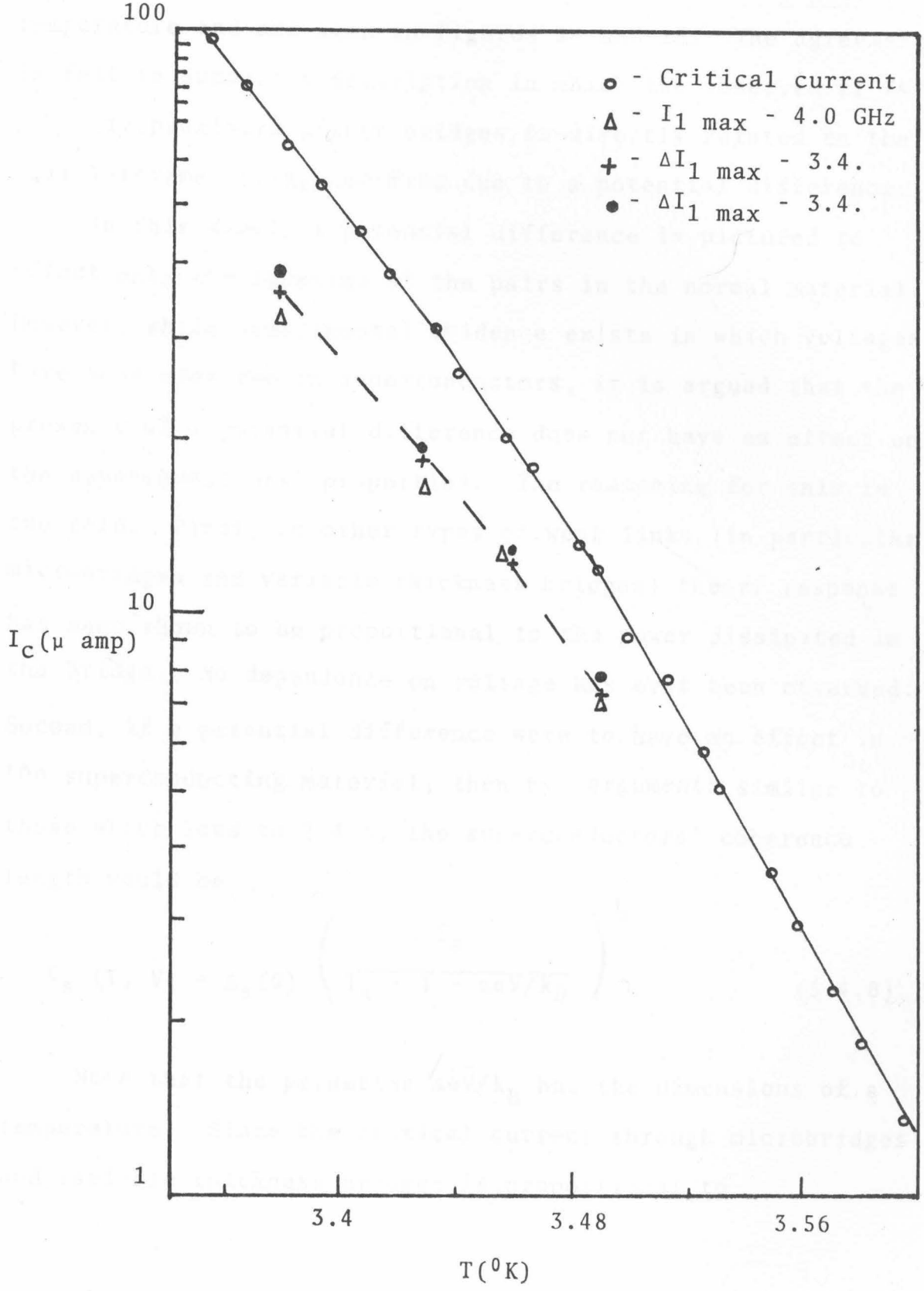


Figure 14 - Comparison of the empirically determined rf response, 3.4.3, and expression 3.4.7 with the experimentally determined rf response for the .5 μ bridge. The maximum width for the nth step, $\Delta I_{n\ max}$ as a function of step number, n, is plotted for a bridge irradiated with 4 GHz microwaves.



Figure 15 - Comparison of the empirically determined rf response 3.4.3, and expression 3.4.7 with the experimentally determined rf response as a function of temperature. The maximum first step, $\Delta I_{1,max}$, as a function of temperature for the .5 μm Ta/Hf bridge irradiated with 4.0 GHz microwaves is seen.


100
10
1
I_c(μ amp)
o - Critical current
Δ - $I_{1\ max}$ - 4.0 GHz
+ - $\Delta I_{1\ max}$ - 3.4.
● - $\Delta I_{1\ max}$ - 3.4.
3.4
3.48
3.56
T(^{0}K)

step number, n and the maximum first step width, $\Delta I_{1\ max}$, vs temperature and are seen in Figures 14 and 15. The agreement is felt to support a description in which the observed rf response in proximity effect bridges is directly related to the pair lifetimes being modified due to a potential difference.

In this model, a potential difference is pictured to affect only the lifetime of the pairs in the normal material. However, while experimental evidence exists in which voltages have been measured in superconductors, it is argued that the presence of a potential difference does not have an effect on the superconductors' properties. The reasoning for this is two fold. First, in other types of weak links (in particular microbridges and variable thickness bridges) the rf response has been shown to be proportional to the power dissipated in the bridge. No dependence on voltage has ever been observed. Second, if a potential difference were to have an effect in the superconducting material, then by arguments similar to those which lead to 3.4.5, the superconductors' coherence length would be

$$\xi_s\ (T,\ V) = \xi_s(0) \left(\frac{T_s}{T_s - T - aeV/k_B} \right)^{\frac{1}{2}} \qquad (3.4.8)$$

Note that the parameter $ae\bar{V}/k_B$ has the dimensions of a temperature. Since the critical current through microbridges and variable thickness bridges is proportional to

$J_c \propto 1/\xi_s(T,V)$, the maximum rf response would then be a function of the temperature difference, $(T_s - T)$. Now Octavio, Skocpol and Tinkham[8] have designed a variable thickness bridge in which the 186th step of a 10 GHz microwave source was observed when $(T_s - T) \sim 1.65^0$K. Assuming the value of a in 3.4.8 is ~ 1/3.35, and ignoring the effect of the microwave drive voltage, V_{RF}, $ae\bar{V}/k_B$ is ~ 12^0K. Thus, the quantum interference effects should have disappeared long before what was experimentally observed. For these reasons, the effect of a potential difference is believed only to have an effect in the normal material.

In conclusion, the experimentally determined rf response of a set of bridges has been compared with several models for the behavior of weak links. No agreement was found between the experimental results and the more common relaxation time and heating models which have been put forth to explain the diminished rf response of weak links. A new model has been developed which is a nonequilibrium extension of the steady state critical current model introduced in Chapter 2., and is consistent with a picture in which the decay length, ξ_n^*, in the normal material is a function of the voltage across the bridge. Good agreement is seen between this model and the measured rf response.

3.5 R.F. Response of Proximity Effect Bridges at 10 GHz

The rf response of proximity effect bridges at 10 GHz is considered in a separate section since the observed behavior appears to be entirely different than the response measured in the frequency range 1-4 GHz. For bridges irradiated at 10 GHz, the maximum first step width, ΔI, was found to be a function of bridge material, length, and temperature. Figure 16 shows the maximum first step width, $\Delta I_{1\ max}$, as a function of temperature for two typical bridges of length .5 and 2.0 μm. The critical current (no applied rf) as a function of temperature is also shown. Two differences become apparent upon comparison of these data with the rf response taken between 1 and 4.0 GHz. First, the maximum step widths at 10 GHz, ΔI_1, are not seen to be constant fraction of the critical current as a function of temperature as reported for the lower frequency response. Second, the maximum step widths, ΔI_1, within a small temperature range, were observed to be larger than those taken at lower frequencies. Again, this trend was never seen in the response measured between 1 and 4.0 GHz.

Variation of the step size, ΔI_n, as a function of applied rf power, V_{RF}, is shown in Figure 17a through 17d. Comparison is made with the RSJ model and the empirical expression 3.4.3. The data in each figure were taken at a different critical current. Note that at the highest temperature (smallest critical current), the step size, ΔI_n, as a function of V_{RF} is exceedingly distorted from the behavior predicted by either the RSJ model or the empirical expression 3.4.3. As the temper-



Figure 16 - Comparison of the maximum step widths $\Delta J_{n,max}$ for two bridges of length .5 μm and 2.0 μm as a function of temperature when irradiated by 10 GHz microwaves.

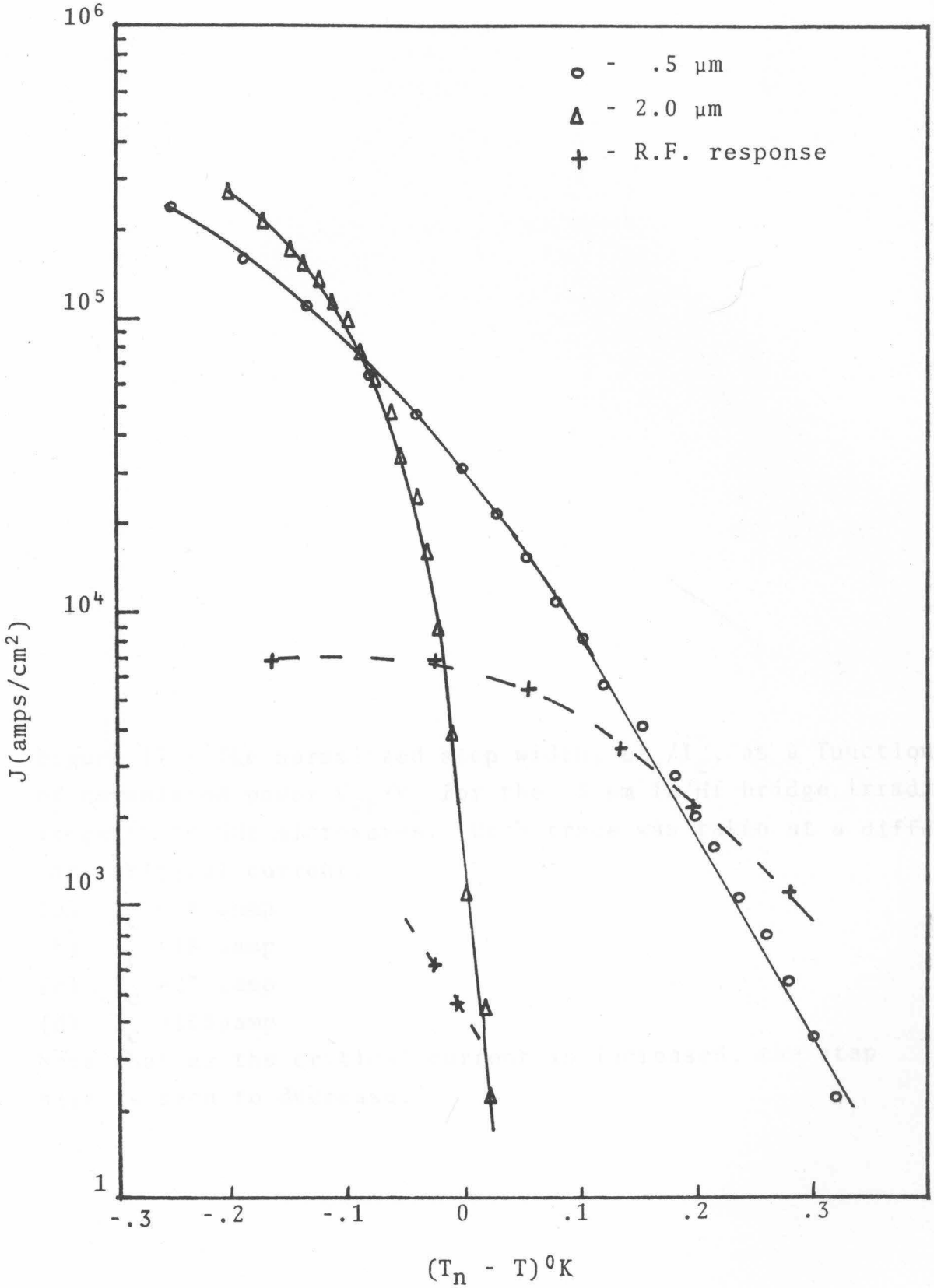
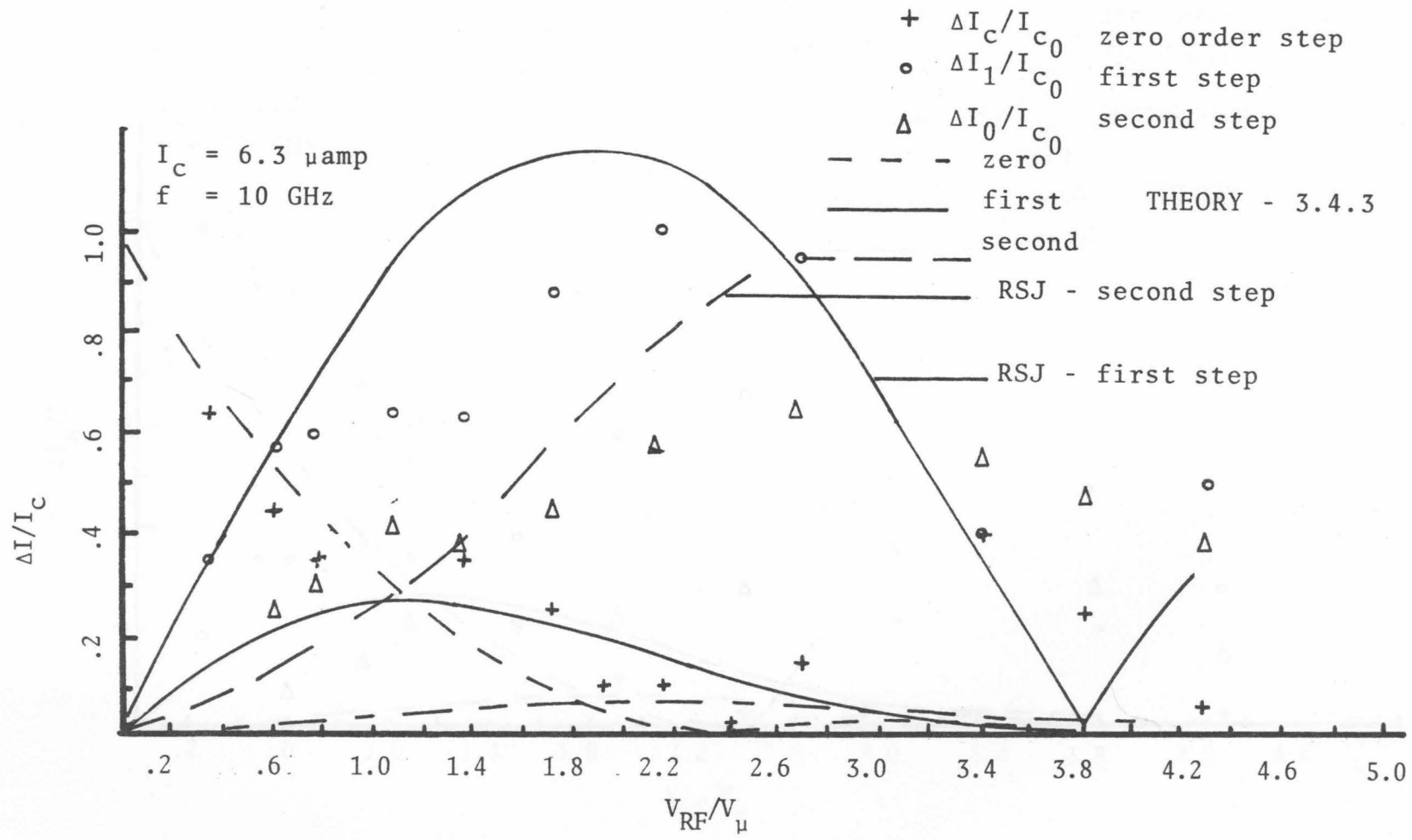
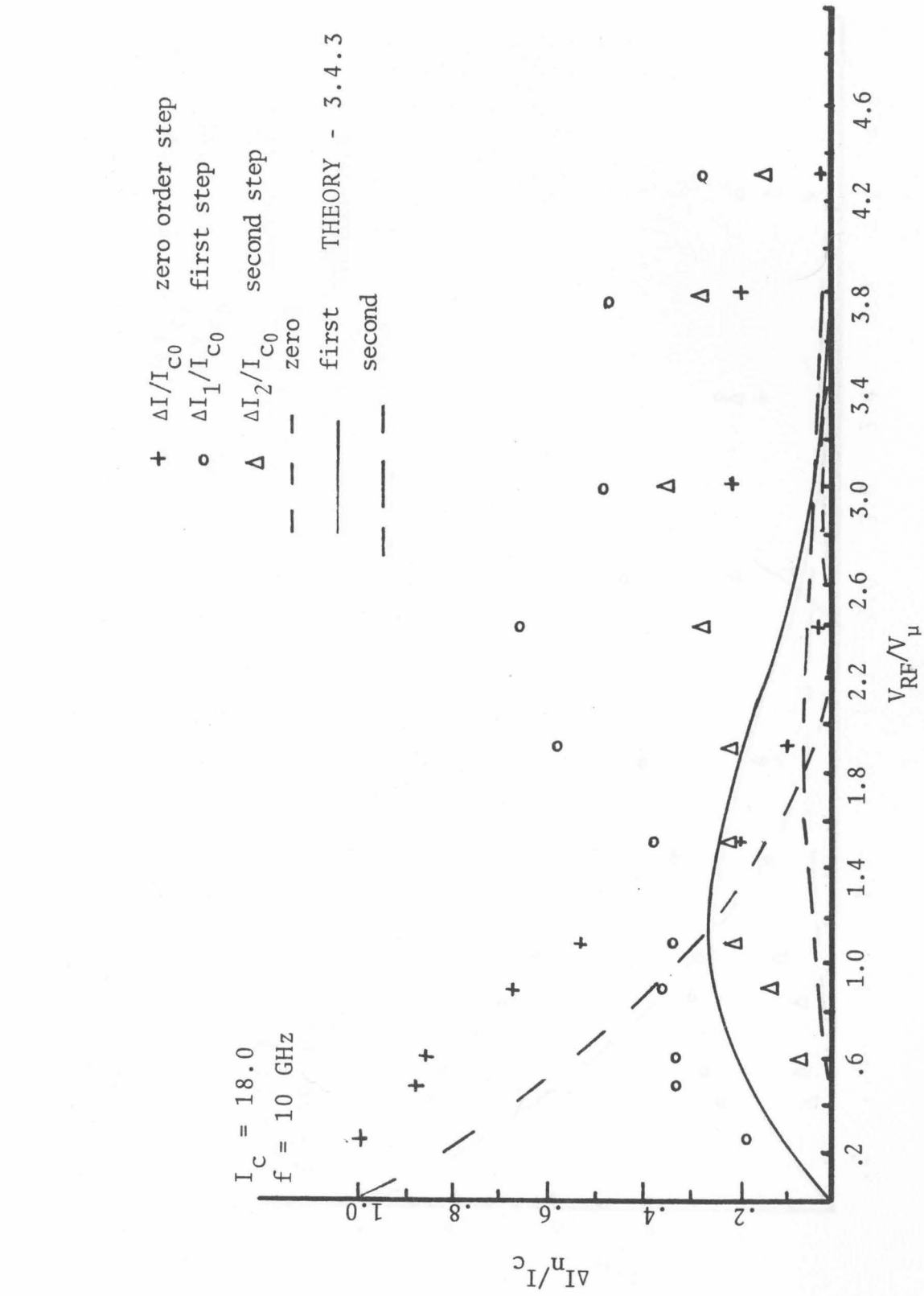

10^6
10^5
10^4
10^3
1
J (amps/cm^2)
o - .5 μm
Δ - 2.0 μm
+ - R.F. response
-.3
-.2
-.1
0
.1
.2
.3
(T_n - T) °K

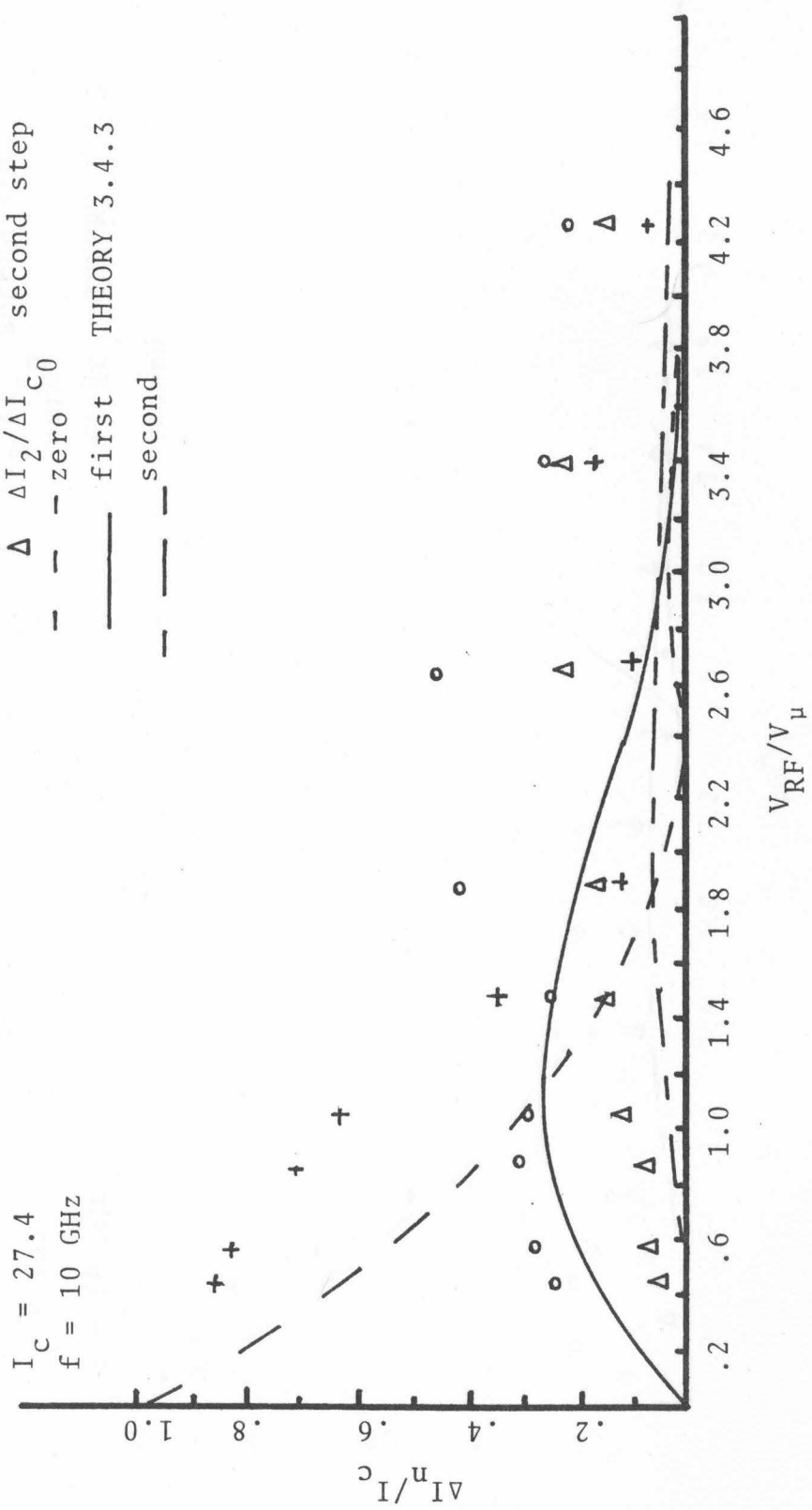
Figure 17 - The normalized step width, $\Delta I_n/I_c$, as a function of normalized power V_{RF}/V_μ for the .5 μm Ta/Hf bridge irradiatedwith 10 GHz microwaves. Each trace was taken at a different critical current.

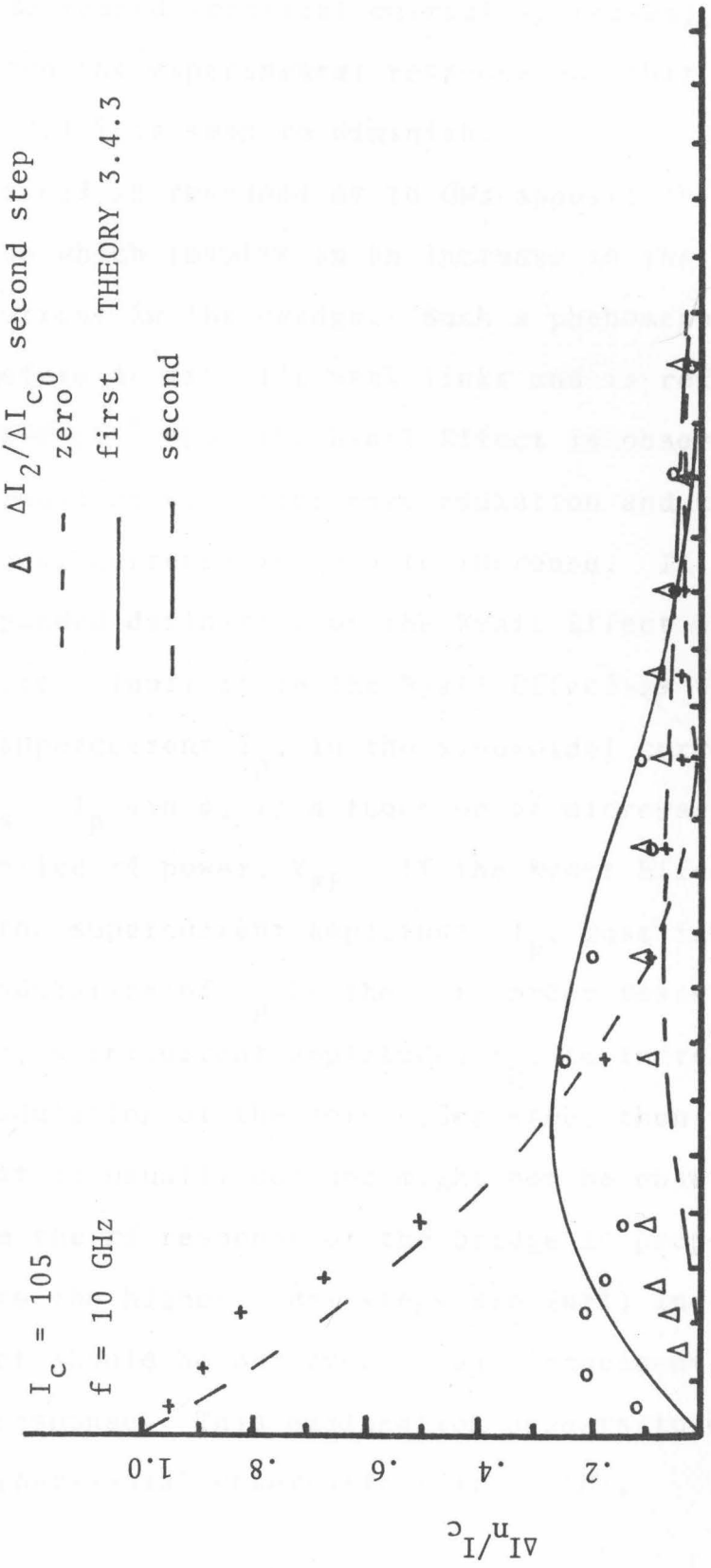
(a) I_c = 6 μamp
(b) I_c =18 μamp
(c) I_c =27 μamp
(d) I_c =105μamp

Note that as the critical current is increased, the step size is seen to decrease.


+ $\Delta I_c/I_{c_0}$ zero order step
o $\Delta I_1/I_{c_0}$ first step
Δ $\Delta I_0/I_{c_0}$ second step
zero
first THEORY - 3.4.3
second
RSJ - second step
RSJ - first step
I_c = 6.3 μamp
f = 10 GHz
$\Delta I/I_c$
.2 .4 .6 .8 1.0
.2 .6 1.0 1.4 1.8 2.2 2.6 3.0 3.4 3.8 4.2 4.6 5.0
V_{RF}/V_μ


+ ΔI/I_c0 zero order step
o ΔI_1/I_c0 first step
Δ ΔI_2/I_c0 second step
zero
first THEORY - 3.4.3
second
I_c = 18.0
f = 10 GHz
ΔI_n/I_c
V_RF/V_μ
.2
.6
1.0
1.4
1.8
2.2
2.6
3.0
3.4
3.8
4.2
4.6
.2
.4
.6
.8
1.0


+ $\Delta I_c/\Delta I_{c_0}$ zero step
o $\Delta I_1/\Delta I_{c_0}$ first step
Δ $\Delta I_2/\Delta I_{c_0}$ second step
— — zero
——— first THEORY 3.4.3
— — — second
I_c = 27.4
f = 10 GHz
$\Delta I_n/I_c$
.2 .4 .6 .8 1.0
.2 .6 1.0 1.4 1.8 2.2 2.6 3.0 3.4 3.8 4.2 4.6
V_{RF}/V_μ


$\Delta I_c/\Delta I_{c_0}$ zero step
$\Delta I_1/\Delta I_{c_0}$ first step
$\Delta I_2/\Delta I_{c_0}$ second step
zero
first THEORY 3.4.3
second
I_c = 105
f = 10 GHz
$\Delta I_n/I_c$
V_{RF}/V_μ
.2
.4
.6
.8
1.0
1.4
1.8
2.2
2.6
3.0
3.4
3.8
4.2
4.6

ature is decreased (critical current increases), the discrepancy between the experimental response and that predicted by expression 3.4.3 is seen to diminish.

The enhanced rf response at 10 GHz appears to be caused by a phenomenon which results in an increase in the amplitude of the supercurrent in the bridge. Such a phenomenon has been observed before in metallic weak links and is referred to as the Wyatt Effect.[9] When the Wyatt Effect is observed, a weak link is irradiated with microwave radiation and the zero order step (critical current) is seen to increase. It is suggested that an expanded definition of the Wyatt Effect should be employed here. Implicit in the Wyatt Effect is that the amplitude of supercurrent I_p, in the sinusoidal current phase relation $I_s = I_p \sin \phi$, is a function of microwave frequency, ω_μ, and applied rf power, V_{RF}. If the Wyatt Effect is to be observed, the supercurrent amplitude, I_p, must increase faster than the modulation of I_p by the zero order Bessel function. Now were the supercurrent amplitude, I_p, to increase slower than the modulation of the zero order step, then the Wyatt Effect as it is usually defined might not be observed. However, since the rf response of the bridge is proportional to I_p and since the higher order steps are ($n \geq 1$) increasing, the Wyatt Effect should be observed by an enhancement in the bridge rf response. This explanation appears to be consistent with the experimental observations at 10 GHz,

The question is what mechanism is responsible for the increased amplitude of the supercurrent in a proximity effect bridge. Eliashberg[10] has pointed out that it is the occupation of the low energy quasiparticle states that most severely interferes with pairing correlations. If a superconductor is driven by microwave radiation at a frequency such that $\hbar\omega < 2\Delta$, pairs cannot be broken and the quasiparticles are redistributed into higher energy states. Such a redistribution of the quasiparticles has been shown to cause an increase in the energy gap for superconducting films.

For the model of the amplitude of the supercurrent presented in this work there are two possible sites where this enhancement can have an effect, either in the superconductor, or in the normal bridge material. If the enhancement of the energy gap were only to occur in the bounding superconductor, in order to account for the 10 GHz experimental results would require a gap enhancement of at least ten times the equilibrium value. However, an order of magnitude gap enhancement does not appear to be consistent with calculations of the nonequilibrium energy gap which show a 10%[11] enhancement and with measurements of the transition temperature of irradiated superconducting films which show an increase of ~ 2%.[12] Thus, an enhancement of the equilibrium energy gap by an order of magnitude does not appear to be justifiable. Therefore, it is concluded that enhanced rf response observed at 10 GHz is due to an interaction

of the rf and the quasiparticles in the normal material, similar to that predicted for a homogeneous superconductor. If so, this implies that the low frequency process causing the rf response to decrease $\propto \exp(-BV)$ is offset by an rf stimulation of the quasiparticles to higher energy so as to give an enhanced rf response. However, further discussion of this point is beyond the scope of this thesis and so will not be considered.

APPENDIX A

Magnetic Field of a Current Carrying Thin Film

When a current is allowed to flow in a superconductor, the current distributes itself in such a way to keep the magnetic field zero inside the superconductor. Conversely, if an external magnetic field is applied to a superconductor, currents are induced sufficient to keep the internal field zero. Consider the situation shown in Figure 29a of a superconducting strip of elliptical cross sectional area with the current direction perpendicular to the plane of the ellipse. In the current free region surrounding the superconductor, $\vec{B}$ can be written as the gradient of the scalar function V, the magnetic vector potential (for this section only, the usual denotation of the vector potential as $\vec{A}$ is changed).

$$\vec{B} = \vec{\nabla} V \qquad \text{A1}$$

Since the divergence of B is always zero in the region of interest

$$\nabla^2 V = 0 \qquad \text{A2}$$

Therefore, the problem of determining the magnetic field distribution around a current carrying superconductor has been reduced to solving Laplace's equation for V. Since Laplace's equation has been solved for the appropriate geometry in the

electrostatic case, this result can directly be applied to this problem. It should be pointed out that one approximation has been made here. Implicit in this sort of a development is that the superconducting penetration depth λ, is smaller than any film dimension, that is, either width, 2b, or thickness, 2a. While the film width, 2b, is almost always much greater than λ, it is seen that the film thickness used here ($2a \sim 300A^0$) is always much less than the penetration depth. However, it is argued that the calculation to be presented is an adequate description of the experimental situation since the magnetic field magnitude and distribution under study is at the film edges $\pm$ b.

To determine the magnetic field around the current-carrying strip, one begins with the conformal transform

$$z=x + iy= b \cos\left(\frac{2\pi}{\mu_0 I} (U + iV)\right) + i a \sin \left(\frac{2\pi}{\mu_0 I}\left(U + iV\right)\right) \quad A3$$

where U is the axial component of the vector potential analagous to the electrostatic potential and V is the magnetostatic potential analogous to the electrostatic flux lines. Expression A3 in conjunction with the formula of the ellipse $(x/b)^2 + (y/a)^2 = 1$ is then used to solve for V. This problem is solved in many E & M texts so that only the result is quoted here.

$$\left(\frac{x}{b \cosh \frac{2\pi V}{\mu_0 I} - a \sinh \frac{2\pi V}{\mu_0 I}}\right)^2 + \left(\frac{y}{-b \sinh \frac{2\pi V}{\mu_0 I} + a \cosh \frac{2\pi V}{\mu_0 I}}\right)^2 = 1 \quad A4$$

The magnetic field is then

$$B_y = \frac{-dV}{dx} \qquad B_x = \frac{dV}{dy} \qquad \text{A5}$$

Using expressions A4 and A5, the magnetic field at the film edge (0,a) is

$$B_x\ (0,\ a) = \frac{\mu_0 I}{2\pi}\ \frac{1}{b} \qquad \text{A6}$$

while at the other film edge (b, 0)

$$B_y(b,\ 0) = \frac{\mu_0 I}{2\pi}\ \frac{1}{a} \qquad \text{A7}$$

It is seen that for a current carrying film, that the magnetic field is concentrated and largest at the narrowest film edge.

REFERENCES

Chapter I

1. V. L. Ginzburg and L. D. Landau, Sov. Phys. JETP 20, 1064 (1950).
2. F. London, Superfluids, Vol. 1, John Wiley & Sons (1950).
3. L. P. Gor'kov, Sov. Phys. JETP 7, 505 (1958).
4. M.Tinkham , Introduction to Superconductivity, McGraw Hill (1975).
5. F. London and H. London, Proc. Roy. Soc. (London) A149, 72(1935); Physica 2, 341 (1935).
6. J. Bardeen, L. N. Cooper, and J. R. Schrieffer, Phys. Rev. 108, 1175 (1957).
7. G. Rickayzen, Superconductivity (ed. by R. D. Parks) pp. 51-113, Marcel Dekker, Inc. (1969).
8. L. P. Gor'kov, Sov. Phys. JETP 10, 998 (1960).
9. R. K. Kuschman, Journal of Low Temperature Physics, Vol. 11, Nos. 1/2, 235 (1973).
10. Tomas Ganz, Ph.D. Thesis (California Institute of Technology, 1976).

Chapter II.

1. B. D. Josephson, Superconductivity (ed. by R. D. Parks) pp. 423-448, Marcel Dekker, Inc. (1969).
2. H. A. Notarys and J. E. Mercereau, J. Appl. Phys., 44, 1821 (1973).
3. David William Palmer, H. A. Notarys, and J. E. Mercereau, Applied Phys. Lett. 26, 204 (1975).

4. E. P. Harris, J. Vac. Sci. Technol. 12, 1383 (1975)
C. H. Arrington III and B. S. Deaver, Jr.,
Applied Phys. Lett. 26, 204 (1975).

5. R. K. Kirshman, J. A. Hutchby, J. W. Burgess,
R. P. McNamara, and H. A. Notarys, JEEE Trans.
MAG-13, 731 (1977).

6. P. Crozat, R. Adde, J. Chaumont, and H. Bernas,
Applications of Ion Beams to Metals, ed by S. T. Picraux,
E. P. Eer Nisse, and F. L. Vook, Plenum Press, p. 27.

7. E. H. Sondheimer, Advan. Phys. 1, 1 (1952).

8. A. F. Mayadas, R. B. Larbowitz and J. J. Cuomo,
J. Appl. Phys. 43, 1287 (1972).

9. F. E. Harper and M. Tinkham, Phys. Rev. 172,
441 (1968). N. E. Aleksejewski, W. M. Sakosarenko,
K. Bluthner, and H. J. Kohler, Phys. Stat. Sol. 34,
541 (1976).

10. W. A. Little, Proceedings of the Symposium on the
Physics of Superconducting Devices, University of
Virginia, Charlottesville (1967) S-1.

11. J. W. Bremer and V. L. Newhouse, Phys. Rev. 116,
309 (1959).

12. Martin Tinkham, Introduction to Superconductivity,
McGraw Hill (1975).

13. W. J.Skocpol , Phys. Rev. B, 14, 1045 (1976).

14. P. G. De Gennes, Superconductivity of Metals and
Alloys, W. A. Benjamin, Inc. (1966).

15. P. W. Anderson, and J. M. Rowell, Phys. Rev. Lett. 10, 230 (1963).

16. R. P. Feynman, Lectures on Physics, Vol. 3, Addison-Wesley Publishing Co. (1965).

17. David William Palmer, Ph.D. Thesis (California Institute of Technology, 1975).

18. P. G. De Gennes, Reviews of Modern Physics, 36, 225 (1964).

19. J. Clarke, Proc. Roy. Soc. A, 308, 447-471 (1969).

20. L. G. Aslamazov and A. I. Larkin, ZhETF Pis, Red., 9, 150 (1969) {JETP Lett., 9, 87 (1969)}.

21. K. K. Likharev and L. A. Yakobson, Sov. Phys. Tech. Phys. 20, 950 (1976).

22. N. R. Werthamer, Phys. Rev. 132, 2440 (1963).

23. P. Morel and P. W. Anderson, Phys. Rev. 125, 1263 (1962).

24. Tomas Ganz, Ph.D. Thesis (California Institute of Technology, 1976).

25. Charles Kittel, Introduction to Solid State Physics, 4th Ed., John Wiley & Sons, Inc. (1971).

26. R. C. Jaklevic et. al., Phys. Rev. 140A, 1628 (1965).

27. J. E. Mercereau, Tunneling Phenomena in Solids, Plenum Press, 461 (1969).

28. H. A. Notarys and J. E. Mercereau, Physica, 55, 424 (1971).

29. C. S. Owen and D. J. Scalopino, Phys. Rev., 164, 538 (1967).

Chapter III

1. B. D. Josephson, Phys. Lett. 1, 251 (1962).
2. Ming Lun Yu, Ph.D. Thesis (California Institute of Technology, 1974). G. J. Dolan and L. D. Jackal, Phys. Rev. Lett., 39, 1628 (1977).
3. R. K. Kushman, Journal of Low Temperature Physics, Vol 11, Nos 1/2, 235 (1973). Tomas Ganz, Ph.D. Thesis (California Institute of Technology, 1976).
4. P. L. Richards, F. Auracher, T. Van Duzer, Proc. IEEE, 61, 36 (1973).
5. J .Franson, Ph.D. Thesis (California Institute of Technology, 1977).
6. P. Russer, J. Appl. Phys., 43, 2008 (1972).
7. T. D. Clark and P. E. Lindelof, Phys. Rev. Lett., 37, 368 (1976).
8. W. J. Skocpol, M. R. Beasley, and M. Tinkham, Rev. Phys. Appl., 9, 19 (1974); M. Octavio, W. J. Skocpol and M. Tinkham, IEEE Trans. MAG-13, (1977).
9. A. F. G. Wyatt, V. M. Dmitriev, S. W. Moore, and F. W. Shreard, Phys. Rev. Lett., 16, 1166 (1966).
10. G. M. Eliashberg, Sov. Phys. JETP Lett. 11, 114 (1970).
11. J. J. Chang and D. J. Scalapino, Nato Advanced Study Institute on Small Scale Superconducting Devices, Lago di Garda, Italy (1976).
12. T. M. Klapwijk and J. E. Modij, Physica 81B, 132 (1976).